5.2.4. Hydrogenation of CO over alumina supported Co catalysts with different metal loading

5.2.4.1. CO spectral region for 1% $Co/\gamma\text{-}Al_2O_3$

The behaviour of alumina supported catalysts with cobalt loadings of 1% and 4.6% was also investigated during CO hydrogenation at different reaction conditions.

Fig. 5.2.4.1-1 shows the difference spectra recorded during CO hydrogenation at 473 and 523K over 1% $Co/\gamma\text{-}Al_2O_3$. At both temperatures, only a flat (or noisy) baseline is observed. Contrary to the observations on the SiO_2 supported catalysts, no infrared bands due to linearly adsorbed CO could be detected on 1% Co/Al_2O_3 under reaction conditions.
The lack of detectable bands ascribed to molecularly adsorbed carbon monoxide can in principle have several explanations.
First, weakly adsorbed CO would be expected to give absorption band(s) in the 2200-2100 cm^{-1} range. These bands would have been masked by the gas phase CO bands in the sample absorbance spectra, but should easily have been recognised when contributions from the gas phase are subtracted in a manner previous described in section 5.2.1. However, no bands were observed in the actual frequency range which could be attributed to CO on $Co^{\delta+}$. Secondly, one could possibly expect a rapid desorption of adsorbed CO, for example in the linear form, in flowing helium and/or hydrogen. This implies however, that linearly adsorbed CO is present during CO hydrogenation. Based on the experience with both the low and high metal loading silica supported cobalt catalysts, significant band(s) should be observable as a shoulder on the low frequency side of the CO gas phase P branch, and as a distinct, resolved band in the difference spectra. This was not confirmed by the experimental observations or post run processing of the spectra. No shoulders on the gaseous CO bands were detected which possibly can be ascribed to linearly adsorbed CO.
A third possibility exists, namely that of dissociative adsorption of carbon monoxide, and the coverage of CO would therefore be too low to be detected by infrared spectroscopy. However, the literature report that low loading alumina supported Co catalysts prepared and treated in a manner similar to the one in the present study do not dissociate CO /6,77/. This is supported by the absence of atomic carbon (α-carbon) on the catalyst surface as deduced from CO-TPD

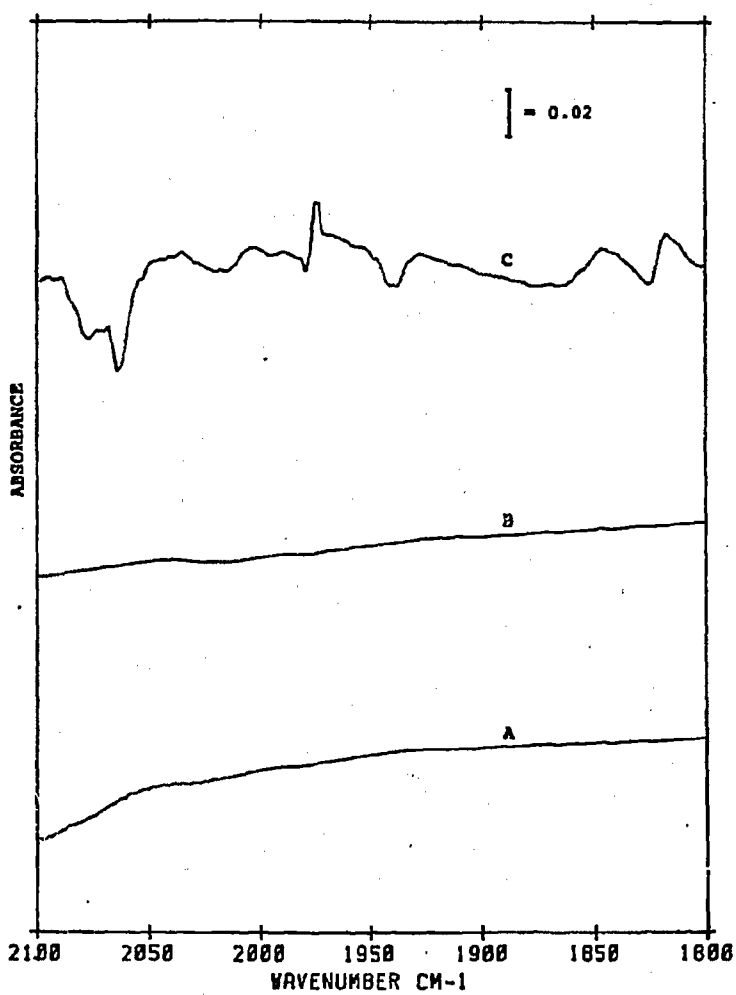

Fig. 5.2.4.1-1: **CO spectral region of 1% Co/γ-Al_2O_3 during CO hydrogenation.**

A: **After 90 min. in synthesis gas at 473K**
B: **After 90 min. in He at 473K (following CO hydrogenation)**
C: **After 180 min. in synthesis gas at 523K**

CO hydrogenation conditions:
P_{Tot} = 6 bar, H_2/CO = 2, 100 Nml/min.

measurements /77/.

Fourthly, several reports /50,52,53,57,58,126/ have emphasized the signification of the interaction between the cobalt in catalysts with low metal loading and the alumina support resulting in the formation of cobalt aluminates (surface or bulk spinels). It has been stated /53,164/ that alumina supported catalysts containing less than 2 wt-% Co experience complete diffusion of the metal ions into the alumina lattice, where they are located either in tetrahedral or octahedral sites /53,55/. Catalysts with low cobalt loadings (1-2%) have been found to have XPS spectra closely resembling those of $CoAl_2O_4$ /53/.

The absence of infrared bands attributable to adsorbed CO most probably indicate that the cobalt atoms associated with the alumina are not exposed to the surface, but located in the subsurface region. This is in accordance with the TPR studies of the 1% $Co/\gamma\text{-}Al_2O_3$ catalyst, showing no peaks attributable to the reduction of cobalt species, except at temperatures higher than 1100K, where reduction of cobalt aluminate is expected to take place.

A qualitative picture of the behaviour of cobalt and its interaction with the alumina carrier depending on the cobalt metal concentration is presented in Fig. 5.2.4.1-2. In the literature, a general agreement exists concerning the incorporation of cobalt into the alumina lattice; diffusion of cobalt ions into the support where they may occupy octahedral or tetrahedral lattice sites /50,53,55/. Low metal loading catalysts (ca. ≤ 2 % Co by weight) experience complete migration of the cobalt ions into the alumina lattice, forming cobalt aluminates, $CoAl_2O_4$. This is usually believed to take place as a result of for example the calcination step. It has been shown, however, in Chapter 5.1, that the interaction between cobalt and alumina is of such a character that it may occur in the impregnation or during the reduction stage

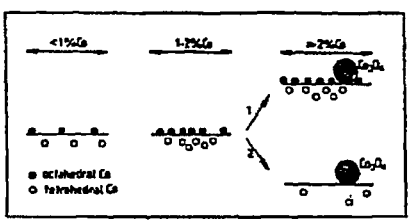

Fig. 5.2.4.1-2: **Schematic representation of Co/Al_2O_3 catalysts. In scheme 1 Co enters the alumina until saturation is attained; excess cobalt is incorporated into Co_3O_4 phase. In scheme 2 the formation of Co_3O_4 is accompanied by a decrease in the amount of Co associated with the alumina /141/.**

/65,126/. If this is the case, bands due to cobalt ions in tetrahedral and/or octahedral positions in the alumina lattice should easily be recognized in UV-VIS spectra of the dried and uncalcined cobalt catalyst with low metal loading (1% Co/γ-Al_2O_3).

Fig. 5.2.4.1-3 shows the diffuse reflectance spectra of the 1% and 4.6% Co/γ-Al_2O_3 catalysts recorded at room temperature in the UV-VIS region, 200-900 nm. The dominating feature in the spectra of the 1% Co/γ-Al_2O_3, Fig. 5.2.4.1-3 spectra A-C, is a broad absorption band in the 350-700 nm range. The two bands located below 300 nm (231 and 270 nm) are probably not a consequence of the interaction between cobalt and the alumina support, but rather believed to be caused by specular reflectance (mirror type reflectance) from the sample surface.

The alumina support itself has been reported to exhibit absorption bands at 1350 nm and in the range around 2200 and 2700 nm, and is consequently outside the region of interest in this section /183/.

Spectrum A in Fig. 5.2.4.1-3 is recorded after impregnation and over night drying of the catalyst in air at 398K. The peaks located around 495 and 523 nm are probably due to a cobalt-water complex, possibly $Co(H_2O)_6^{2+}$ (cobalt hexa-aqua complex) /71/. In this frequency region, one would also expect to find bands due to the metal precursor, cobalt nitrate.

The absorption triplet at 543, 587 and 627 nm is in excellent agreement with bands in the literature ascribed to Co^{2+} located at tetrahedral interstices surrounded by oxygen ions in the spinel structure of Co-Al oxide /54,57,71,85,183,184/. The lack of any absorption bands due to octahedric coordinated Co^{2+} in the cobalt aluminate is probably due to the high extinction coefficient of the tetrahedric coordinated Co^{2+} species. Chung et al. /54/ suggested that octahedric Co^{2+} should result in an absorption band around 500 nm, but since the intensity of this band is an order of magnitude lower than that of tetrahedric Co^{2+} /183/, this band will probably be masked by the strong absorption of the tetrahedral positioned Co^{2+}.

Absorption bands due to octahedrally coordinated Co^{3+} and Co_3O_4 have been reported near 700-750 nm and 250-350 nm, respectively. Cobalt oxide (Co_3O_4) would be expected to give strong absorption bands around 675-750 nm and 370-400 nm /60,183,184/. Although a broad peak is observed in the 300-350 nm range, the high frequency band is absent or at least poorly resolved. Thus, it is believed that the amount of cobalt oxide after impregnation and drying is low or non-existing. The UV-VIS spectrum (A in Fig. 5.2.4.1-3) suggests that the

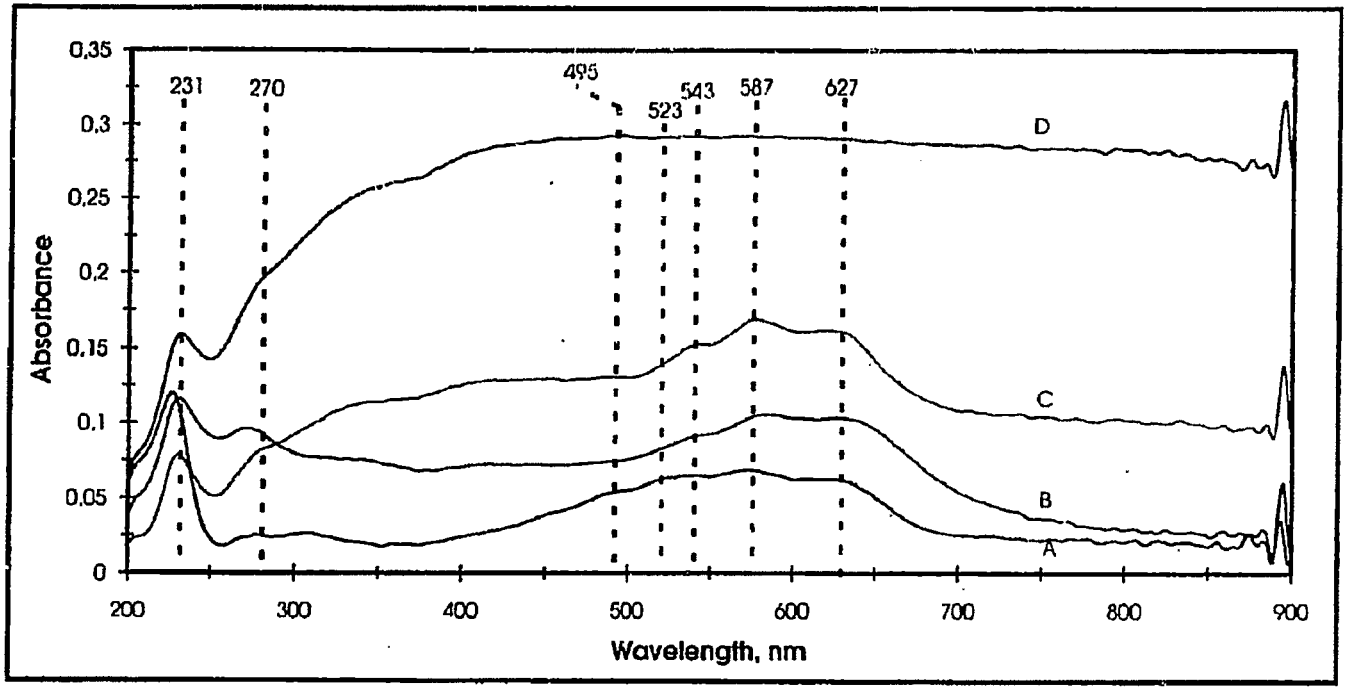

Fig. 5.2.4.1-3: **UV-VIS diffuse reflectance spectra of 1% and 4.6% Co/γ-Al_2O_3.**

A: **Impregnated and dried 1% Co/γ-Al_2O_3**
B: **1% Co/γ-Al_2O_3 heated in air to ~573K**
C: **1% Co/γ-Al_2O_3 after subjected to a TPR run; 294-1203K**
D: **4.6% Co/γ-Al_2O_3 after subjected to a TPR run; 298-1203K**

cobalt ions (Co^{2+}) are stabilized in tetrahedral/octahedral positions in the alumina matrix. After heating the catalyst in air to approximately 573K, the triplet structure remains intact, although slightly shifted in frequency, see Fig. 5.2.4.1-3, spectrum B. The calcination treatment causes the absorption bands ascribed to the cobalt-water complex or residual cobalt nitrate to decrease in intensity, while no features appear which can be ascribed to cobalt oxide.

Spectrum C and D are recorded at room temperature in flowing CO after the catalyst had been exposed to a normal TPR-run, as described in further details in Chapter 5.1. Their corresponding TPR profiles are previously given in Fig. 5.1.2-1. Even though these samples had been stored in sample bottles for some time before the UV-VIS measurements, it is not believed that this has had any serious influence on the state of cobalt in the case of the low metal loading catalyst, 1% $Co/\gamma\text{-}Al_2O_3$. Neubauer /185/ stated that cobalt/alumina catalysts strongly resisted oxidation during exposure to air after reduction. It must be expected, though, that exposure of the reduced 4.6% $Co/\gamma\text{-}Al_2O_3$ catalyst to air will result in oxidation, at least of the surface layer.

Except from the absorption due to cobalt hexa-aqua complex/cobalt nitrate, there is a striking similarity between the UV-VIS diffuse reflectance spectra of the "raw" 1% $Co/\gamma\text{-}Al_2O_3$ catalyst (spectrum A) and the same catalyst investigated according to the TPR procedure (spectrum C) in terms of dominating absorption bands in the 500-700 nm range, due to Co^{2+} in tetrahedric configurations. Also the colour of the catalyst samples after the different treatments was similar, the "TPR" sample being slightly more bluish than the "raw" catalyst. The bluish colour has in the literature been regarded as an strong indication of the cobalt aluminate formation /54/. This points towards a formation of the cobalt aluminate already during the impregnation or drying step, although it is also possible that additional migration of Co^{2+} into the alumina lattice may occur during the reduction stage as well, thus explaining the slightly deeper blue colour of the sample run in the TPR apparatus.

Spectrum D in Fig. 5.2.4.1-3, that of 4.6% $Co/\gamma\text{-}Al_2O_3$, differed from the diffuse reflectance spectra of the low metal loading catalyst. The DRS signal from the absorption triplet assigned to Co^{2+} in tetrahedral positions has vanished or is possibly hidden under the broad absorption band extending over almost the entire frequency range. The lack of any distinct features due to tetrahedric divalent cobalt ions could indicate that (additional) structure(s) are deposited over the spinel structure, creating an overlayer phase. It would seem that the excess cobalt,

not participating in the cobalt aluminate formation is deposited over the spinel structure. It is tempting to assign this structure-less absorption to cobalt oxide, either of the type Co_3O_4 or CoO. Absorption bands attributable to Co_3O_4 have been reported to appear at 350-450 and around 700 nm /60/. The DRS-spectra of a Co_3O_4 sample, as given by Tung et al. /57/ do not bear any significant resemblance to spectrum D in Fig. 5.2.4.1-3. This is understood, since the formation of cobalt oxide occuring during storage of the catalyst sample at room temperature between the TPR and the DRS measurements is of a lesser extent than it would have been upon exposure of the catalyst to oxygen (at higher temperatures). Still, it is possible that the absorption bands appearing in the low frequency regions represents cobalt oxide formed due to oxidation of the surface layer. Neither can the possibility of a metallic cobalt phase being the reason for the rather strong, structurless absorption characteristic for this sample be totally excluded. Also, it might be that the continous absorption band in the region 400-700 nm represents cobalt interacted with the alumina support, forming an amorphous surface oxide overlayer, consisting of cobalt ions. This mixed oxide phase would be deposited over the cobalt aluminate, thereby precluding the observations of any bands due to tetrahedric Co^{2+} in the Co-Al spinel structure. It is expected that this overlayer phase is easier to reduce than the cobalt aluminate phase. Tung et al. /57/ reported a distorted overlayer structure of Co_3O_4 with peaks at 400 and 700 nm, deposited over the Co-Al spinel.

Fig. 5.2.4.1-4 shows the UV-VIS spectrum of 0.82% Co/SiO_2 and 4.7% Co/SiO_2 in air at room temperature after impregnation and drying. Two broad peaks at 428 and 710 nm dominate the spectrum. In accordance with Okamoto et al. /60/, these peaks are assigned to Co_3O_4 as a result of nitrate decomposition during drying of the catalyst. The broad features of the two bands could imply the presence of additional structures, for example coordinated water. Other possible compounds could include Co_2SiO_4 (cobalt silicate) and the metal precursor, $Co(NO_3)_2 \cdot 6H_2O$, due to incomplete or partial decomposition. Peaks due to Co_2SiO_4 is expected near 730, 645, 565, 520, 515, 487 and 465 nm /60/, while $Co(NO_3)_2$ supported on silica have been reported to give absorption bands in the vicinity of 505, 490 and 465 nm. As can be seen, the small frequency separation and the overlap of bands between the cobalt silicate and the supported metal precursor makes it difficult to clearly distinguish between the two species. All of the bands above may in principle be accounted for by just considering the relatively broad bands. To conclusively confirm or exclude the presence of either of the two

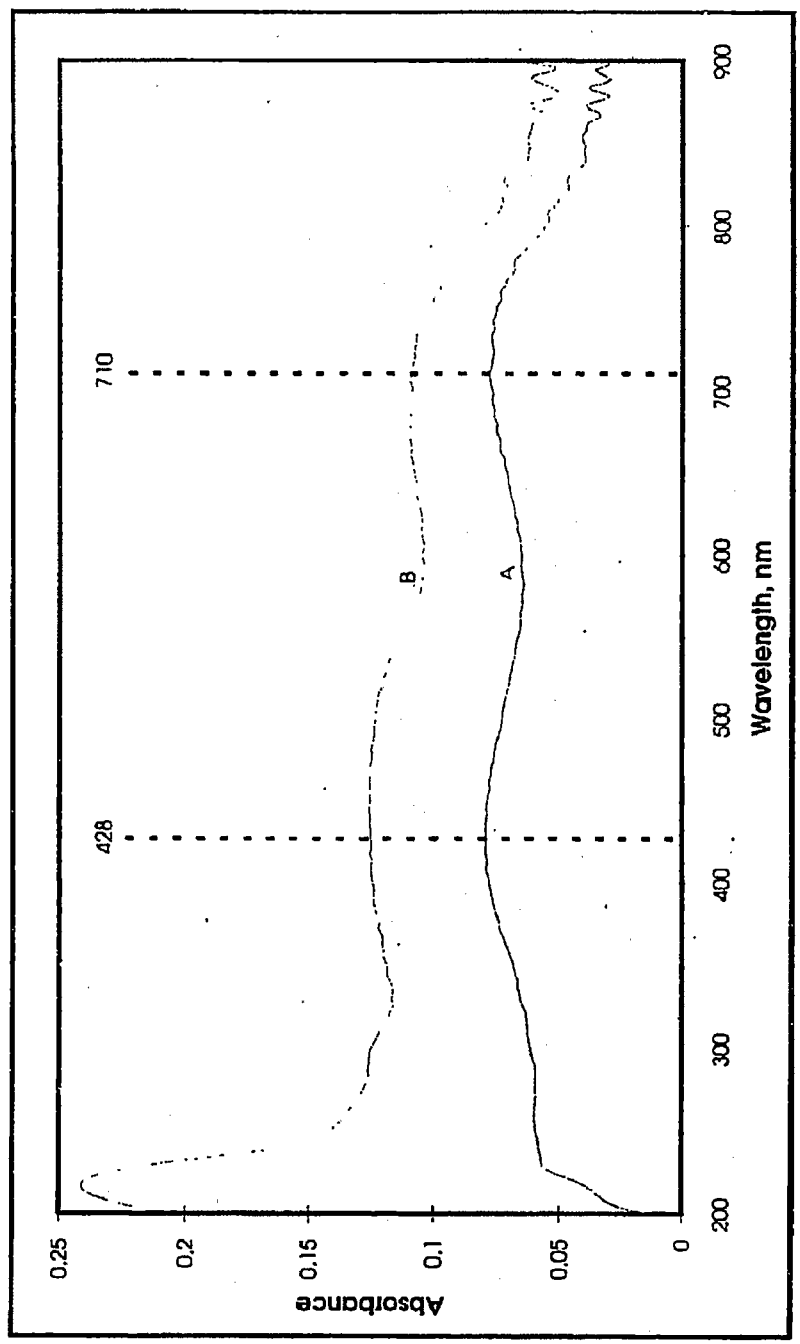

Fig. 5.2.4.1-4: UV-DRS spectra of 4.7% Co/SiO_2 (A) and 0.82% Co/SiO_2 (B).

compounds based on the limited amount of available experimental data is not possible. The spectra in Fig. 5.2.4.1-4 does however confirm the assumption that the peaks observed below 300 nm can be ascribed to specular reflectance. The 4.7% Co/SiO_2 sample was diluted in $BaSO_4$ (14%) before collecting the spectrum, while the 0.82% Co/SiO_2 catalyst was analysed without dilution of the catalyst sample.

The UV-VIS DRS measurements carried out at room temperature illustrate the difference in the surface composition of the silica and alumina supported cobalt catalyst after impregnation and drying. While the cobalt aluminate spinel phase dominates on the alumina supported low metal loading catalyst, Co_3O_4 is the major phase on 0.82% Co/SiO_2. For the catalysts with higher metal loading, the picture is not altered for the 4.7% Co/SiO_2 catalyst, while additional contributions from cobalt oxide and possibly the non-stoichiometric cobalt oxide overlayer phase are registred for 4.6% Co/γ-Al_2O_3. The essential picture obtained from the UV-VIS DRS measurements is in qualitative agreement with the conclusions from the TPR investigations.

In the infrared portion of the electromagnetic spectrum, the skeletal vibrations of $CoAl_2O_4$ is believed to result in an absorption band around 670 cm^{-1}, ascribed to octahedrally coordinated Al^{3+}. Adsorption of CO on cobalt aluminate have been reported to give infrared bands in the 2250-2100 cm^{-1} range, due to CO adsorbed on octahedric and tetrahedric Al^{3+} (2170 and 2210 cm^{-1}, respectively) in addition to CO on Co^{2+} (~2140 cm^{-1}) /95/.

It is believed that the absence of infrared absorption bands in the CO spectral region for 1% Co/γ-Al_2O_3 may be due to the lack of cobalt available for CO adsorption. TPR studies of this catalyst showed no cobalt oxide reduction peaks, while hydrogen consumption was detected above 1100K, where reduction of the surface cobalt aluminate spinel phase is expected to occur. UV-VIS diffuse reflectance spectra of dried and impregnated 1% Co/γ-Al_2O_3, before and after a TPR run, showed distinct absorption bands due to Co^{2+} in tetrahedric interstices in the alumina matrix. Since CO hydrogenation occurs readily on metal atoms having the ability to adsorb and dissociate CO, the assumption of inaccessible cobalt is consistent with later results showing negligible CO hydrogenation activity for the 1% Co/γ-Al_2O_3 catalyst.

5.2.4.2. CO spectral region for 4.6% $Co/\gamma\text{-}Al_2O_3$: $H_2/CO = 2$, $P_{Tot} = 6$ bar, T = 473-523K

During CO hydrogenation over the 4.6% $Co/\gamma\text{-}Al_2O_3$ catalyst at 473 and 523K, bands appeared at 2062 and 2050 cm^{-1}, respectively, which can be attributed to linearly adsorbed carbon monoxide, see Fig. 5.2.4.2-1. As seen from this figure, an increase in the reaction temperature from 473 to 523K led to a decline in the band intensity and a shift to lower frequencies. In addition, the spectrum of 4.6% $Co/\gamma\text{-}Al_2O_3$ during CO hydrogenation showed a doublet structure with peak maxima at 1996 and 1952 cm^{-1}.

A curious feature of these bands is their behaviour during exposure to synthesis gas, during flushing with inert gas (He) and as a function of temperature.

The two bands appeared after short times in synthesis gas. Their intensities increased with time in H_2/CO, passed through a maximum and then declined, as illustrated in Fig. 5.2.4.2-2. During this period, the intensity of the linear CO band at 2062 cm^{-1} increased with time in synthesis gas until reaching an approximately constant value.

Flushing with inert gas (He) following CO hydrogenation at reaction temperature (473K) weakened and shifted the 2062 cm^{-1} linear CO band to lower frequencies, as seen in Fig. 5.2.4.2-3. Similarly, the pair of bands at 1996 and 1952 cm^{-1} also decreased in intensity with time in He, but without any apparent frequency shift.

The effect of increasing reaction temperature on the peaks in the CO spectral region is illustrated in Fig 5.2.4.2-4. An increase in the temperature from 473K to 573K during CO hydrogenation resulted in a gradual disappearance of the 1996/1952 cm^{-1} bands. Subsequent cooling to 473K did neither restore the 1996/1952 cm^{-1} doublet nor the intensity or the frequency of the 2062 cm^{-1} band.

Repeating the experiment at a fixed CO hydrogenation temperature of 473K with a fresh catalyst yielded spectra identical to those in Fig. 5.2.4.2-2.

Adsorption of CO (He:CO=9:1) at low temperature (303K) and low pressure (2 bar) on 4.6% $Co/\gamma\text{-}Al_2O_3$ revealed the presence of linearly adsorbed CO, but the low frequency doublet structure could not be detected in the same resolved manner as earlier described.

Absorption bands in the 2000-1800 cm^{-1} range have generally been ascribed to bridgebonded CO /50,73,74,78,85-87/. Several of these studies report two bands for the bridgebonded form

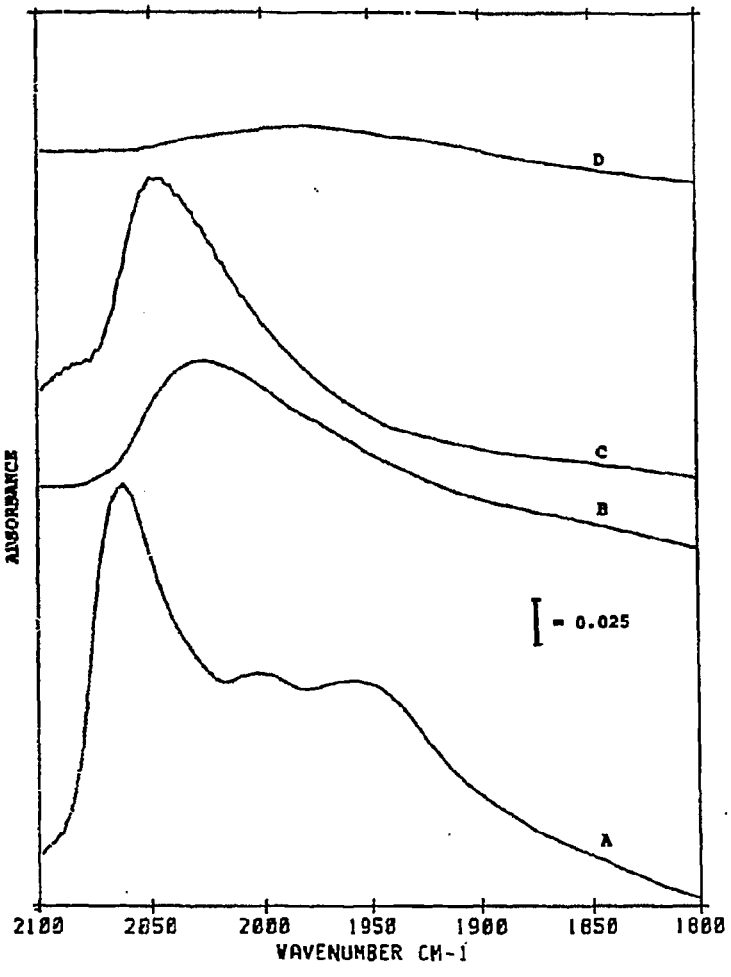

Fig. 5.2.4.2-1: **Infrared spectra of adsorbed CO during CO hydrogenation over 4.6% Co/γ-Al_2O_3 and subsequent elution of synthesis gas with He.**

A: **After 70 min. in synthesis gas at 473K**
B: **After 70 min. in He at 473K (following CO hydrogenation)**
C: **After 70 min. in synthesis gas at 523K**
D: **After 60 min. in He at 523K (following CO hydrogenation)**

CO hydrogenation conditions:
P_{Tot}= 6 bar, H_2/CO = 2, 100 Nml/min.

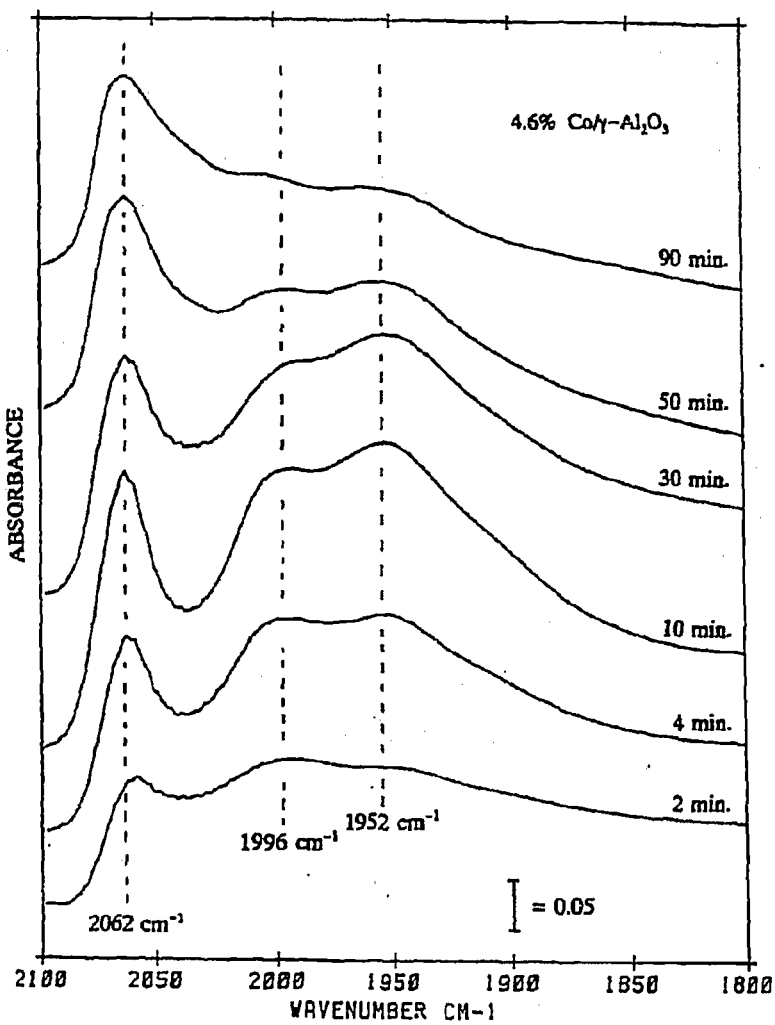

Fig. 5.2.4.2-2: **Development of infrared bands with time during CO hydrogenation over 4.6% Co/γ-Al_2O_3.**
The times given in the figure represent those at which the IR scan was initiated.

CO hydrogenation conditions:
P_{Tot}= 6 bar, H_2/CO = 2, T = 473K

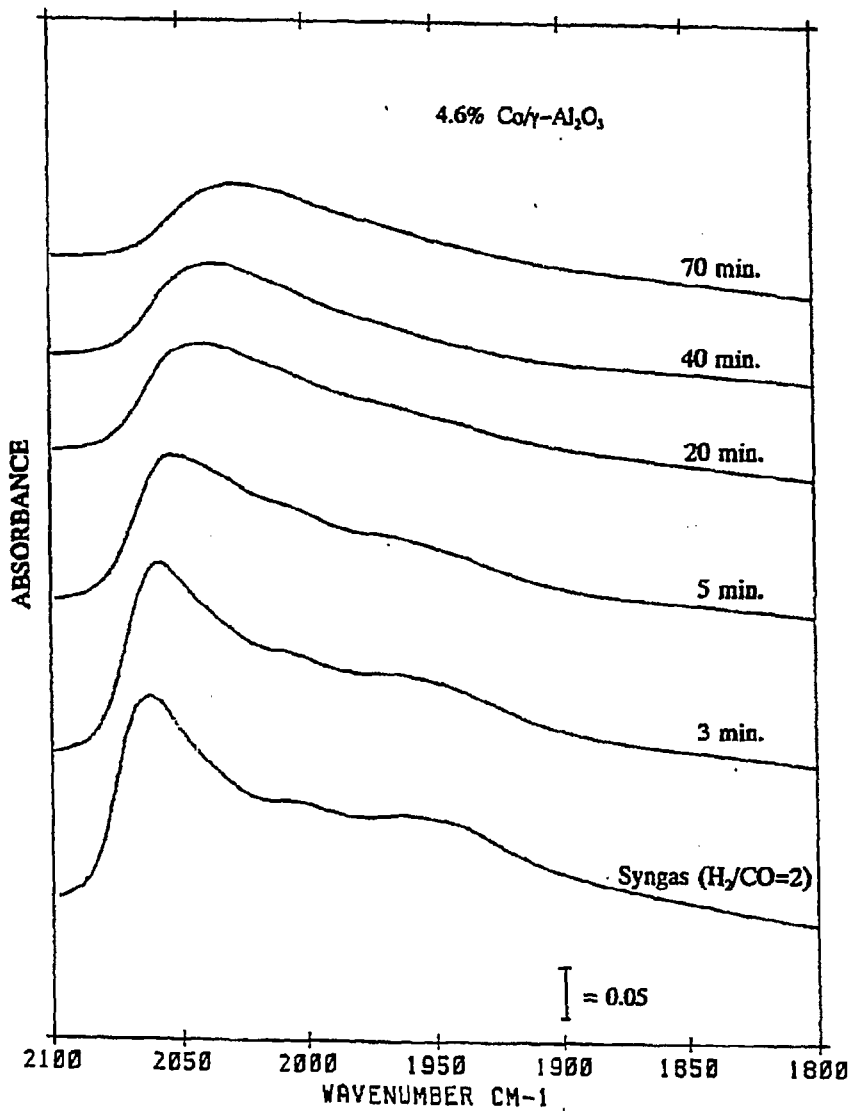

Fig. 5.2.4.2-3: **Infrared spectra of 4.6% Co/γ-Al_2O_3 after various times in He following CO hydrogenation.**

CO hydrogenation conditions:
P_{Tot}= 6 bar, H_2/CO = 2, T = 473K

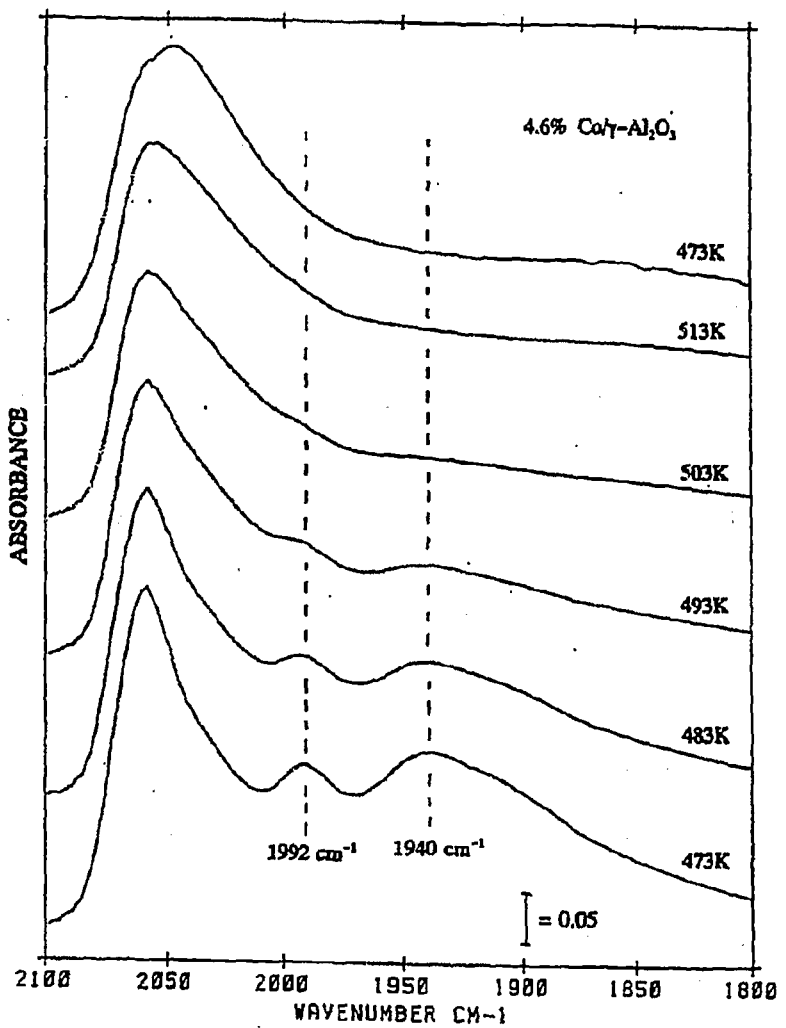

Fig. 5.2.4.2-4: **Infrared spectra of 4.6% Co/γ-Al_2O_3 at various temperatures while increasing the reaction temperature in H_2/CO from 473K to 573K followed by cooling to 473K in H_2/CO.**

Heating and cooling rate: 2K/min.

CO hydrogenation conditions:
P_{Tot}= 6 bar, H_2/CO = 2, 100 Nml/min.

/50,74,85,87/, while others assigned only a single band to this species /78,86/. The parallel behaviour of the two bands during prolonged exposure to H_2/CO, in inert gas and upon heating, may also suggest that they arise from the same adspecies. The 1996 and 1952 cm^{-1} bands can therefore possibly be assigned to bridgebonded carbon monoxide, but it must be emphasized that this assignment is not conclusively established. This is because of the unexpected high frequencies and the behaviour of the bands with time in synthesis gas, He and upon heating. Also, in general, one would expect only one absorption band for bridgebonded CO.

Both the reactivity and the frequency are atypical for bands ascribed to bridgebonded carbon monoxide in the literature /50,73,78,80/. Usually, bridgebonded CO is found at lower frequencies, and is more resistent to evacuation (or flushing with inert gas) than observed in the present study /50,73/. In these investigations, the multicoordinated CO species were believed to be adsorbed on fully reduced Co particles.

The cobalt catalyst used in this study exhibited a low degree of reduction, 42%, as deduced from the TPR measurements. This indicates a relatively large fraction of unreduced cobalt in the form of $Co^{\delta+}$ species, carrying excess positive charge, present on the surface or coordinated with the support in amorphous surface or subsurface oxidic phases. The relatively high frequency of the bands (1996 and 1952 cm^{-1}) can possibly be due to CO adsorbed in a bridgebonded form strongly influenced of or in the proximity of cobalt ions in a state resembling that described above. The anticipated effect of CO in such a coordination would be withdrawal of electrons from the bonding site of CO to the electron deficient $Co^{\delta+}$ site, thus decreasing the backbonding and increasing the C-O bond strength, hence a shift to higher frequency would be expected. It is not believed that CO is adsorbed on cationic cobalt, Co^{2+}/Co^{3+}, because a greater frequency separation than that observed would most probably be the case. The rather high frequency of the two bands tentatively assigned to bridgebonded CO could therefore possibly be related to the surface coordination of the CO in terms of adsorption on reduced cobalt particles deposited over or interactive with cobalt ions or oxygen atoms of the surface oxide or spinel. Thus, one could speculate if the somewhat higher frequencies than those usually found for bridgebonded carbon monoxide (1950-1800 cm^{-1}) could indicate a link with the oxidic cobalt phases found on Co/Al_2O_3.

Two bands for the multicoordinated CO can then be explained by the difference in the electronic environment or density experienced by the adsorbed CO, inducing different degrees

of back-bonding and hence different CO stretching frequencies. An electron deficient environment would then be expected to result in a higher frequency compared to an adsorption site exhibiting higher electron density.

Another possible explanation relates to the presence of oxygen atoms on the surface. Cobalt atoms surrounded by oxygen atoms, either from dissociation of carbon monoxide or due to incomplete reduction of the catalyst, may influence the electron density on the cobalt atoms. Oxygen attracting electrons from Co would result in decreasing occupation of the $2\pi^*$ orbital of CO, giving a higher CO frequency. But it could be speculated if oxygen also would influence the 5σ bonding. As to compensate for the low electron density, cobalt could attract electrons from the 5σ orbital, resulting in increasing 5σ donation, and hence a strengthening of the C-O bond.

The possibility of a dicarbonyl species giving rise to the pair of bands at 1996 and 1952 cm^{-1} can not be excluded. It can be assumed that the asymmetric and symmetric oscillations of two CO molecules coordinated to a single Co atom would result in a high and low frequency band. One should anticipate that an increasing population of Co with CO would lead to an increased competition for the metal *d*-electrons available for back-donating, hence a higher frequency than < 2000 cm^{-1} is to be expected when considering multiple CO adsorption. Ferreira et al. /74/ ascribed a band at 2070 cm^{-1} to structures in which two, three or four CO ligands were chemisorbed on single sites. In the study of Li et al. /186/ two bands were observed at 2027 and 2002 cm^{-1}, which were attributed to a M-$(CO)_2$ structure. Thus, the observed frequencies of 1996 and 1952 cm^{-1} are probably too low to justify an assignment to dicarbonyl species. Of further interest is the frequency separation between the two bands, which is 44 cm^{-1}. According to Li et al. /186/, the frequency separation between two butterfly CO molecules is approximately 23-27 cm^{-1}, which is lower than the one found in the present study. It should also be noted that with the expected orientation of such a structure, the metal surface selection rule implies that only one vibration would be infrared active. Furthermore, by cross plotting the intensity of the 1996 and 1952 cm^{-1} bands, they would be expected to lie on a straight line if they were attributable to a dicarbonyl structure. Fig. 5.2.4.2-5 shows the intensity of the 1996 cm^{-1} band plotted versus the 1952 cm^{-1} band intensity. Hence, based on the above argumentation, it is doubtful whether the pair of bands at 1996 and 1952 cm^{-1}

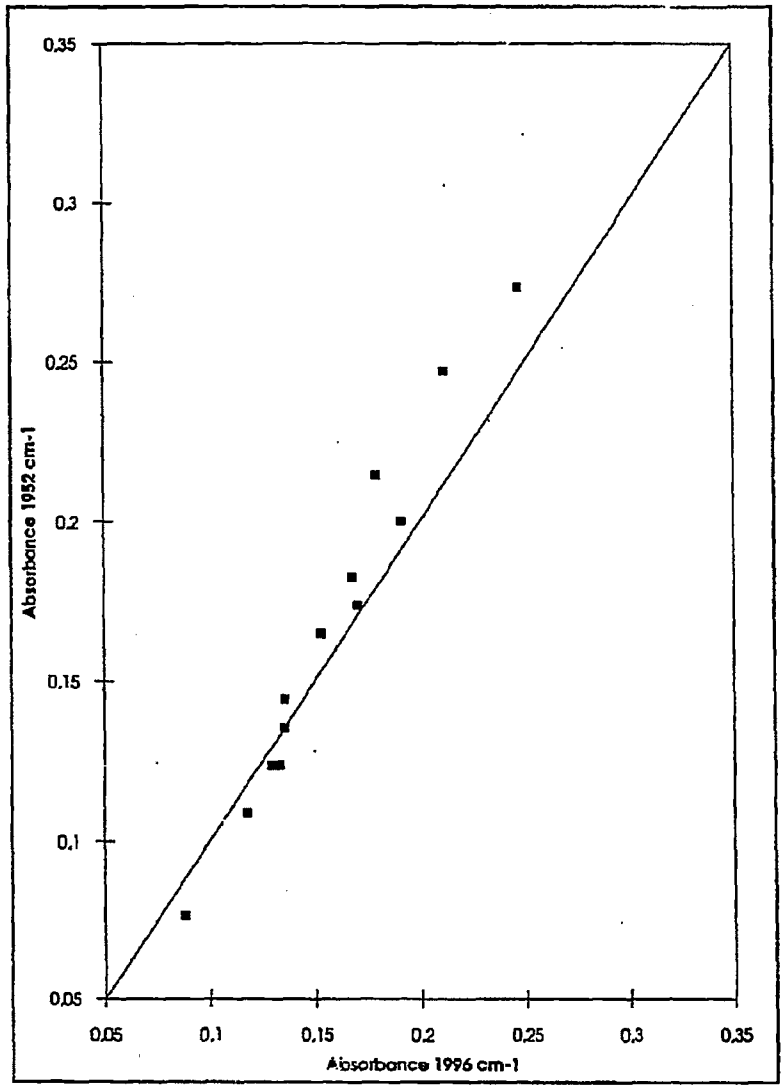

Fig. 5.2.4.2-5: **Crossplot of the intensities (as peak heights) of the 1996 and 1952 cm^{-1} bands recorded at different times during CO hydrogenation over 4.6% $Co/\gamma\text{-}Al_2O_3$.**

CO hydrogenation conditions:
P_{Tot}= 6 bar, H_2/CO = 2, T = 473K

belong to a butterfly structure. It has been found for supported Rh catalysts that the linear CO band frequency was in an intermediate position between the bands arising from the asymmetric and symmetric stretching vibrations of the butterfly molecules /187/, while twin CO adsorption on Ru catalysts gave bands whose frequencies were located above that of the linear CO absorption band.

The band frequencies in the present study compare well with those of a previous report; Zaitsev et al. /85/ reported bands at 1990 cm^{-1} and 1950 cm^{-1} on 1.5% Co/Al_2O_3. The behaviour of these bands during evacuation at 300K resembled that observed here during He-flushing, i.e. the disappearance of the bands upon removal of CO from the feed. However, no specific assignments were given other than that they were due to CO adsorbed on Co^0 /85/.

The above suggestions concerning the pair of bands at 1996 and 1952 cm^{-1} are put forward more as a scenario and/or examples than finite, specific assignments for the origin of the bands and their adsorption sites.

As mentioned earlier, the intensity of the pair of bands increased with time in H_2/CO, passed through a maximum and then declined. If the decrease in the intensity of the 1996 and 1952 cm^{-1} bands was due to a displacement of bridgebonded CO by CO adsorbed in a linear form, due to reconstructions, f.ex. the breaking up of islands, one would possibly expect to observe an increase in the intensity of the terminal CO band, which, however, remained rather constant with time in synthesis gas.

The time dependent behaviour of the pair of bands in synthesis gas at 473K could possibly be explained by the formation of infrared inactive species or the effect of surface hydroxyl groups.

The disappearance of the two bands with time in H_2/CO may indicate that the adsorption sites are covered with carbon or carbonaceous deposits. This would be expected to reduce the probability of bridgebonding, requiring two adjacent sites. The disappearance of the bands at a constant frequency may suggest the lack of interaction between the CO adsorption site and the carbonaceous deposits. CO would be adsorbed on the remaining sites, with decreasing intensity of the bands reflecting the progress of the deposition process. This could possibly imply that the deposition of carbon proceeds via island formation, suppressing CO adsorption.

Hydroxyl groups on the surface may act as potential oxidizing agents. Water can also be formed by hydrocondensation of hydroxyl groups from the alumina support. Diminishing intensity of the absorption bands at 1996 and 1952 cm^{-1} may be ascribed to oxidation of cobalt, thereby decreasing the surface coverage of adsorbed CO.

Even though a quantitative estimation of the amount of surface hydroxyl groups present during treatment with synthesis gas has not been performed, the spectra indicate an increase in the intensity of the absorption bands in the 3800-3400 cm^{-1} region. During the initial period of reaction (< 10 min.), the hydroxyl band intensity was relatively low, whereafter a gradual increase in the band intensities could be observed, paralleling the decrease in the intensity of the 1996/1952 cm^{-1} bands. If hydroxyl groups or water, formed in the Fischer-Tropsch reaction, have an oxidizing effect on the cobalt, one would anticipate that also the linear CO band would be influenced. A band could be observed at 2135/2165 cm^{-1} in the difference spectra, but it is not believed that this band represents CO adsorbed on Co^{2+}, but rather is a result of the subtraction procedure.

The observed differences in the linear CO band intensity and position during CO hydrogenation over the silica and alumina supported cobalt catalysts are evident by looking at Fig. 5.2.4.2-6. Characteristicly, both the frequency and intensity of the linear CO band on the alumina supported catalyst is lower than on the SiO_2 supported cobalt catalyst. At 473K, for example, the band ascribed to "on-top" adsorbed CO shifted 10 cm^{-1} to lower wavenumber. One can argue, that in view of the applied resolution (4 cm^{-1}) the downscale shift is of minor importance, but it does suggest that stronger metal-carbon bonds exist for the alumina supported sample. This could perhaps imply that the cobalt metal *d*-electrons participate to a greater extent in bonding of carbon monoxide when alumina is the support. Thus, one may suggest that alumina assist the metal in donation of electrons for bond formation. Eischens et al. /80/ reported similar characteristic features in the spectra upon CO adsorption on silica (Cabosil) and alumina (Alon C) supported platinum catalysts. Two bands (at 2040 and 1810 cm^{-1}) were observed over the alumina supported catalyst, while only a single band (at 2070 cm^{-1}) was observed on the silica supported catalyst. The differences were explained by the different electron donor properties of the supporting materials. The increased donation of electrons with the alumina support will result in an increase in the carbon-metal bonding strength due to electrons entering the π-antibonding orbital. The carbon-oxygen bond

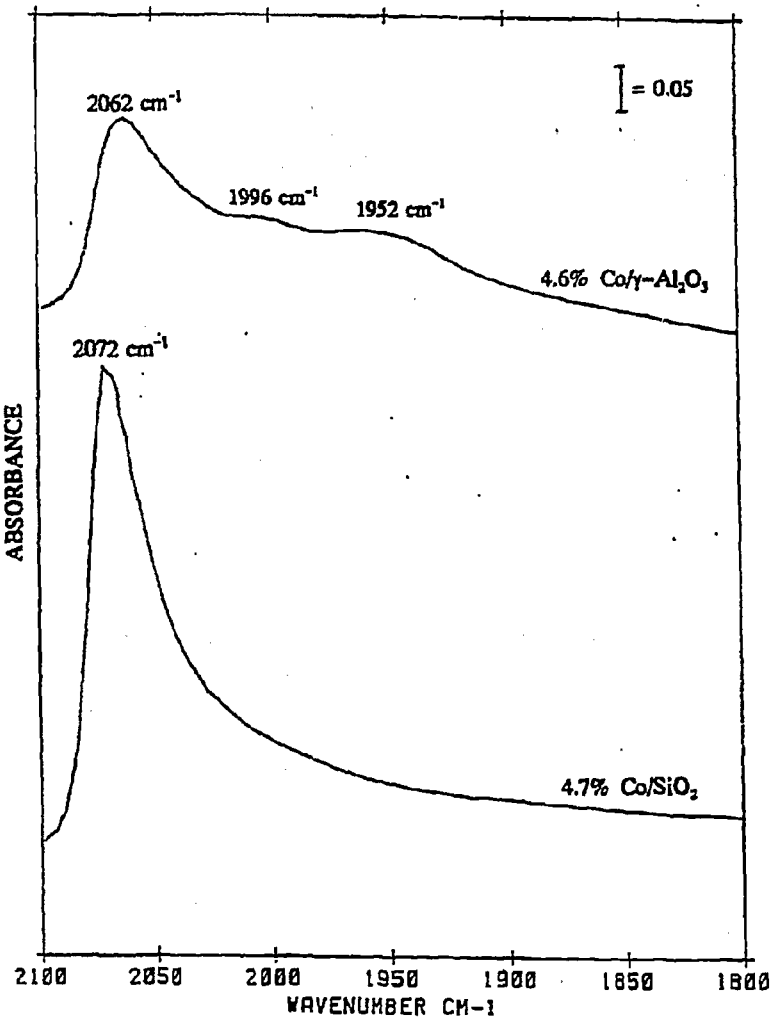

Fig. 5.2.4.2-6: **Infrared spectra obtained during CO hydrogenation over 4.6% $Co/\gamma\text{-}Al_2O_3$ and 4.7% Co/SiO_2.**

CO hydrogenation conditions:
P_{Tot}= 6 bar, H_2/CO = 2, T = 473K

Spectrum of 4.7% Co/SiO_2 was recorded after 120 min. in H_2/CO, that of 4.6% $Co/\gamma\text{-}Al_2O_3$ after 90 min. of reaction.

is weakened, and a shift to lower wavenumbers would be expected. On the other hand, γ-Al_2O_3 is amphoteric by nature, containing both acidic and basic sites. It is possible that acid sites (Lewis sites), which are electron deficient, may tend to coordinate the metal *d*-electrons, thus preventing the formation of π-bonding between the metal and carbon monoxide. For silica, Lewis acid/base sites are absent unless it has been activated at very high temperatures (>1000 K), and Brönsted acidity is low or non-existent. Stoop et al. /188/ stated that the difference in the spectra (between Pt/SiO_2 and Pt/Al_2O_3) could be due to the influence of the support on the crystal surface structure. Rao et al. /72/ reported that the vibrational frequency of CO on Co/MgO was 10 cm^{-1} lower than CO on Co/SiO_2. It was suggested that this could be due to metal-support interactions (donation of electrons from MgO) or different exposed metal faces.

It is understood, that a definitive explanation can not yet be given for the observed differences in the frequency of the linear CO band on the silica and alumina supported cobalt catalyst. The spectral data are conclusive only in the sense that a downscale shift in the frequency of linearly adsorbed CO does occur when shifting from silica to alumina as the applied support.

The effect of temperature, total reaction pressure and H_2/CO ratio upon the intensity and frequency of the band corresponding to linearly adsorbed CO on alumina and silica supported catalysts with high metal loading can be summarized by the following points:

1. The CO pressure affected the intensity, but not the frequency at each temperature and H_2/CO ratio.
2. At a fixed CO pressure, the coverage of CO is strongly dependent upon the CO hydrogenation temperature.
3. The influence of the H_2/CO ratio was more ambiguous; at 473K a higher intensity but similar frequencies were observed, while at 573K the intensities were comparable but the frequency appeared to be slightly reduced (by 6 cm^{-1}).

A common feature of the spectra in Fig. 5.2.3.2-1 to 5.2.4.2-4 was a downscale shift in frequency and a decrease in the linear CO band intensity with increasing CO hydrogenation temperature. Several infrared studies of CO hydrogenation reports shifts to lower CO frequencies and decreased intensity with increasing reaction temperature /189-192/.

This effect can in principle be due to hydrogen influencing the C-O bond strength or to a temperature dependency of the CO coverage. Table 5.2.3.6-1 indicate a decrease in the amount of CO with higher temperature at otherwise constant reaction conditions. The reduced coverage of CO at higher temperatures could be explained by the temperature dependence of the equilibrium constant for CO adsorption. K_{CO} has been determined to 1.57, 0.35 and 0.29 at 473, 523 and 573K, respectively (4.7% Co/SiO_2, $H_2/CO=2$, $P_{Tot}=2.5$-11 bar). That is, K_{CO} decreases with increasing CO hydrogenation temperature.

Since H_2 adsorption on cobalt catalysts is an activated process /193/, increasing amounts of hydrogen could be expected with increasing temperature. One may suspect an interaction, i.e. electronically, between coadsorbed hydrogen and CO, resulting in a weakening and/or strengthening of the CO bond. The possibility of hydrogen and CO attached to the same adsorption site, for example in the configuration H-Co-CO should be considered. Assuming electron donor properties of hydrogen, electron transfer through the metal increase the extent of π-backbonding, hence weakening the CO bond. This could be thought of as hydrogen assisted disproportionation of adsorbed CO. On the other hand, if hydrogen acts as an electron acceptor, competition for *d*-electrons would be expected to shift the CO frequency to higher wavenumbers, which was not observed experimentally.

The changes in the characteristica of the linear CO band can also be explained in view of the previous mentioned dipole-dipole interactions. The CO frequency will probably be affected by the distance between the neighbouring CO molecules and thus the coverage. The frequency shift can possibly be ascribed to a reduction in the vibrational coupling as the surface coverage decreases due to, for example, thermal desorption or hydrogen decoupling the vibrational coupling. This would then be a geometrical effect not influencing the CO bond strength.

In an attempt to further investigate the reason for the dependence of the CO band intensity/frequency on the temperature, an experiment was performed in which a freshly reduced disk of 4.6% Co/γ-Al_2O_3 was exposed to H_2/CO at 473K for 30 min. The temperature was then raised (2K/min.) to 573K before subsequent cooling to 473K in synthesis gas. The experimental procedure included dwell periods of 30 min. at 523K and 573K.

With increasing temperature, a downscale shift in the position of the linear CO band and a reduction of the intensity could be observed. Neither the intensity nor the band frequency was

restored upon cooling to 473K, see Fig. 5.2.4.2-4. This was also the case for the pair of bands at 1996 and 1952 cm^{-1}. The disappearance of the doublet upon heating to 573K can not be due to thermal desorption alone, since the bands did not reappear after lowering the temperature in the syngas mixture.

The irreversible changes in the CO band intensity and position with temperature are most likely due to a decrease in the coverage of CO, which may have been caused by deposition of carbon or carbonaceous deposits. This is supported by the irreversible changes in the CO band frequency and intensity upon heating form 473K to 573K followed by recooling to 473K. The presence of such species may be expected to influence the CO adsorption by the donation of electrons, increasing the back-donation from the metal *d*-orbital to CO's π^*-antibonding orbital, hence a shift to lower frequencies would be expected. The accumulation of carbon on stepped Co(1012) faces /39,47/ as well as on supported Co-catalysts /49,70,77,105,194/ are well established. However, there is a significant difference between the results obtained in this study and of those referred to above. The previous studies revealed a frequency shift in the opposite direction, that is, the linear CO band was located at higher frequencies after a disk of 10% Co/SiO_2 had been heated to 518K in He/CO and then cooled to room temperature followed by readmittance of CO /77/. Higher frequencies and lower intensity were observed when 7.5% Co/SiO_2 was exposed to CO (P_{CO}=0.3 torr), evacuated at 573K and re-exposed to CO /70/. Choi et al. /49/ argued that the greater electronegativity of carbon (2.5) compared to 1.8 for cobalt would result in a withdrawal of electrons from Co towards carbon, weakening the binding strength of CO (weaker carbon-metal bonding), resulting in a shift to higher frequencies. It should be noted that these experiments were conducted in the absence of hydrogen. Contrary to these observations, Dalla Betta et al. /189/ reported decreasing coverage of CO at increasing temperature (downscale shift in frequency and reduced intensity) which was irreversible with respect to a lowering of the reaction temperature.

It is also noticed that the half height width of the linear CO band is larger at higher reaction temperatures, see Fig. 5.2.3.2-1, 5.2.3.3-1 and 5.2.3.4-1. This could indicate a certain disorder in the sense that CO islands of different sizes experience or are influenced by different environment. One can envisage a situation where the spectra obtained at higher reaction temperatures do not represent a "uniform" coverage of CO, but that some particles/clusters are covered with CO and some are partly covered with CO and partly with carbon. Then, the

degree of interaction between the CO molecules will depend on the size of the island and the density of the carbon patches, either neighbouring or in close proximity of the CO island. CO molecules in islands far apart, separated by carbon patches, will interact more weakly, and thus be expected to give absorption bands of lower frequency. Islands consisting of a number of CO molecules separated by i. e. the van der Waals diameter (3.5 Å for CO) would overlap orbitally and be less influenced. The broadening of the linear CO peak with increasing CO hydrogenation temperature is therefore interpreted in terms of CO island molecules positioned in and experiencing different surroundings with respect to the carbon entities. The lower absorbance at higher reaction temperature can possibly be explained with suppression of CO adsorption due to carbon poisoning of the cobalt sites.

Some reflections can be done about the process of carbon deposition. One may speculate that the formation of carbon species take place from the edges of the island, since CO molecules in these positions have a lower coordination number and higher heats of adsorption. Thus, dissociation of CO is facilitated on defect sites, kinks and steps. This would then mean that the linear CO band should loose intensity from the low frequency side. Based on the spectra in Fig. 5.2.4.2-4, it is difficult to judge whether this is the case or not, since the tailing of the linear CO peak becomes more pronounced with increasing temperature, possibly as a consequence of the diminishing of the 1996 and 1952 cm^{-1} doublet. As the carbon deposition proceeds, smaller and smaller islands of CO would be expected, surrounded by increasing carbon patching, both in size and number. Eventually, one may reach a point where the carbon entities not only has a geometrical dilution effect, but can be transformed into a less active (reactive) form, given sufficient time. This would seem plausible if the coverage of hydrogen is low and the removal of the carbon species is slow with respect to the rate of CO dissociation.

In principle, the decline in the intensity and downscale shift in frequency of the major CO band with increasing temperature could also possibly be considered to be due to oxidation of the cobalt metal, for example by water formed in the Fischer-Tropsch reaction. In the majority of the experiments, the GHSV was higher than 333000 Nml (H_2 + CO)/g catalyst·h, which would imply that the conversion in the infrared reactors is relatively low. This would mean that the partial pressure of water is low, and hence oxidation is believed to be of minor importance. No bands were observed in the 2200-2100 cm^{-1} region during reaction which could be assigned to CO on Co-ions.

5.2.5. Bands observed in the 3050-2800 cm^{-1} spectral range over silica alone and silica supported Co catalysts (0.82 and 4.7% Co/SiO_2) at different reaction conditions

Infrared spectra obtained in the 3050-2800 cm^{-1} (C-H) range during CO hydrogenation over 0.82% Co/SiO_2 are shown in Fig. 5.2.5-1. It should be noted that the noise level in most cases was equal or slightly smaller than the absorbance associated with adsorbed species. This imposes severe difficulties in distinguishing between baseline noise and "true" peaks. However, absorption bands are apparently present at 3017, 2961, 2949 and 2860 cm^{-1}, all of which show some evidence of increasing intensity with time in H_2/CO.

A sequence of spectra recorded during the course of the H_2/CO reaction over 4.7% Co/SiO_2 are presented in Fig. 5.2.5-2. After 2 minutes of reaction only a noisy baseline is observed due to the relatively poor transmission in this frequency region. After 20 minutes, weak absorption bands located near 2934 cm^{-1} and 2960 cm^{-1} are detectable. Further exposure to synthesis gas results in the additional appearance of a band near 2860 cm^{-1}. The intensity of the peaks increase steadily with time during CO hydrogenation and after 130 minutes the major features in the spectra consists of the three bands located at 2965, 2934 and 2860 cm^{-1}. During this time period, both the intensity and the frequency of the linear CO band remained invariable.

The preferred assignment for the observed bands in the C-H stretching region during CO hydrogenation over the silica supported catalysts with different metal loading is as follows: The band at 2965 cm^{-1} is assigned to the asymmetric stretch of a terminal CH_3-group, while the 2934 cm^{-1} band is attributed to the asymmetric stretching vibration of saturated CH_2-groups. The symmetric stretches of CH_2- and CH_3-groups have been reported to 2850 and 2870 cm^{-1}, respectively /91/. Thus, the intermediate position of the 2860 cm^{-1} band makes it difficult to exclude one assignment at the expense of the other. Usually, however, bands observed in the vicinity of 2860 cm^{-1} are reported to be due to the symmetric stretch of CH_2-groups /78,91,108/. The corresponding weak CH_2/CH_3 deformation bands are expected around 1450 cm^{-1}. Bands in the 1800-1200 cm^{-1} range will be discussed in section 5.2.8.

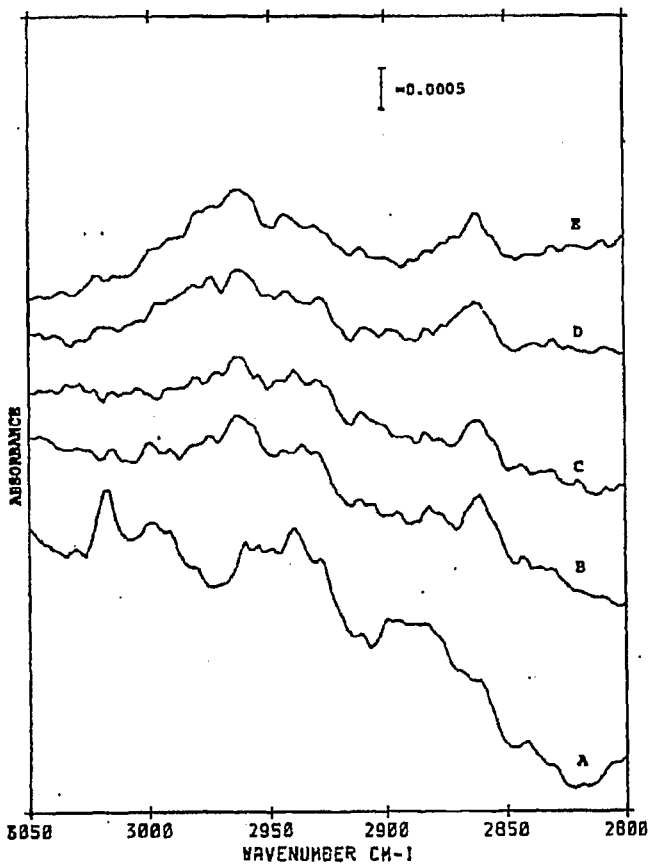

Fig. 5.2.5-1: **Infrared spectra of adsorbed species on 0.82% Co/SiO_2 obtained during CO hydrogenation and subsequent flushing with inert gas.**

Spectrum A was recorded after 26 min. in H_2/CO.
Spectra B-E were recorded at various times in He following CO hydrogenation:

B: **3 min.**
C: **22 min.**
D: **38 min.**
E: **55 min.**

CO hydrogenation conditions:
P_{Tot} = 6 bar, H_2/CO = 2, T = 473K

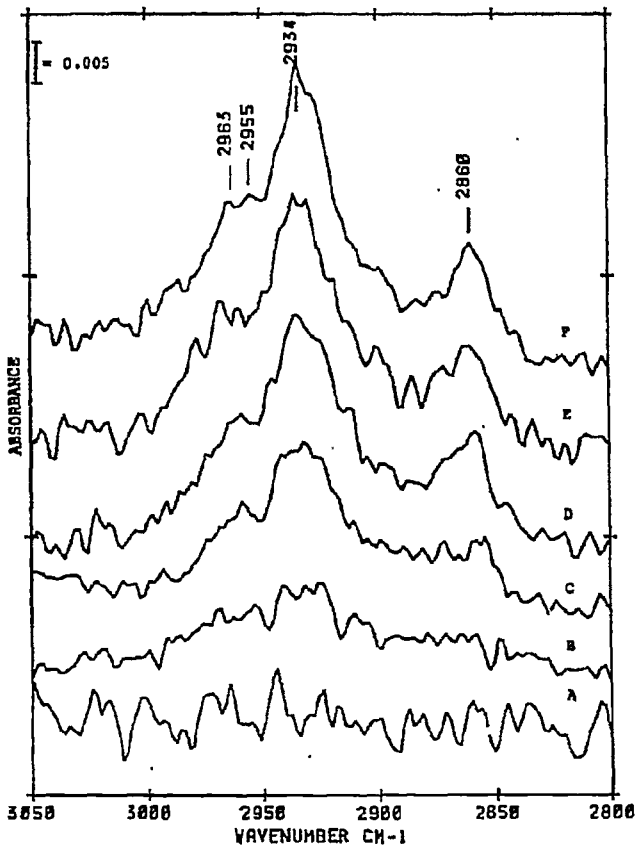

Fig. 5.2.5-2: **Infrared spectra of adsorbed species on 4.7% Co/SiO_2 as a function of time in synthesis gas.**

Spectra were obtained after:

A: **2 min.**
B: **20 min.**
C: **60 min.**
D: **90 min.**
E: **110 min.**
F: **130 min.**

The indicated times represent initiation of the IR-scans.

CO hydrogenation conditions:
P_{Tot} = 6 bar, H_2/CO = 2, T = 473K

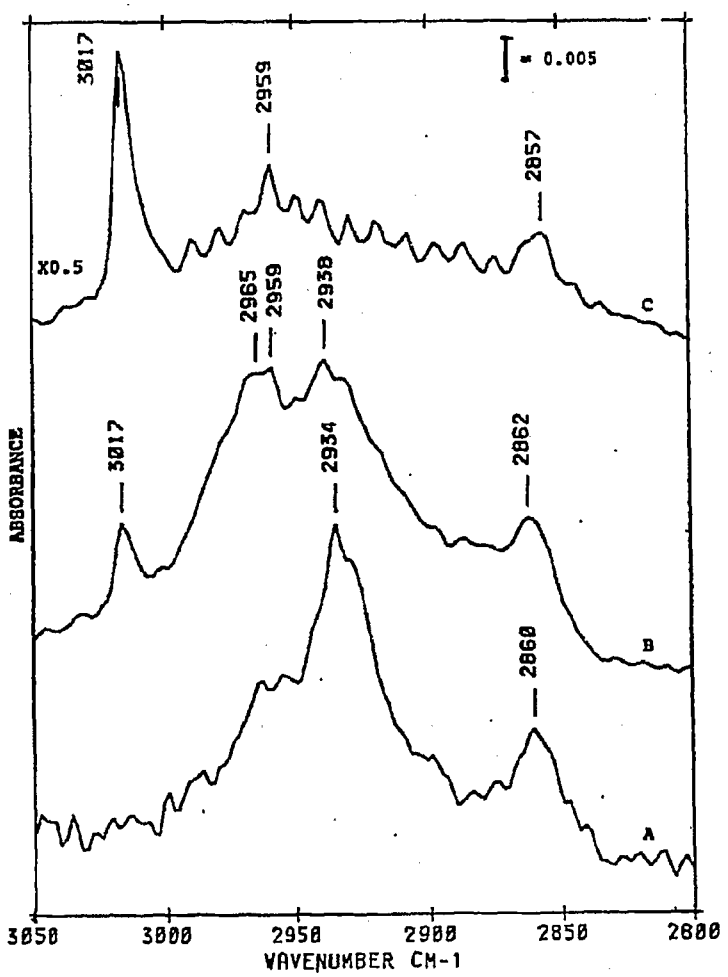

Fig. 5.2.5-3: Effect of reaction temperature on the intensities of bands in the 3050-2800 cm^{-1} region during CO hydrogenation over 4.7% Co/SiO_2.

A: after 130 min. in synthesis gas at 473K
B: after 120 min. in synthesis gas at 523K
C: after 130 min. in synthesis gas at 573K

CO hydrogenation conditions:
P_{Tot} = 6 bar, H_2/CO = 2, 100 Nml/min. unless otherwise stated

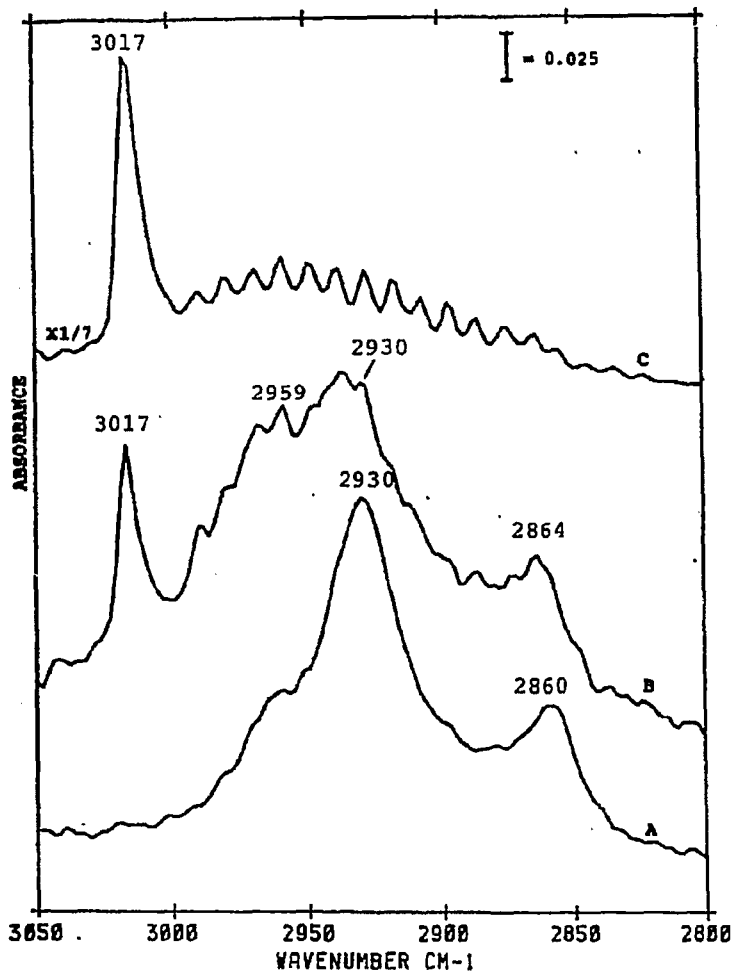

Fig. 5.2.5-4: **Infrared bands in the 3050-2800 cm^{-1} range during CO hydrogenation over 4.7% Co/SiO_2 at different reaction temperatures.**

A: **after 130 min. in H_2/CO at 473K**
B: **after 120 min. in H_2/CO at 523K (50 Nml/min.)**
C: **after 120 min. in H_2/CO at 573K (30 Nml/min.)**

CO hydrogenation conditions:
P_{Tot} = 11 bar, H_2/CO = 2, 100 Nml/min. unless otherwise stated

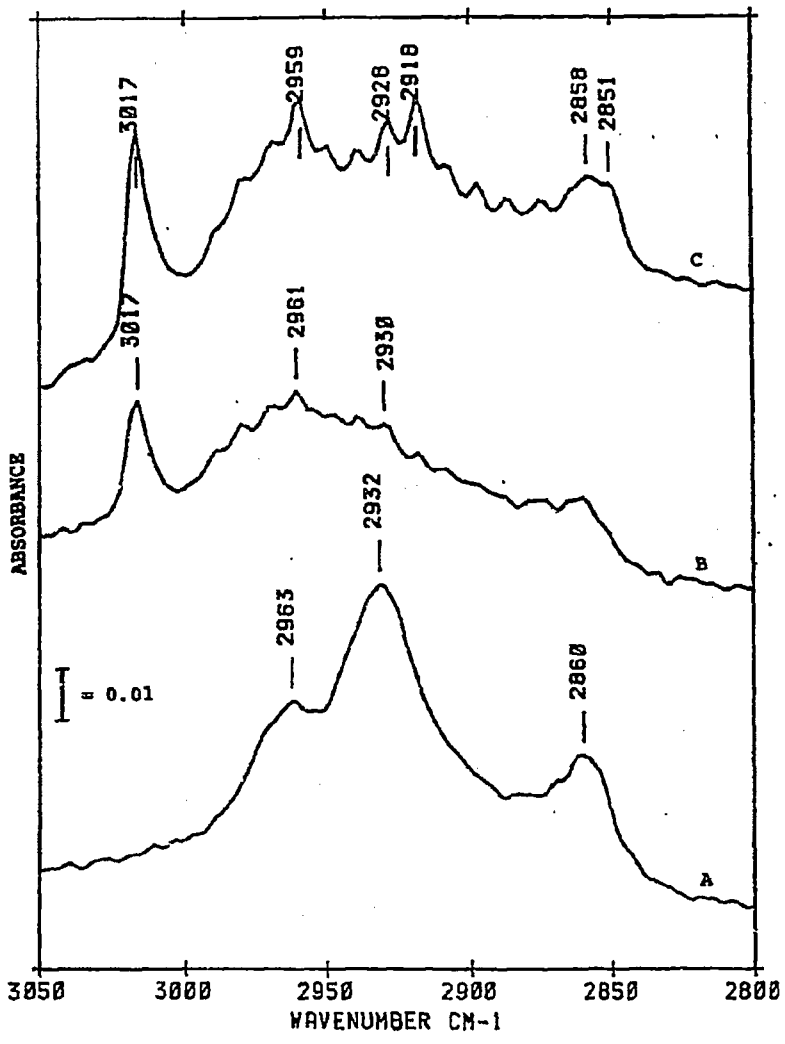

Fig. 5.2.5-5: Infrared spectra of adsorbed species in the 3050-2800 cm^{-1} region during CO hydrogenation over 4.7% Co/SiO_2 at various temperatures.

A: after 120 min. in H_2/CO at 473K (100 Nml/min.)
B: after 90 min. in H_2/CO at 523K (50 Nml/min.)
C: after 120 min. in H_2/CO at 573K (200 Nml/min.)

CO hydrogenation conditions:
P_{Tot} = 6 bar, H_2/CO = 3

The behaviour of the species in the frequency range 3050-2800 cm^{-1} was investigated at different temperatures, pressures and H_2/CO ratios. In addition, the effect of varying flow rate was also briefly examined.

The spectra shown in Fig. 5.2.5-3, 5.2.5-4 and 5.2.5-5 at different CO hydrogenation conditions exhibited basically the same groups of absorption bands, although the intensities and frequencies varied slightly from one experiment to another, but within the limits of experimental accuracy.

Three characteristic features can be noted when studying Fig. 5.2.5-3 to 5.2.5-5, all being dependent on the CO hydrogenation temperature.

The intensity of the C-H stretching bands increased with increasing reaction temperature, see Fig. 5.2.5-3. Kellner /195/ stated that such behaviour could be explained by a more rapid rate of accumulation of species at higher temperatures.

Next, the band previously assigned to asymmetric CH_3 stretches becomes more prominent with higher CO hydrogenation temperatures. This indicate a higher fraction of shorter chained hydrocarbons with increasing temperature. This is in agreement with what is known about the temperature dependency of α (the chain growth probability), i.e. decreasing value of α with increasing temperature /6/. Dry /26/ stated that increasing operating temperature shifted the product selectivity to lighter molecular mass compounds.

In the spectra given in Fig. 5.2.5-3, 5.2.5-4 and 5.2.5-5, a distinct band appear near 3017 cm^{-1} at elevated temperatures (> 523K), regardless of the H_2/CO ratio and partial pressure of carbon monoxide. The existence of bands in this range is generally expected for olefinic CH-stretching. However, the 3017 cm^{-1} band in the present study is assigned to gas phase CH_4, an interpretation which was confirmed by varying the flowrate (of H_2/CO) and/or flushing with He. Especially at 573K, see Fig. 5.2.5-3 and 5.2.5-4, the gas phase methane band was accompanied by the R and P branches, having fine rotational bands. The presence of the P branch precludes to a certain extent the observation of bands in the 3000-2800 cm^{-1} range. The enhanced selectivity to methane with increasing CO hydrogenation temperature is in agreement with the higher activation energy for methane formation compared to that of hydrocarbon formation /196/.

An anticipated effect of increasing H_2/CO ratio (2→3) would be a decline in the production of higher molecular weight species and increased methane formation, corresponding to a

decline in α with increasing H_2/CO ratio. By comparison of the C-H band intensities, the spectra indicate a lower fraction of CH_2 groups with a H_2/CO ratio of 3. Also, it seems that the intensity of the C-H stretching bands at 473K is higher with $H_2/CO=3$ than with a ratio of two.

The effect of varying the total reaction pressure while keeping the temperature fixed (at 473K) can clearly be seen in Fig. 5.2.5-6. The intensity of all the C-H stretching bands increased with increasing pressure. Note also that the dominating bands are those ascribed to CH_2-groups, with the C-H stretch in CH_3-groups appearing as a shoulder on the 2930-2934 cm^{-1} band. Increasing total reaction pressure leads to an increase in the CH_2 and CH_3 bands, but the CH_3 peak becomes less resolved at higher total pressure. One may therefore conclude that higher hydrocarbons are being formed with higher total reaction pressure. Longer hydrocarbon chains would mean that the surface is covered with more carbon containing entities relative to adsorbed hydrogen. Thus, the probability of chain growth will most likely be higher, and it can be speculated whether the CO island formation favour the production of long chained hydrocarbon species.

The ratio between the intensity of the asymmetric CH_2 and CH_3 peak has been used as an estimate of the average chain length of the adsorbed hydrocarbon structures, provided no branching occurs in the hydrocarbon molecule.

If long chained hydrocarbons are responsible for the observed C-H stretching bands, the CH_2/CH_3 ratio would be expected to be higher than unity. That this indeed is the case can be seen from Table 5.2.5-1. Also the temperature dependence of the CH_2/CH_3 ratio is further noticed, suggesting that the concentration of methyl groups becomes increasingly higher with increasing reaction temperature.

The lower CH_2/CH_3 ratio with $H_2/CO=3$ and generally at higher reaction temperature indicate shorter chain lengths of the hydrocarbon structures at these conditions.

The reactivity of the adsorbed hydrocarbon species towards hydrogen is consistent with the observed CH_2/CH_3 ratios.

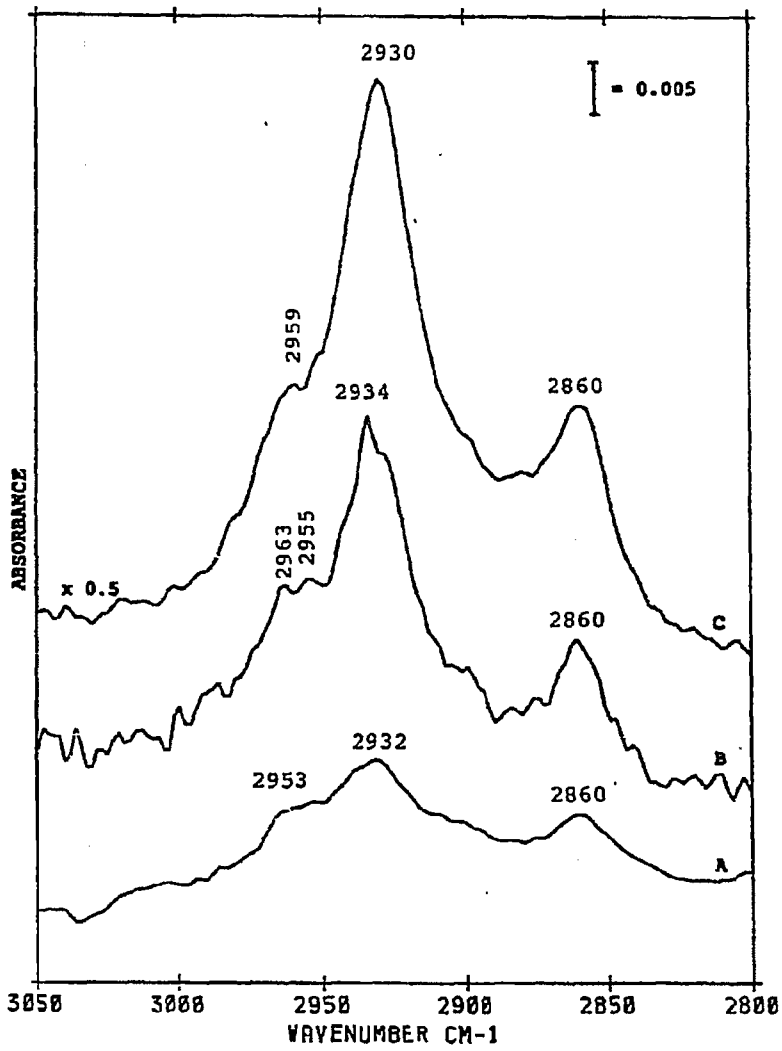

Fig. 5.2.5-6: Effect of the total pressure on the intensity of the infrared bands observed in the 3050-2800 cm^{-1} region over 4.7% Co/SiO_2.

A: P_{Tot}=2.5 bar
B: P_{Tot}=6 bar
C: P_{Tot}=11 bar

CO hydrogenation conditions:
H_2/CO = 2, T = 473K

Table 5.2.5-1: **Intensity ratio of the asymmetric CH_2/CH_3 bands over 4.7% Co/SiO_2 at different CO hydrogenation conditions.**

Temperaiure (K)	*Pressure (bar)*	*H_2/CO-ratio*	*CH_2/CH_3-ratio*	*Asymmetric C-H stretching bands (cm^{-1})*
473	6	2	>1	2934/2965
523			>1	2938/2959
573			--^	------
473	6	3	>1	2930/2961
523			>1	2932/2961
573			<1	2918/2939
473	11	2	>1	2928/2968
523			>1	2938/2959
573			<1	2928/2959
473	2.5	2	>1	2932/2963

^ : Estimation of the CH_2/CH_3 ratio at these reaction conditions was not possible due to the poorly resolved asymmetric CH_2 peak.

The CH_2/CH_3 ratios in Table 5.2.5-1 is based upon the use of peak heights as a measure for the absorbance of the C-H stretching bands. It is of interest to get a more specific quantification of the amount of adsorbed hydrocarbon structures, in order to validate the CH_2/CH_3 ratios in Table 5.2.5-1, but also with respect to the gravimetric studies in Chapter 5.4. One can roughly estimate the respective amounts of adsorbed CH_2 and CH_3 by using the data from Wexler /197/. Wexler reports the structural unit intensities for methyl and methylene stretching bands to 4460 and 3740 $cm^{-2}\cdot dm^3\cdot mol^{-1}$, respectively. Since

$$B_{CH_n} = \int_{\gamma_1}^{\gamma_2} \varepsilon_\gamma \cdot d\gamma \qquad 5.9$$

and

$$\varepsilon_\gamma = \frac{I}{b \cdot c} \cdot \log_{10}\left(\frac{I_0}{I}\right) \qquad 5.10$$

the experimental integrated intensity is given by:

$$S_{CH_x} = \int_{\gamma_1}^{\gamma_2} \log_{10}\left(\frac{I_0}{I}\right) d\gamma = B_{CH_x} \cdot C_{CH_x} \cdot L \qquad 5.11$$

S_{CHx} = area under C-H stretching bands belonging to CH_2- and CH_3- structures (cm^{-1})

C_{CHx} = concentration ($mol \cdot dm^{-3}$)

L = pathlength (cm)

B_{CHx} = structural unit intensity for methyl or methylene ($cm^{-2} \cdot dm^3 \cdot mol^{-1}$)

Replacing $C_{CHx} \cdot L$ with $(n_{CHx} \cdot m_{cat})/A_C$ in the same manner as previously described on page 132-133, gives the following expression for the amount of methyl and/or methylene residing on the catalyst surface at reaction conditions:

$$n_{CH_x} = \frac{S_{CH_x} \cdot A_C \cdot 10^{-3}}{B_{CH_x} \cdot m_{cat}} \qquad 5.12$$

Details of the calculations and assumptions employed are shown in Appendix A8. The above equation 5.12 and equation 5.7 on page 133 are both based on the integrated intensity of the actual absorption bands.

Applying the equation above (5.12) makes it possible to obtain a quantitative estimate of the respective amounts of $>CH_2$ (a) and $-CH_3$(a).

Table 5.2.5-2 gives a summary of selected results obtained for the 4.7% Co/SiO_2 catalyst at the reaction conditions: H_2/CO=2, P_{Tot}=6 bar and 100 Nml/min. of H_2/CO. The experiment carried out at 573K over 4.7% Co/SiO_2 is not included in Table 5.2.5-2 due to the poorly resolved CH_2-stretching band. Neither are the calculations done for the 4.6% Co/γ-Al_2O_3 catalyst. This was because of the suspected influence of contributions from vibrations related

to the adsorbed surface structures like for example formates. Also, the intensity of the asymmetric CH-stretch in CH_3-groups is hardly discernable from baseline noise. Table 5.2.5-2 nevertheless confirm the previous observation that higher fractions of hydrocarbons with shorter chain length appears at higher temperatures.

Table 5.2.5-2: Estimated amounts of CH_2 and CH_3 species residing on the surface of 4.7% Co/SiO_2 during CO hydrogenation.

Temperature (K)	*$>CH_2$(a) (cm^3)*	*$-CH_3$(a) (cm^3)*	*Chain length (CH_2/CH_3)*
473	0.00109	0.00014	~8
523	0.00066	0.00042	~2

5.2.6. Bands observed in the 3050-2800 cm^{-1} spectral region over 4.6% Co/γ-Al_2O_3 and pure alumina during CO hydrogenation

The hydrogenation of CO over 1% Co/γ-Al_2O_3 was also studied by infrared spectroscopy, but spectra in the C-H region of this catalyst are not shown here due to serious problems with back-diffusion of oil from the vacuum pump at the time these experiments were performed. Oil accumulated on the mirrors located before and after the sample chambers, thus obscuring observations of C-H stretching bands formed due to the Fischer-Tropsch reaction. Procedures carried out in order to check and ensure that the bands presented in this section really were due to reaction species adsorbed on the catalyst disks, have already been given in section 4.3.5 on page 77.

Fig. 5.2.6-1 shows infrared spectra obtained during CO hydrogenation over 4.6% Co/γ-Al_2O_3 at 473 and 523K with a H_2/CO ratio of 2. In contrast to the observations in Fig. 5.2.5-3 to 5.2.5-5, only a broad band with peak maxima near 2926-2914 cm^{-1} and a low frequency shoulder around 2857 cm^{-1} can be seen when CO hydrogenation is carried out at 473K.
A steady increase in the intensity of the bands with time in synthesis gas was observed. Decreasing the flowrate of synthesis gas (at 473K) resulted in an increasing band intensity, in accordance with the behaviour of the C-H-stretching bands on the silica supported cobalt catalyst.

CO hydrogenation at 523K resulted in a band peaking at 2924 cm^{-1} accompanied by a low frequency shoulder located at approximately 2860 cm^{-1}. Due to the severe shift in the baseline of the experiment carried out at 523K, it is not possible to draw any definitive conclusions regarding the effect of the temperature upon the development of the bands observed over the alumina supported cobalt catalysts in the investigated temperature range, 473-523K.

Nevertheless, by comparing the bands appearing in Fig. 5.2.6-1 with the C-H stretching bands observed in Fig. 5.2.5-3 to 5.2.5-6, three observations are evident:

1. The downscale shift in position of the main absorption band (2926-2914 cm^{-1})
2. The lack of resolved bands due to asymmetric CH_3 (generally near 2960 cm^{-1})

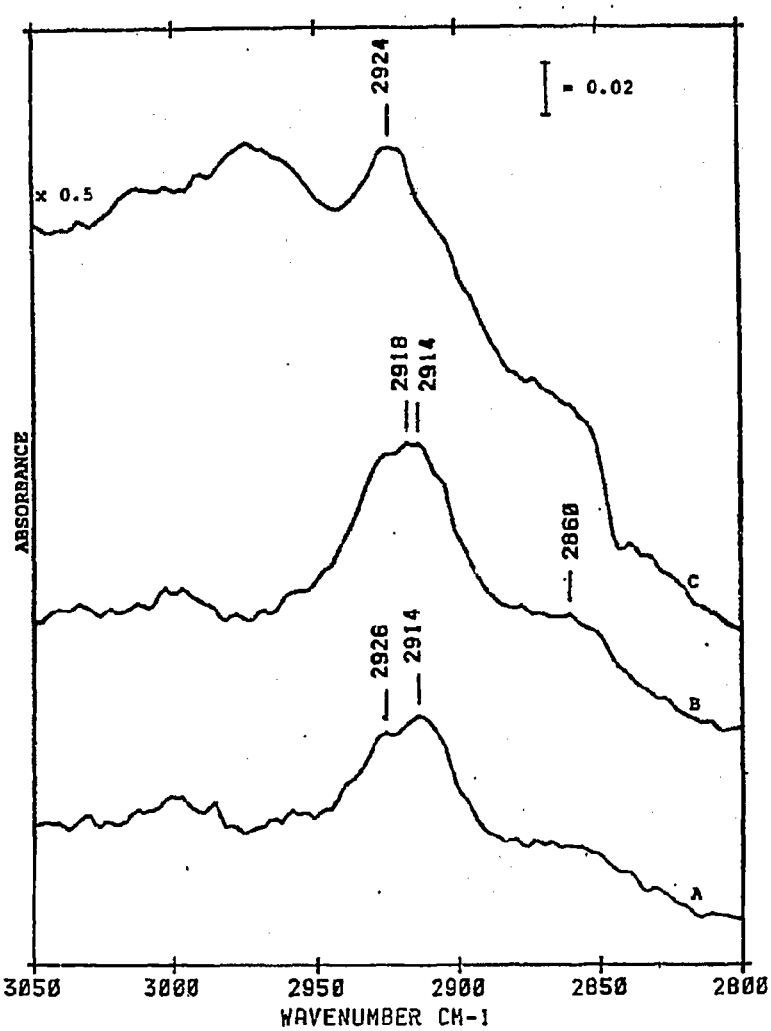

Fig. 5.2.6-1: Infrared absorption bands in the C-H stretching region during CO hydrogenation over 4.6% Co/γ-Al_2O_3 at different reaction conditions.

A: after 50 min. in H_2/CO at 473K
B: after 90 min. in H_2/CO at 473K (33 Nml/min.)
C: after 70 min. in H_2/CO at 523K

CO hydrogenation conditions:
P_{Tot} = 6 bar, H_2/CO = 2, 100 Nml/min. unless otherwise stated

3. The inherent weak absorbance of the ~2860 cm^{-1} peak relative to the major absorption band (2926-2914 cm^{-1}), which may be a baseline problem

These observations point towards the fact that the C-H stretching region on the γ-Al_2O_3 supported cobalt catalysts possibly contains C-H stretching vibrations in other structures than just adsorbed hydrocarbons.

Spectra in the 1800-1200 cm^{-1} range of alumina alone and the 4.6% Co/γ-Al_2O_3 catalyst are dominated by intense absorption bands attributable to formate and carbonate species, see section 5.2.8.

The C-H stretching band of formic acid adsorbed on alumina has been reported to appear at 2915 cm^{-1} /198/. This may explain why the main C-H stretching band on the alumina supported cobalt catalysts is centered around 2926-2914 cm^{-1}. Consequently, it can be assumed that the C-H stretching in formate groups as well as in hydrocarbon species contributes to the observed bands in the 3050-2800 cm^{-1} region over 4.6% Co/γ-Al_2O_3 at 473 and 523K.

The absorption band caused by terminal CH_3 groups is weak or at least poorly resolved on 4.6% Co/γ-Al_2O_3. This could mean that the fraction of CH_3 groups is low, implying the formation of longer chained hydrocarbons on the alumina supported catalyst compared to on 4.7% Co/SiO_2. In this respect, the infrared results tend to support the conclusions drawn from the microreactor experiments (Chapter 5.3). However, the shift in the baseline (at 523K) put some restrictions in drawing such a conclusion.

5.2.7. Discussion of the behaviour and nature of the absorption bands observed in the frequency range 3050-2800 cm^{-1}

Experiments were performed in order to try to establish if the observed hydrocarbon structures are attached to cobalt or at least associated with reactions on Co.

The reaction of H_2 and CO over a disk of silica void of Co at 523K did not result in any resolved bands attributable to CH_2/CH_3-groups in the frequency range 3050-2800 cm^{-1}.

Weak bands were observed, however, in the temperature interval 473K to 573K when a silica disk was placed downstream of the cell containing pressed disks of the silica supported cobalt catalysts. The positions of the bands were similar to those observed in Fig. 5.2.5-3 to 5.2.5-5,

indicating that these absorption bands most likely are due to hydrocarbon species adsorbed on the silica support.

A slightly different situation arose when similar experiments were carried out using alumina. Passing a mixture of H_2 and CO over a blank γ-Al_2O_3 at 473K ("single cell" experiment) resulted in the formation of absorption bands resembling those in Fig. 5.2.6-1, but with the main absorption band shifted to a lower frequency of 2907 cm^{-1}, in addition to a weak band near 2957 cm^{-1}. The behaviour and intensity of these two bands were comparable to those observed on 4.6% Co/γ-Al_2O_3 in synthesis gas, although the half-height width of the major peak at 2907 cm^{-1} is less compared to the dominant band on 4.6% Co/γ-Al_2O_3. Furthermore, the two bands also appeared to be quite unaffected by flushing with He and subsequent treatment with hydrogen.

Placing an alumina disk downstream of the cell containing a cobalt catalyst disk produced bands similar to those described above for 4.6% Co/γ-Al_2O_3, in addition to a band appearing near 2849 cm^{-1}.

The band positions of the hydrocarbon structures on the alumina supported Co-catalysts are located at slightly higher frequencies than the corresponding bands on γ-Al_2O_3.

Thus, one could tentatively propose that the dominating absorption band on γ-Al_2O_3 is due to the C-H stretch in adsorbed formate species, possibly formed in a reaction between CO and the surface hydroxyl groups of the alumina support. This would also be valid for alumina alone placed downstream of the alumina supported cobalt catalyst and for 4.6% Co/γ-Al_2O_3. In the latter cases, however, the broadening of the major peak and appearance of additional absorption bands is believed to reflect the presence of hydrocarbon species.

Since the bands are present on pure alumina, one can thus probably associate these peaks with the support rather than the cobalt metal.

Adsorption on the support is indicated by the presence of hydrocarbon structures (C-H species) on disks of either silica or alumina alone placed downstream of the catalyst sample. The lack of a reasonable reaction capability with H_2 at CO hydrogenation conditions and the absence of any influence on the position and intensity of the principle CO band, suggest that these species are unlikely to be on the cobalt surface.

Some efforts were also made in an attempt to evaluate the significance of the observed

hydrocarbons, that is, whether they are to be regarded as reaction products or reaction intermediates in the Fischer-Tropsch synthesis.

The stability of the adsorbed species in the 3050-2800 cm^{-1} range were investigated by replacing synthesis gas with He and then H_2, or directly with H_2, at reaction conditions. Switching from H_2+CO to He resulted in a relatively rapid decline in the intensity of the bands on the silica supported cobalt catalysts, while subsequent treatment with hydrogen led to practically no alteration in the band absorbances, as shown by way of illustration in Fig. 5.2.7-1. The negligible influence of He and/or H_2 treatment on the absorption bands over alumina and the alumina supported cobalt catalyst can most probably be related to the stability of the formate species, further discussed in Chapter 5.2.8.

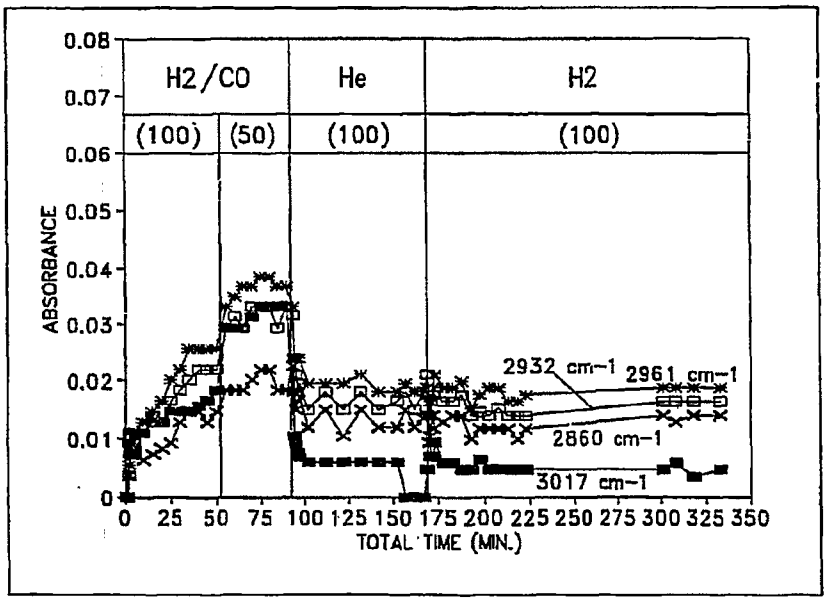

Fig. 5.2.7-1: Variation in the intensity of the CH-stretching bands during CO hydrogenation (P_{Tot}=6 bar, H_2/CO=3, T=523K), He- and H_2 treatment on 4.7% Co/SiO_2.
The applied flowrate is given in brackets.

The intensity of the bands were slowly attenuated in flowing hydrogen following cessation of synthesis gas. While the intensity of the linear CO band decreased in H_2 and shifted to

Fig. 5.2.7-2: **Infrared spectra of adsorbed species in the 3200-2700 cm^{-1} region obtained during CO hydrogenation over 4.7% Co/SiO_2 and subsequent treatment with hydrogen.**

A: **After 130 min. in synthesis gas.**

Spectra B-F were recorded after various times in hydrogen following CO hydrogenation:

B: **40 min.**
C: **90 min.**
D: **180 min.**
E: **360 min.**
F: **22.5 hr.**

CO hydrogenation conditions:
P_{Tot} = 6 bar, H_2/CO = 2, T = 473K, 100 Nml/min.

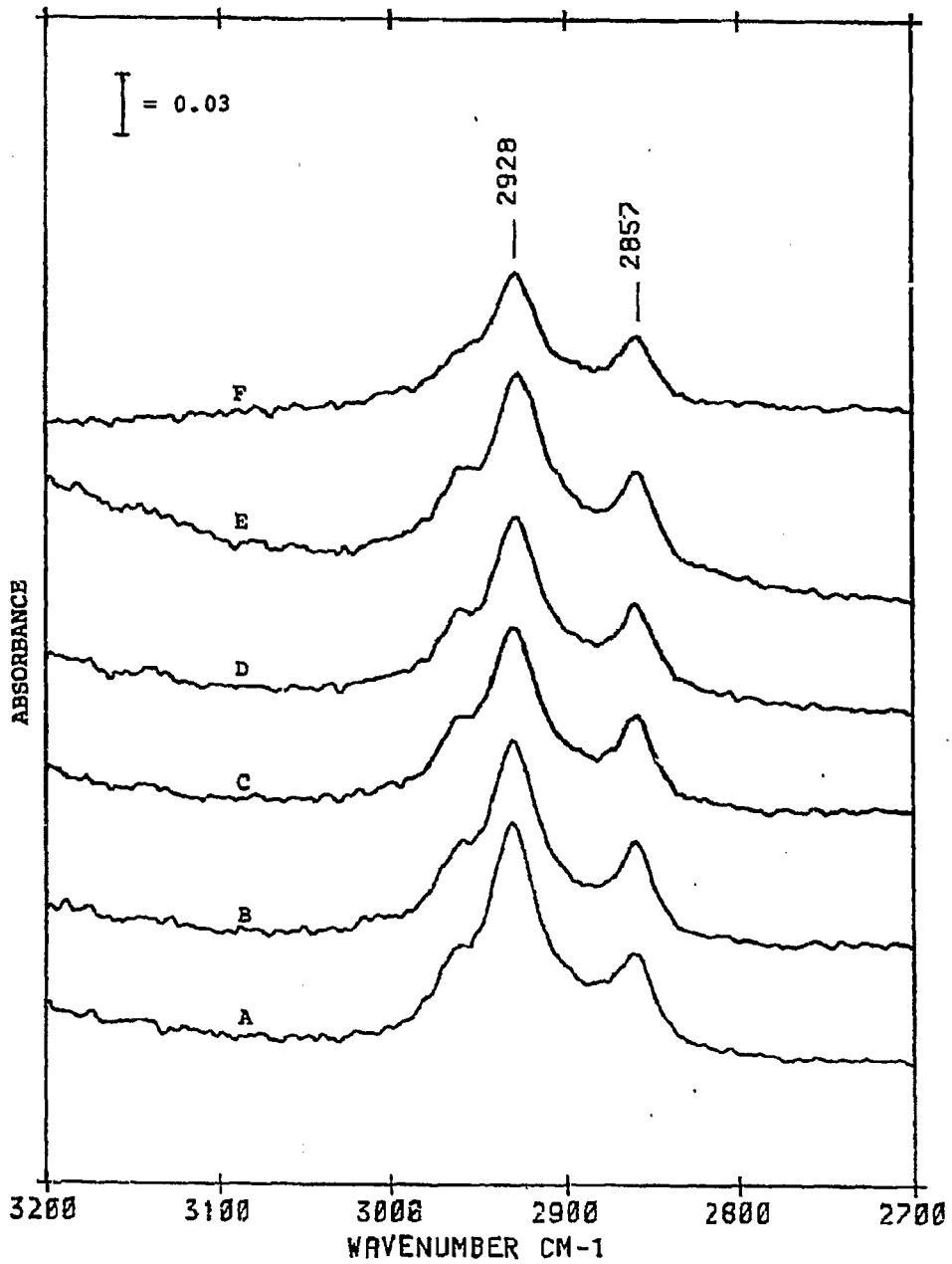
= 0.03
2928
2857
F
E
D
C
B
A
ABSORBANCE
3200
3100
3000
2900
2800
2700
WAVENUMBER CM-1

lower frequencies (possibly because of a decrease in the dipole-dipole interactions as a result of dilution by adsorbed hydrogen), the intensities of the hydrocarbon bands were little influenced by flowing hydrogen, as shown in Fig. 5.2.7-2. After several hours of hydrogen treatment absorption bands in the CH region could still be observed.

The development of the intensity for selected bands is shown in Fig. 5.2.7-1 and 5.2.7-3 during CO hydrogenation, purging with He and hydrogen treatment. The variation of the band intensity as a function of time suggests that these species do not represent active reaction intermediates in the Fischer-Tropsch synthesis, but rather reaction products. This is supported by the fact that the intensity of the infrared bands continue to grow beyond the point at which the rate of CO hydrogenation is expected to have reached a "pseudo" steady state /189/. The continuing growth of the hydrocarbon bands does not influence the position or the intensity of the principal CO absorption band. Furthermore, the rate of decay of band intensities in H_2 is less than expected from reaction intermediates. On iron, it has been shown /138/ that the time constant associated with the decay of the infrared band intensities is two orders of magnitude too low to agree with the observed turnover frequencies. Finally, the assumption of adsorbed spectator products is consistent with the behaviour of the bands in He, i.e. relatively rapid decline in intensity.

Inert surface hydrocarbons have also been reported during CO hydrogenation on alumina supported Ru catalysts /189,199/. Formation of the hydrocarbon species on the Ru metal followed by migration onto the alumina support was suggested as a possible reaction pathway.

Fig. 5.2.7-3 shows the effect upon the intensity (as peak heights) of C-H stretching bands when the flow of H_2/CO was varied during the course of a run. Increasing the flowrate resulted generally in decreasing intensity, and vica versa. Fig. 5.2.7-4 shows the corresponding spectra recorded in the three flow regimes of Fig. 5.2.7-3, 100, 200 and 50 Nml/min. The most intense absorption bands in Fig. 5.2.7-4 (due to $CH_{4(g)}$) are accompanied by P and R branches exhibiting rotational fine structures. The spectra in Fig. 5.2.7-4 and the intensity versus time curves in Fig. 5.2.7-3 serves to illustrate two main points.

One being that the variation in the intensity of the C-H stretching bands upon an increase or decrease in the flowrate of synthesis gas confirms the proposed explanation of the bands being caused by reaction products interacting with the catalyst surface.

Secondly, the rates of adsorption and desorption of reaction products will depend on the

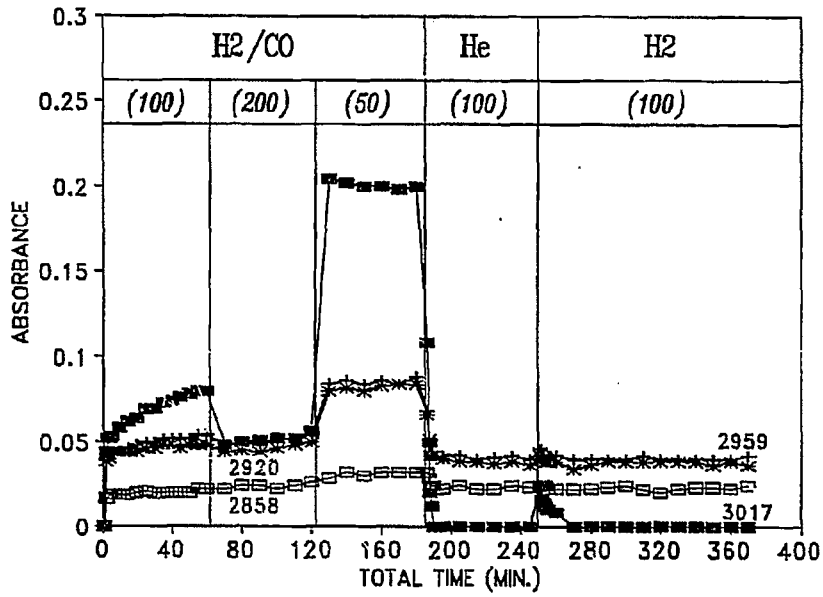

Fig. 5.2.7-3: Variations in the C-H stretching band intensities as a result of changing the flowrate (Nml/min.) during CO hydrogenation (P_{Tot}=6 bar, H_2/CO=3, T=573K) on 4.7% Co/SiO_2.

temperature and concentration of the products in the gas phase. Increasing temperature will favour the formation of reaction products, thus increasing their concentration, but desorption will also be favoured at higher temperatures. The variation in the band intensity with the flowrate may suggest that the amount of adsorbed species is dependent on the concentration of the gas phase compounds. The observed increase in the C-H stretching band intensities upon a decrease in the flowrate of synthesis gas to 50 Nml/min. can be explained by a higher gas phase concentration of reaction products due to the increased conversion of carbon monoxide. The gas phase methane absorption band at 3017 cm^{-1} is a typical example, its intensity is clearly a function of the applied flowrate.

The lack of detectable infrared bands belonging to C_xH_y reaction intermediates has been suggested /130,138/ to be due to a too low steady state concentration, masking of these bands by similar bands from adsorbed hydrocarbon products or to a low value of the chain growth probability (α).

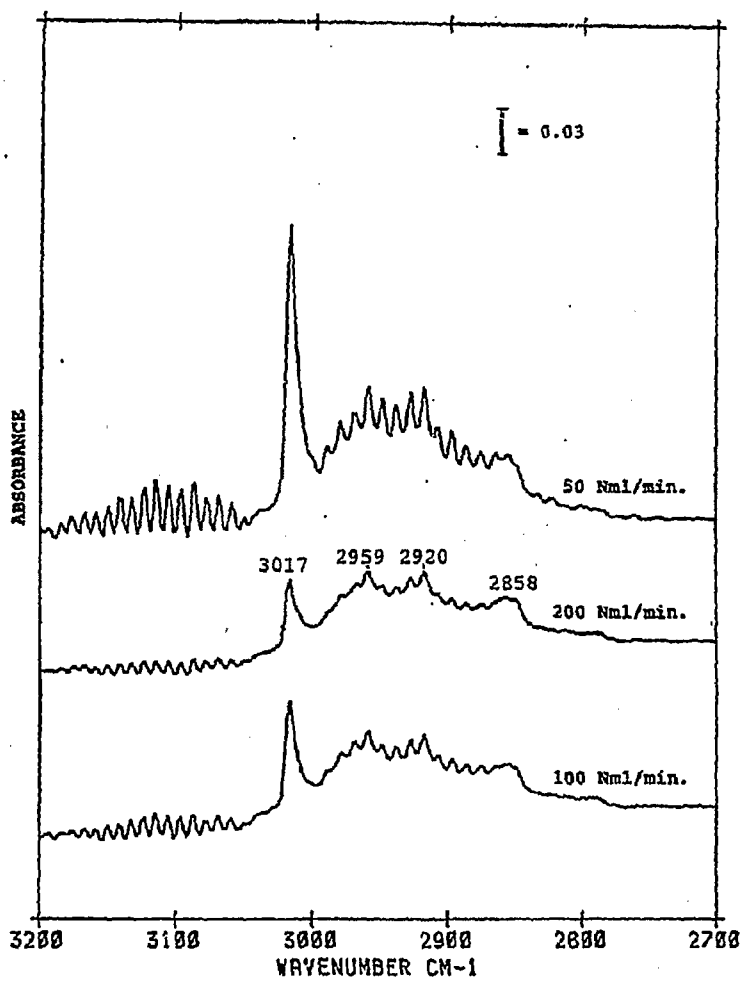

Fig. 5.2.7-4: Infrared spectra in the frequency range 3200-2700 cm^{-1} obtained during CO hydrogenation over 4.7% Co/SiO_2 with varying flowrates of synthesis gas.

Key as for Fig. 5.2.7-3.

5.2.8. Bands observed in the 1800-1200 cm^{-1} spectral range during CO hydrogenation over silica and alumina supported Co catalysts

5.2.8.1. Introduction

Spectra in this frequency region, 1800-1200 cm^{-1}, showed the presence of several absorption bands, which nature and behaviour depended on the type of catalyst and the applied reaction conditions. The intensities of the bands on the silica supported cobalt catalyst were generally less intense than the band intensities in the preceding frequency range, 3050-2800 cm^{-1}, while by far the strongest bands were observed in this range (1800-1200 cm^{-1}) over the alumina supported catalysts and alumina alone. It must also be remembered that silica itself gives rise to absorption bands in the 1800-1200 cm^{-1}, as briefly discussed in section 5.2.2.

Spectra of the supported cobalt catalysts with low metal loading (≤ 1%) are not reported in this section. Infrared spectra of 0.82% Co/SiO_2 in the present range of interest showed only a noisy baseline without any resolved peaks attributable to adsorbed species during CO hydrogenation. Elution of synthesis gas with He revealed bands resembling those presented in Fig. 5.2.2-1.

Absorption bands in the range 1800-1200 cm^{-1} were observed during CO hydrogenation over 1% $Co/\gamma\text{-}Al_2O_3$. The positions of the bands and their development with time in synthesis gas, He and hydrogen were similar to the bands observed over 4.6% $Co/\gamma\text{-}Al_2O_3$. Since the species causing these bands are of particular interest in connection with the microbalance experiments, and since only the 4.6% $Co/\gamma\text{-}Al_2O_3$ catalyst was studied in this apparatus, it was chosen not to include the spectra of the 1% $Co/\gamma\text{-}Al_2O_3$ catalyst in this frequency range.

5.2.8.2. 4.7% Co/SiO_2

Infrared spectra of silica alone during CO hydrogenation at 523K and 6 bar total pressure ($H_2/CO=2$) ("single cell" experiment) featured no absorption bands in the 1800-1200 cm^{-1} range. During flushing with He following CO hydrogenation, bands characteristic of silica overtone vibrations could be observed.

Fig. 5.2.8.2-1 shows spectra in the 1700-1350 cm^{-1} range obtained with the 4.7% Co/SiO_2 catalyst at different CO hydrogenation temperatures.

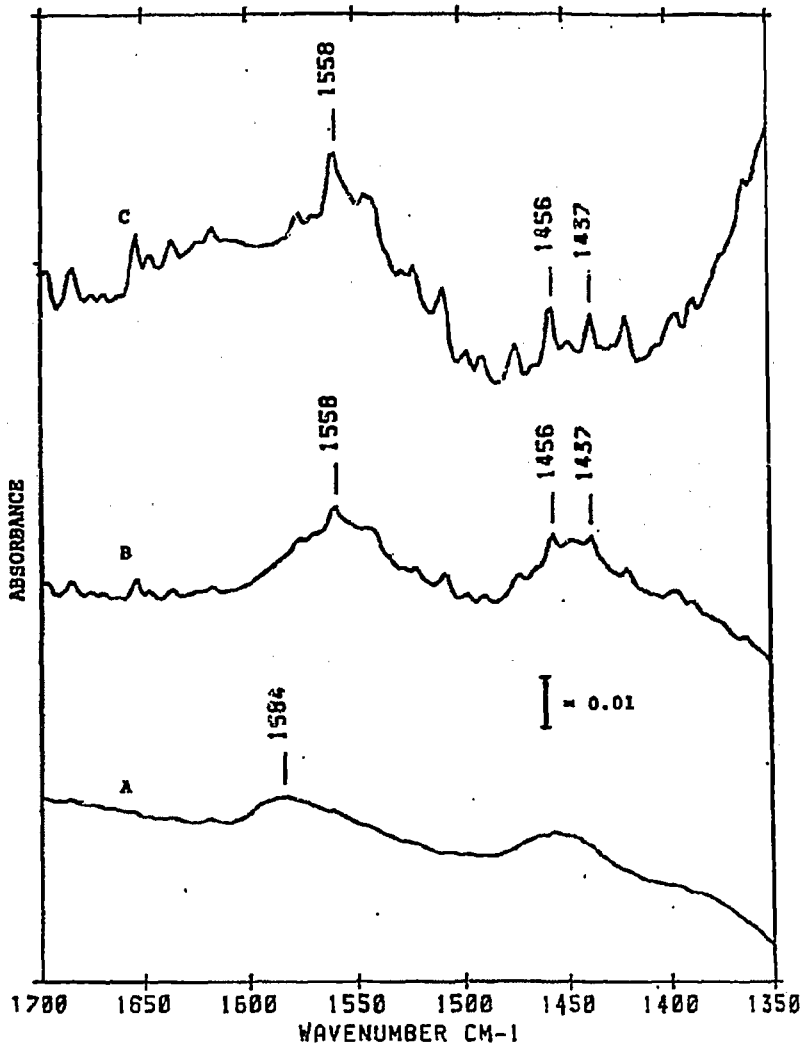

Fig. 5.2.8.2-1: Infrared spectra in the 1800-1350 cm^{-1} range during CO hydrogenation over 4.7% Co/SiO_2.

A: After 120 min. in synthesis gas at 473K
B: After 120 min. in synthesis gas at 523K
C: After 120 min. in synthesis gas at 573K

CO hydrogenation conditions:
P_{Tot} = 6 bar, H_2/CO = 2, 100 Nml/min.

At the lowest temperature investigated, 473K, two absorption bands are present in the 1600-1500 cm^{-1} and 1500-1400 cm^{-1} range, with distinguishable peak maxima appearing at 1584 and 1458 cm^{-1}, respectively.

Two broad bands are also evident in the spectra obtained at higher reaction temperatures, 523 and 573K, but the frequency of the principal absorption band in the 1600-1500 cm^{-1} range has apparently shifted to lower wavenumbers, while no pronounced changes in the positions of the bands in the 1500-1400 cm^{-1} range can be observed.

It appears that this downscale frequency shift is a common feature when the reaction temperature is raised from 473K to 523K, regardless of the total pressure or the hydrogen to carbon monoxide ratio. This is illustrated in Fig. 5.2.8.2-2 and 5.2.8.2-3.

At least two possible explanations can be rationalized which may account for the difference in the infrared spectra. Either the downscale shift is due to the same adspecies absorbing at different wavenumbers at different temperatures, or the increase in temperature implies the formation of new surface compounds, f.ex. by a decomposition mechanism. The frequency shift seems to be solely due to a temperature effect, occuring when the CO hydrogenation temperature is raised to 523/573K. The band frequencies are quite similar at 523 and 573K. In anticipation of the assignment of these bands, discussed later in this section, it is clear that both carbonates and formates are possible surface species which in principle can be responsible for the absorption bands observed in this frequency range.

On a catalyst surface, two main reaction pathways can be envisaged for the formate species, that is, dehydration or dehydrogenation:

$$CO_{(a)} + H_2O_{(a)} \rightleftharpoons HCOO^- + H^+ \rightleftharpoons CO_{2_{(a)}} + H_{2_{(a)}} \qquad 5.13$$

According to Grenoble et al. /200/, the dehydration reaction is catalyzed by acid oxides, and the dehydrogenation by metals and basic metal oxides.

One could possibly interprete the spectra at 523K and 573K as being a result of formate decomposition, yielding for example carbonate species, such as coordinated CO_2. An explanation like that above is favoured by the observed frequency shift and the additional appearance of (sub)bands in the 1600-1500 cm^{-1} range at 523K compared to the lower

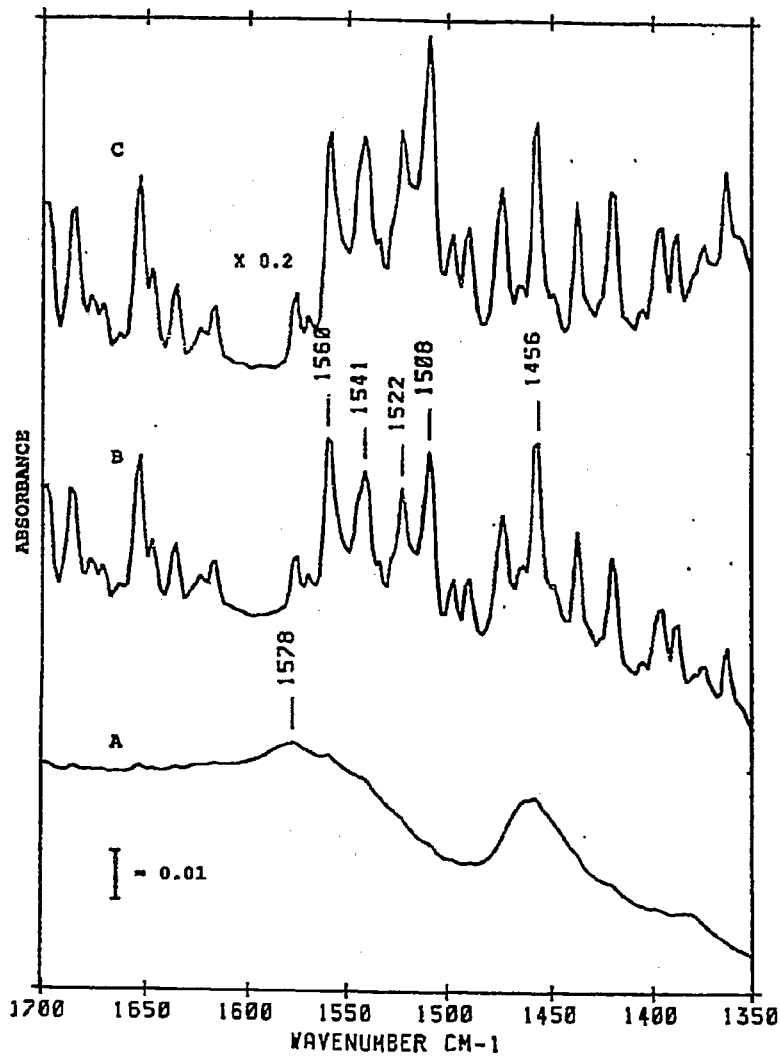

Fig. 5.2.8.2-2: **Infrared bands in the 1700-1350 cm^{-1} range during CO hydrogenation over 4.7% Co/SiO_2.**

A: **After 130 min. in synthesis gas at 473K**
B: **After 120 min. in synthesis gas at 523K (50 Nml/min.)**
C: **After 120 min. in synthesis gas at 573K (30 Nml/min.)**

CO hydrogenation conditions:
P_{Tot} = 11 bar, H_2/CO = 2, 100 Nml/min. unless otherwise stated

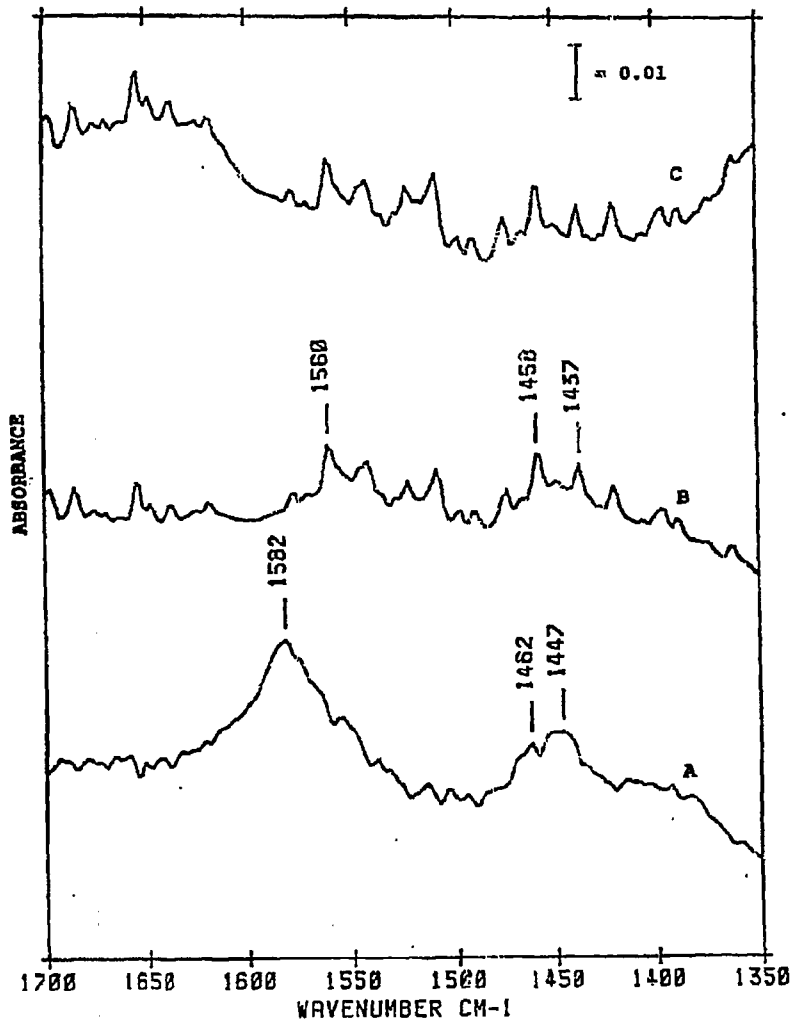

Fig. 5.2.8.2-3: **Infrared bands observed in the 1700-1350 cm^{-1} range during CO hydrogenation over 4.7% Co/SiO_2.**

A: **After 120 min. in synthesis gas at 473K**
B: **After 90 min. in synthesis gas at 523K**
C: **After 120 min. in synthesis gas at 573K**

CO hydrogenation conditions:
P_{Tot} = 6 bar, H_2/CO = 3, 100 Nml/min. unless otherwise stated

temperature (473K), but may be contradicted by the apparently low decomposition temperature of 473K-523K. Surface formate species have been reported to be stable up to at least 523K /111/ or even 673K /201/. It can be questioned whether the temperature used is sufficiently high enough for decomposition reactions. A third possibility also exists, namely the existence of not only formate species, but also acetate and propionate species. A common feature of these three compounds is the presence of O-C-O asymmetric and symmetric stretching vibrations occuring in close vicinity of each other, see Table 5.2.8.2-1. The sodium salts of the corresponding acids have asymmetric O-C-O stretches at 1583, 1565 and 1551 cm^{-1} /202/. As Blyholder et al. /203/ pointed out, this indicates a downscale shift in the O-C-O frequency with an increasing number of carbon atoms. Thus, due to the different thermal stability of the formate, acetate and propionate species, the red shift in frequency when going from 473K to 523K can possibly be explained by a higher fraction of adspecies containing at least 2, or possibly more than two carbon atoms. The difficulties in distinguishing the three adspecies from each other at 473K could arise from the overlap of the band positions (Table 5.2.8.2-1) and the inaccessible frequency region below 1350 cm^{-1}, where one would expect

Table 5.2.8.2-1: Assignment of infrared stretching frequencies of adsorbed formic, acetic and propionic acid on 9% Co/SiO_2 /203/.

COMPOUND	*O-C-O asymmetric str.*	*O-C-O symmetric str.*
Formic acid	1580 cm^{-1}	1350 cm^{-1}
Acetic acid	1580 cm^{-1}	1450 cm^{-1}
Propionic acid	1570 cm^{-1}	1425 cm^{-1}

O-C-O and CH_3 deformation bands, CH_3 rock and the O-C-O bending frequencies to occur. The presence of bidentate and unidentate acetate species has been observed on the SiO_2 support at 473K /204/.

As long as it presently is not possible to give an reasonable explanation for the observed frequency shift upon an increase in the reaction temperature (473K→523K), it is chosen - in the following treatment and discussion of the origin and nature of these adspecies - to regard

these bands as arising from the same adsorbed surface species. This is done in order to at least provide a qualitative picture of the surface composition in this frequency range (1700 - 1350 cm^{-1}) during CO hydrogenation at the different reaction conditions.

As already mentioned, the most pronounced differences are observed by an increase in the reaction temperature from 473 to 523K. At 523 and 573K, the band frequencies are similar, although variations in the intensity of the bands are observed depending on the reaction conditions. The intensities of the 1456 cm^{-1} and 1558 cm^{-1} bands increased with increasing temperature while keeping the total reaction pressure at 6 or 11 bar, see Fig. 5.2.8.2-1 and 5.2.8.2-2. On the other hand, increasing the H_2/CO ratio from 2 to 3 (Fig. 5.2.8.2-3) resulted in decreasing intensity of the 1560 cm^{-1} band and increasing intensity of the 1458 cm^{-1} with increasing temperature.

Before any further discussion of the origin of the species giving rise to the observed infrared bands, it is necessary to ensure that these bands are not related to changes in the transmission of the silica deformation bands. It has been shown in Chapter 5.2.2 that at least three absorption bands can be associated with and explained to be due to silica lattice vibrations. In this respect, the 1580 cm^{-1} band is of considerable interest, since its frequency closely corresponds to the wavenumbers of surface compounds appearing in the spectra obtained at CO hydrogenation conditions. The behaviour of the 1584 cm^{-1} and 1578 cm^{-1} bands during CO hydrogenation are contrary to what would be expected if they were due to the SiO_2 support itself. The intensity of the two bands increased steadily with time in syngas. Similarly, their behaviour during He and H_2 treatment and upon changes in the syngas flowrate paralleled the observed behaviour of the CH_x ($x=2 \vee 3$) bands in the 3050-2800 cm^{-1} range. Furthermore, when the reaction temperature is kept constant (at 473K) and the H_2/CO ratio (of 2) is fixed, Fig. 5.2.8.2-4 shows that increasing total reaction pressure resulted in an increasing intensity of the bands. It is hard to believe that the overtone vibrations depend to such an extent on the pressure. As evident from the spectra in Fig. 5.2.8.2-5, no distinct changes in the intensity of the silica overtone bands are observed with increasing total reaction pressure. More likely, they are rather sensitive to changes in the temperature, as shown previously in Fig. 5.2.2-1, 5.2.2-2 and 5.2.3.4-3. Thus, it seems reasonable to assume that the major bands appearing in the frequency range 1700-1350 cm^{-1} during CO

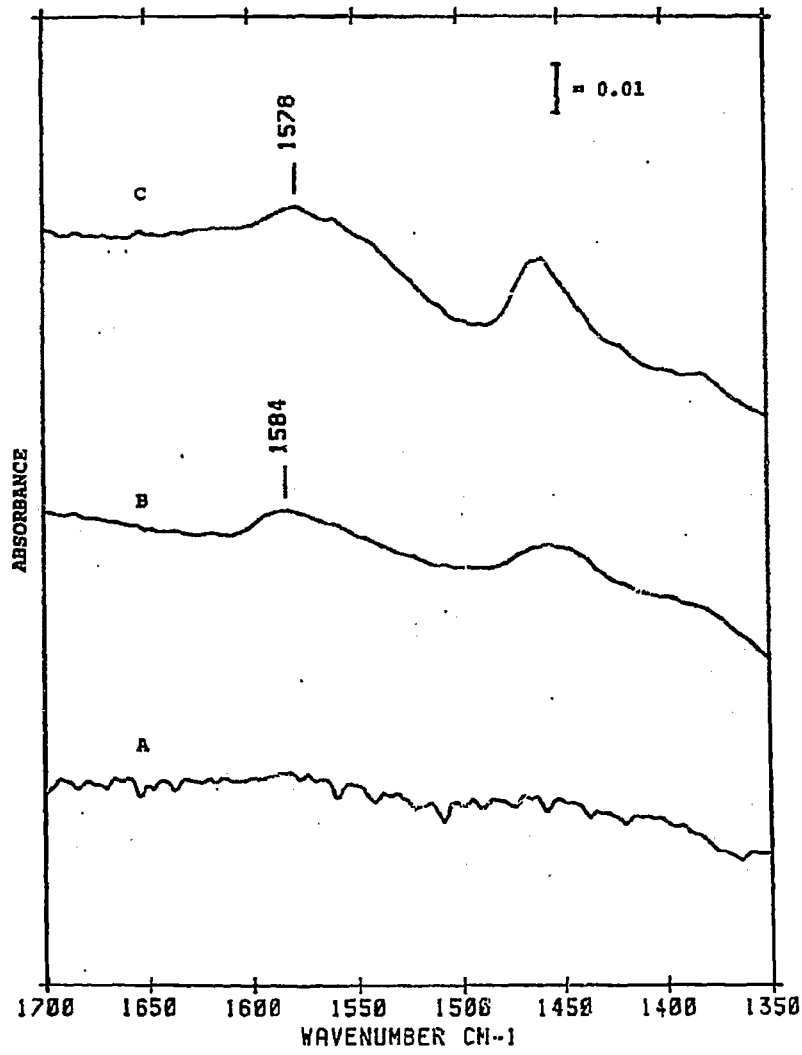

Fig. 5.2.8.2-4: Infrared bands in the 1700-1350 cm^{-1} range during CO hydrogenation over 4.7% Co/SiO_2.

A: After 120 min. in synthesis gas at 2.5 bar total pressure
B: After 120 min. in synthesis gas at 6 bar total pressure
C: After 130 min. in synthesis gas at 11 bar total pressure

CO hydrogenation conditions:
T = 473K, H_2/CO = 2, 100 Nml/min.

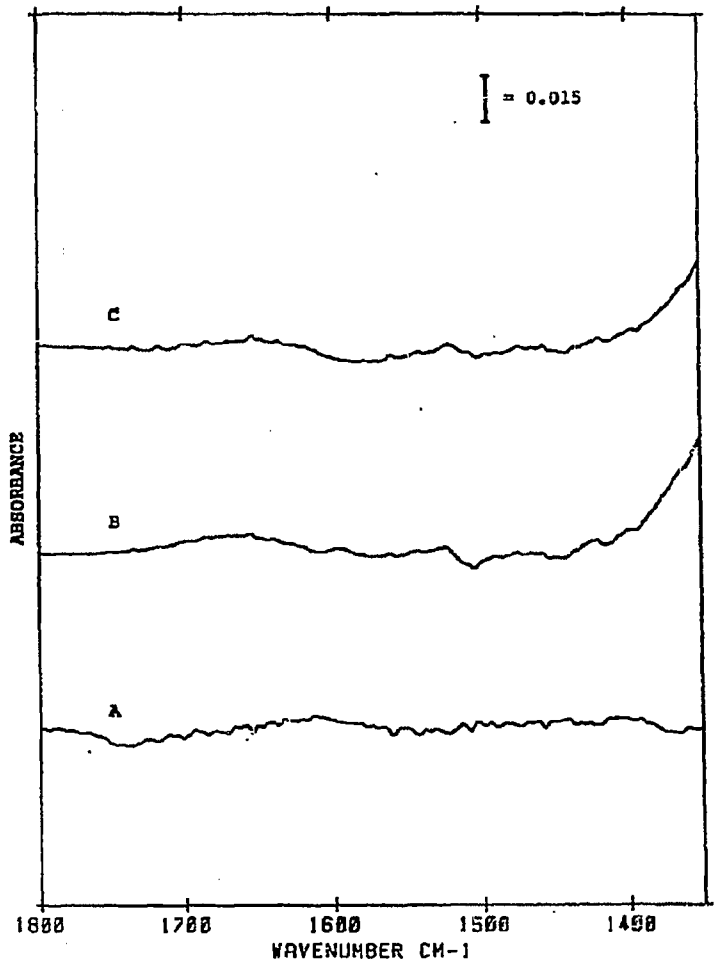

Fig. 5.2.8.2-5: Infrared bands in the 1700-1350 cm^{-1} range during CO hydrogenation over the silica support.

A: After 120 min. in synthesis gas at 2.5 bar total pressure
B: After 130 min. in synthesis gas at 6 bar total pressure
C: After 130 min. in synthesis gas at 11 bar total pressure

CO hydrogenation conditions:
T = 473K, H_2/CO = 2, 100 Nml/min.

hydrogenation over the silica supported catalysts belong to species formed during CO hydrogenation, and can not be related to the effect of support lattice vibrations.

When it comes to the assignment of these bands, it is important not only to consider the 1700-1350 cm^{-1} spectral region, but also relate the suggested structures and their corresponding absorption bands to other appropriate frequency regions. During CO hydrogenation at different reaction conditions, the development of bands in the C-H stretching region (3050-2800 cm^{-1}) have been demonstrated, see section 5.2.5 and 5.2.6.
The corresponding bending modes of the asymmetric and symmetric stretching of CH_2- and CH_3 groups would be expected to appear in the range 1375-1465 cm^{-1} /91/. Species responsible for the observed 1458 cm^{-1} band can therefore possibly be assigned to CH_2-deformation (1465 cm^{-1}) and/or to the asymmetric or symmetric CH_3-deformation at 1450 and 1375 cm^{-1}, respectively. The frequency of the 1458 cm^{-1} band is in an intermediate position between the CH_2 and CH_3 deformation bands, thus making it difficult to discriminate between the two species based on the wavenumber alone. One could, however, consider the behaviour of the band at the different reaction conditions, thereby getting an indication of the most probable structure (CH_2- or CH_3-deformation) giving rise to this band. As already mentioned, the intensity of the 1458 cm^{-1} band increased with increasing temperature. When the intensity of this band at 473, 523 and 573K is compared at different H_2/CO ratios, 2 or 3, it follows that the intensity of the band is higher at a H_2/CO ratio of 3 than of 2 at each temperature. Furthermore, when the total reaction pressure was increased to 11 bar, the intensities of the band were by far higher at this reaction pressure compared to those at lower total pressure (6 bar). These observations can then be related to what is known about the probability of chain growth in the Fischer-Tropsch chemistry as a function of reaction conditions. Generally, the chain growth probability decreases with increasing temperature and partial pressure of hydrogen, and increases with increasing CO partial pressure. As the ratio of H_2/CO increases, thereby increasing the surface hydrogen coverage and thus favouring termination (hydrogenation) reactions, the production of high molecular weight species would be expected to decrease and the formation of lighter products to be favoured. This manifests itself in the spectra as an increase in the intensity of the bands in the 3050-2800 cm^{-1} frequency range ascribed to asymmetric (and symmetric) stretching of CH_3 groups and the appearance of gas phase methane at 3017 cm^{-1}. One may therefore suggest, that the observed behaviour of the

1458 cm^{-1} band upon changes in the temperature and H_2/CO ratio indicate that the band is caused by asymmetric deformation of a CH_3 group. The assignment of the band to such an adspecies would imply the existence of the corresponding symmetric CH_3 deformation band, expected to occur near 1375 cm^{-1}. Indeed, a band located at 1381 cm^{-1} can be observed in the spectra. It is, however, rather difficult to follow exactly the behaviour of this band because of its inherent weakness and the shift occuring in the baseline due to the progressive absorption by the silica support. The broadness of the band indicates that it could encompass several absorption processes. Nevertheless, the presence of the band at 1381 cm^{-1} and the general development of the 1458 cm^{-1} band at the different reaction conditions, which parallels the behaviour of the CH_3 bands in section 5.2.5, suggest an assignment of the 1458 cm^{-1} band to the deformation mode of CH_3-groups. If the 1458 cm^{-1} band was due to CH_2-deformation in long chained hydrocarbons, it should be expected that the intensity of this band varied in a manner similar to the chain growth probability with for example temperature, namely, decreasing intensity with increasing temperature. Instead, the intensity behaviour of the band is believed to reflect reaction conditions favouring the production of hydrocarbons with shorter chain lengths. That these bands can be related to adsorbed hydrocarbons is further supported by the variation in their intensity with time during prolonged exposure to syngas followed by either He and the H_2 treatment or by direct replacement of synthesis gas with hydrogen, as shown in Fig. 5.2.8.2-6. In addition, the reactivity of the adspecies towards hydrogen was similar to that found for the CH_x structures giving absorption bands in the

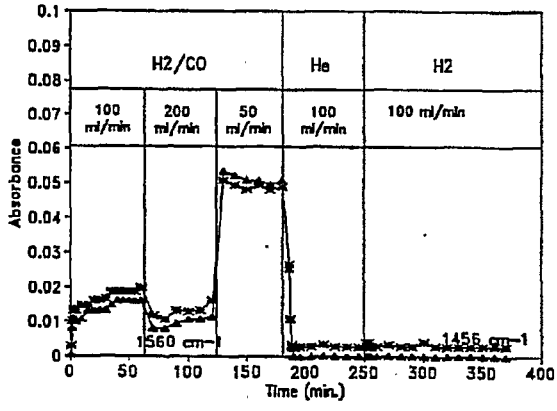

Fig. 5.2.8.2-6: Development of the intensity of infrared bands observed during CO hydrogenation, He-flushing and H_2-treatment of 4.7% Co/SiO_2. CO hydrogenation conditions: P_{Tot}=6 bar, H_2/CO=3, T=573K.

3050-2800 cm^{-1} region, that is, a slow decline in intensity with time in H_2.

A number of studies have reported infrared bands in the C-H stretching region ascribed to asymmetric/symmetric stretching vibrations of CH_2- and/or CH_3-groups during CO hydrogenation over silica supported Co catalysts /78,108/ and supported Ru catalysts /189,190,195,196,205,206/. Arakawa et al. /78/ ascribed a band at 1459 cm^{-1} to CH_2 groups, while a band near 1378 cm^{-1} was not accounted for. Similarly, Yamasaki et al. /205/ observed weak C-H deformation bands at 1470-1440 cm^{-1} (methylene and methyl) and 1380 cm^{-1} (methyl). Pien et al. /206/ ascribed bands in the range 2970-2860 cm^{-1} and at 1461 cm^{-1} to hydrocarbon species. Apart from these studies, no bands due to the bending modes of CH_2 and CH_3 groups have been reported. The absence of any resolved absorption band attributable to the CH_2 or CH_3 deformation mode was by Ansorge et al. /108/ assumed to be due to the masking of the band(s) by their strong bidentate carbonate band at 1590 cm^{-1}. King /207/ explained the lack of the C-H bending mode with the weakness of the band.

Even though an assignment of the 1458 cm^{-1} band to asymmetric CH_3 deformation mode (and the 1381 cm^{-1} band to symmetric CH_3 deformation) seems plausible, this does not exclude the possibility of ascribing these and other bands at higher frequencies in this region to alternative adspecies.

Strong absorption bands in the OH stretching region (3800-3400 cm^{-1}), assigned to surface bound hydroxyl groups and chemisorbed water, was observed during the CO hydrogenation reaction. Since the presence of carbon monoxide is evident, one can possibly envisage a reaction between CO and water resulting in the formation of formate species. In fact, the presence of a surface formate species has recently been suggested by Li et al. /111/ as a result of interaction between water vapour and adsorbed carbon monoxide over a 4.6% Co/SiO_2 catalyst. The adsorption of formate species on silica alone was characterized by three bands appearing at 2950, 1725 and 1390 cm^{-1}. Formic acid adsorbed on cobalt sites was reported to give absorption bands at 2945, 1580 and 1380 cm^{-1}. The latter species was reported to be stable at least up to 523K, while formate species adsorbed on the silica support was completely desorbed at 473K /111/. Duchinskii et al. /208/ found that cobalt (and Ni) formates decomposed at 673K. Thus, the dominating bands in the 1600-1500 and 1500-1400 cm^{-1} ranges can possibly be ascribed to a surface formate species.

When comparing the band intensities of the major bands in each of the above mentioned

frequency regions, several different trends could be observed. The intensity of the 1460 cm^{-1} band was lower than those of the 1582/1560 cm^{-1} bands at 473K. At 523K, both groups of bands exhibited similar intensities, while at the highest temperature investigated, 573K, the intensity of the 1460 cm^{-1} band exceeded that of the 1560 cm^{-1} band. This situation was the case when CO hydrogenation was carried out at a total pressure of 6 bar with a H_2/CO ratio of 3. With a H_2/CO ratio equal to 2, but applying otherwise the same reaction conditions, the intensities of the 1584/1558 cm^{-1} bands were higher at all temperatures compared to the 1456 cm^{-1} band, and the relative difference in intensity increased with increasing temperature. Increasing the reaction pressure from 6 to 11 bar, but keeping the same H_2/CO ratio (of 2), resulted in a diversifying correlation, as seen from the spectra shown in Fig. 5.2.8.2-1 and 5.2.8.2-2. These ambigious relationships is somewhat contrary to what would be expected if the bands in the two frequency regions should be ascribed to a formate species, and can not be regarded as effects of the different reaction conditions. Nor is it believed that they are related to the formation of new or additional surface structures as a result of for example decomposition reactions, since the major features of the spectra are generally retained showing no pronounced signs of disappearance or appearance of absorption bands. Rather, the inconsistent behaviour must be considered as an indication of the existence of two different adspecies, each absorbing infrared light in their own characteristic frequency region. The asymmetric and symmetric C-O stretching vibration of a adsorbed surface formate species is expected to appear between 1600 and 1500 cm^{-1} and 1400-1300 cm^{-1}, respectively. One may therefore suggest that the dominating band in the 1600-1500 cm^{-1} range can be ascribed to the asymmetric C-O stretch, while the weak, broad band centered around 1381 cm^{-1} - rather than the principle absorption band in the 1480-1400 cm^{-1} domain - can be due to the corresponding symmetric C-O stretching vibration. Also, applying the criteria of frequency separation (discussed in detail later in this section) on the asymmetric/symmetric C-O bands indicate that the corresponding band positions preferentially is to be located in the region 1600-1500 cm^{-1} and below 1400 cm^{-1}. Such an assignment is, however, complicated by the low intensity of the 1381 cm^{-1} band and the disturbance in the baseline due to increasing absorption of the fundamental transverse and longitudinal vibrations of the silica lattice in addition to the SiO_2 overtone bands.

Plausible explanations have been given for the principle bands appearing in the spectral range

1600-1500 and 1500-1400 cm^{-1}, but also other types of surface species giving rise to the main absorption band located near 1560 cm^{-1} can be proposed in addition to the formate species. Several studies have reported the presence of different kinds of surface carbonate structures, i.e. bidentate and unidentate carbonate, on the catalyst surface during reaction. Two types of carbonate complexes are shown in Fig. 5.2.8.2-7. Such compounds may arise as a result of strong interactions of CO and CO_2 with metals and metal oxides. The unidentate carbonate complex with cobalt is reported to give two C-O_{II} stretching bands in the 1470-1450 cm^{-1} and 1380-1350 cm^{-1} ranges in addition to a C-O stretching band in the 1070-1050 cm^{-1} range /210/. Bidentate carbonate complexes have a stretching vibration between 1640-1590 cm^{-1} (C-O_{II}) and asymmetric and symmetric C-O_I stretching vibrations in the spectral range 1290-1260 cm^{-1} and 1040-1020 cm^{-1}. Ansorge et al. /108/ reported a band at 1590 cm^{-1} to the stretching vibration of bidentate surface carbonate. The bands observed in the present study do not exactly coincides with the above cited band frequencies. Nevertheless, it would seem that the frequency of the principle absorption band in the 1600-1500 cm^{-1} region (1582/1560 cm^{-1}) is somewhat high to allow an assignment to unidentate carbonate species. Therefore, by just considering the band positions, the 1582/1560 cm^{-1} bands could indicate the presence of bidentate carbonate structures. The expected low frequency bands are of reasons earlier mentioned not accessible. This further implies that any *conclusive* assignment of the bands in this region (1700-1350 cm^{-1}) can not be made unless frequencies below 1350 cm^{-1} are examined. In this frequency domain, the symmetric, carbon-out-of-plane and torsional vibrations of carbonate and carboxylate species are predicted to occur.

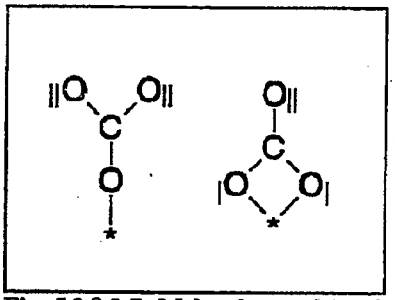

Fig. 5.2.8.2-7: Molecular models of the 1:1 unidentate and bidentate carbonate complexes /209/.

Another likely candidate responsible for the 1582/1560 cm^{-1} band could be carboxylate species. The asymmetric and symmetric stretching vibrations of C-O in surface carboxylate compounds have been reported at 1570 and 1377 cm^{-1} /211/, 1560 and 1410 cm^{-1} /212/ and at 1560 and 1330 cm^{-1} /213/, respectively. In the study of Blyholder et al. /203/ two bands at 1557 and 1435 cm^{-1} were reported to be indicative of carboxylate formation on a 9.1%

Co/SiO_2 catalyst upon interaction of C_2H_4 and CO at 373K. Hence, the absorption bands at 1582/1560 cm^{-1} and the broad band between 1400 and 1350 cm^{-1} are in such a position that they can be caused by adsorbed carboxylate species. If this is the case, then the behaviour of these bands could possibly be expected to be related to that of adsorbed carbon monoxide, since this species probably would act as a source for the CO_2 involved in the carboxylate compounds. Carbon dioxide can be formed either from the Boudouard reaction; $2CO \rightarrow C + CO_2$, or by the water gas shift reaction; $CO + H_2O \rightarrow CO_2 + H_2$. By using a H_2/CO ratio of 2 and varying the total reaction pressure between 6 and 11 bar, the intensity of the 1582/1560 cm^{-1} band increased with increasing temperature, while the opposite trend was found to occur with a H_2/CO ratio of 3 (at a total pressure of 6 bar). Also, the intensity of the band was higher at the highest total reaction pressure (11 bar) compared to that obtained with a total pressure of 6 bar. It is not presently clear if the observed behaviour of the band intensitites reflects the influence of the reaction conditions on the formation of CO_2, for example from the water-gas shift reaction, and consequently, if the bands can be assigned to coordinated CO_2.

5.2.8.3. 4.6% Co/γ-Al_2O_3 and γ-Al_2O_3

Considerable more complex spectra featuring strongly absorbing species were obtained in the 1800-1200 cm^{-1} range during CO hydrogenation over 4.6% Co/γ-Al_2O_3 and the alumina support alone.

Fig. 5.2.8.3-1 illustrates the development of infrared bands in the 1750-1250 cm^{-1} region with time in synthesis gas over 4.6% Co/γ-Al_2O_3 at 473K.
A number of bands appear after short times of reaction and continue to grow in intensity during prolonged exposure to H_2/CO. After 80 minutes of reaction, distinct absorption bands are evident at 1620, 1595, 1460, 1393 and 1377 cm^{-1}.

Increasing the reaction temperature to 523K (but keeping a total pressure of 6 bar and H_2/CO ratio of 2) resulted in major bands appearing at identical positions (as at 473K), as shown in Fig. 5.2.8.3-2. The behaviour of the bands is analogous to that observed in Fig. 5.2.8.3-1; the band intensities increased steadily with time in synthesis gas.
The main difference is that the intensity of the absorption bands is highest at the highest of the two CO hydrogenation temperatures investigated, 523K.

Spectra obtained during CO hydrogenation over an alumina disk void of cobalt placed downstream of the cell containing the supported catalyst sample are shown in Fig. 5.2.8.3-3 and 5.2.8.3-4. Furthermore, Fig. 5.2.8.3-5 presents the spectral features of γ-Al_2O_3 alone during CO hydrogenation at 473K (H_2/CO=2, P_{Tot}= 6 bar, "single cell" experiment).
By comparison of the spectra in Fig. 5.2.8.3-1 to 5.2.8.3-4, several effects are noticed, below summarized by points:

1. The presence of a distinct absorption band near 1327 cm^{-1} on γ-Al_2O_3, which is poorly resolved on 4.6% Co/γ-Al_2O_3.
2. The reduced intensity of the 1377 cm^{-1} band relative to the 1393 cm^{-1} peak on γ-Al_2O_3, while the intensity of the 1393 cm^{-1} band is higher than that of the 1377 cm^{-1} peak on 4.6% Co/γ-Al_2O_3 at both temperatures, 473 and 523K.
3. The difference in the intensity of the band located at 1458 cm^{-1}. On γ-Al_2O_3,

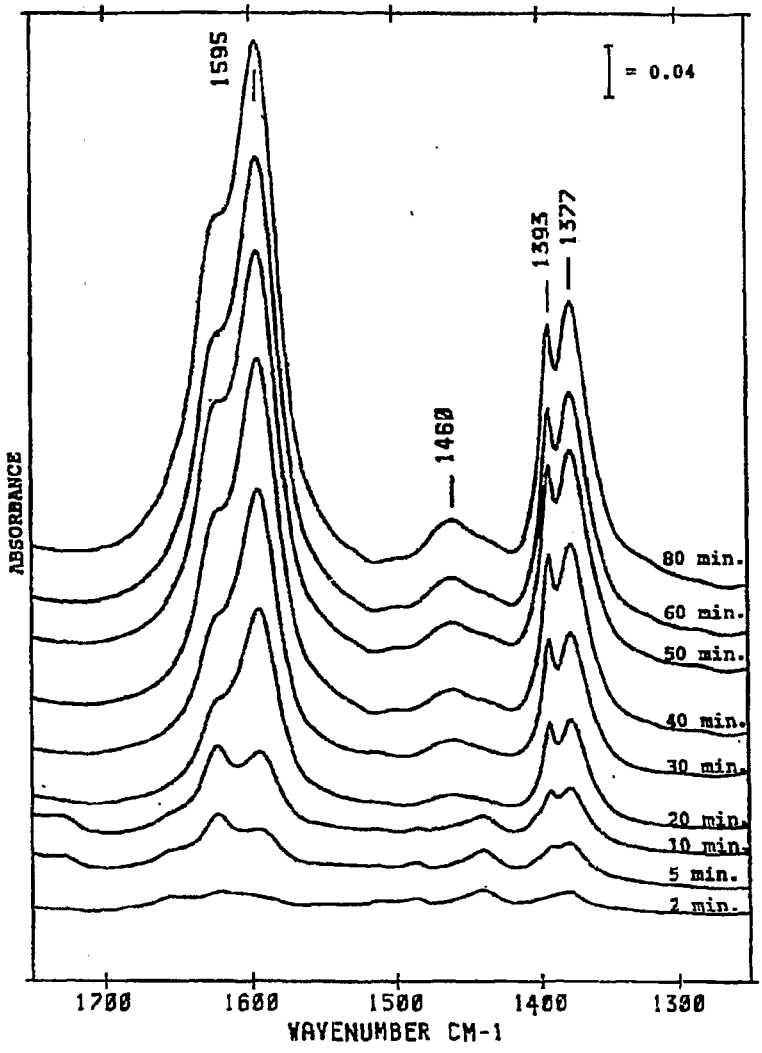

Fig. 5.2.8.3-1: **Infrared spectra in the spectral range 1750-1250 cm^{-1} during prolonged exposure of 4.6% $Co/\gamma-Al_2O_3$ to synthesis gas at 473K.**

The times indicated represent those at which collection of interferograms was initiated.

CO hydrogenation conditions:
P_{Tot} = 6 bar, H_2/CO = 2, T = 473K, 100 Nml/min.

Fig. 5.2.8.3-2: Infrared spectra of 4.6% Co/γ-Al_2O_3 with time in synthesis gas at 523K.

A: 2 min.
B: 5 min.
C: 10 min.
D: 20 min.
E: 30 min.
F: 40 min.
G: 50 min.

The times indicated represent those at which the IR scans were started.

CO hydrogenation conditions:
P_{Tot} = 6 bar, H_2/CO = 2, T = 523K, 100 Nml/min.

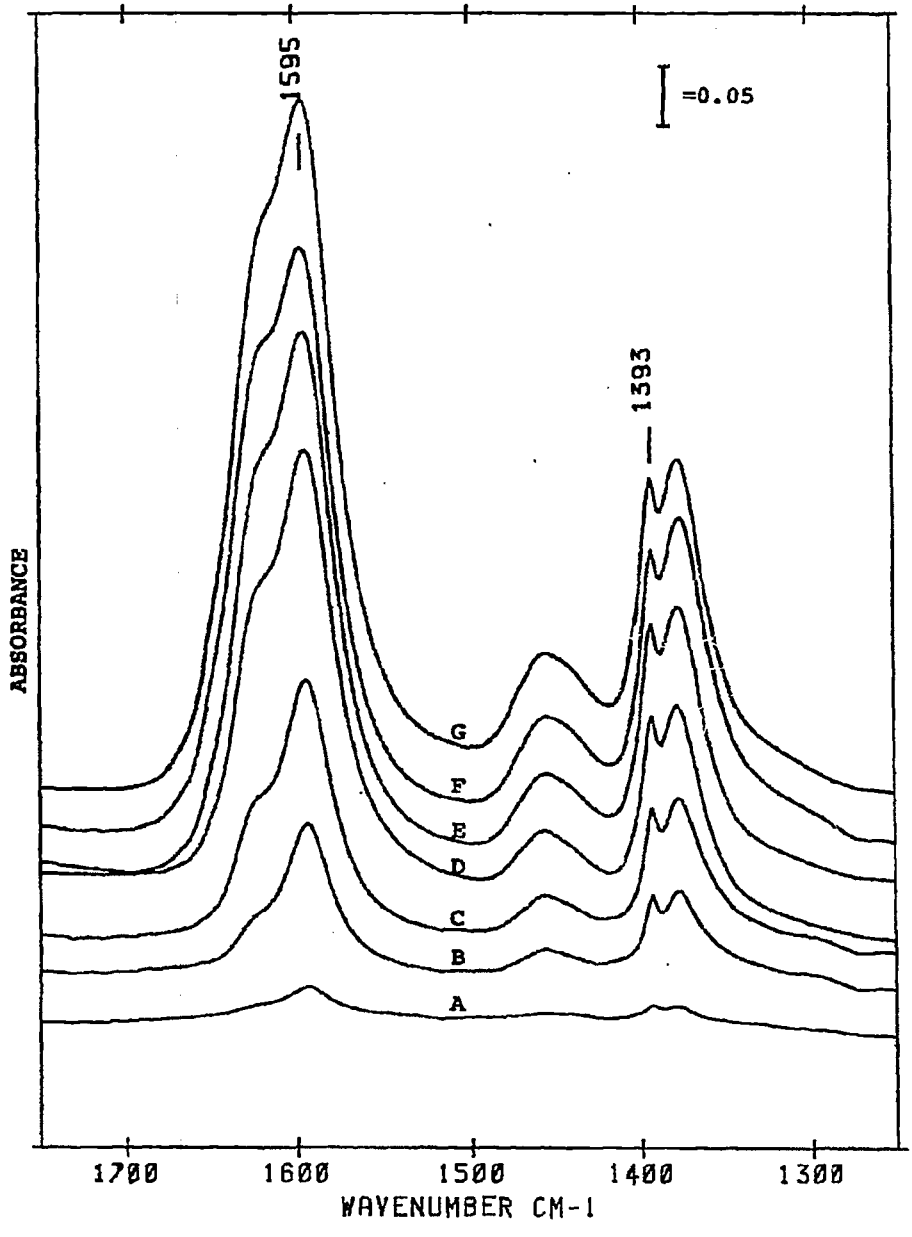
1595
1393
=0.05
ABSORBANCE
G
F
E
D
C
B
A
1700
1600
1500
1400
1300
WAVENUMBER CM-1

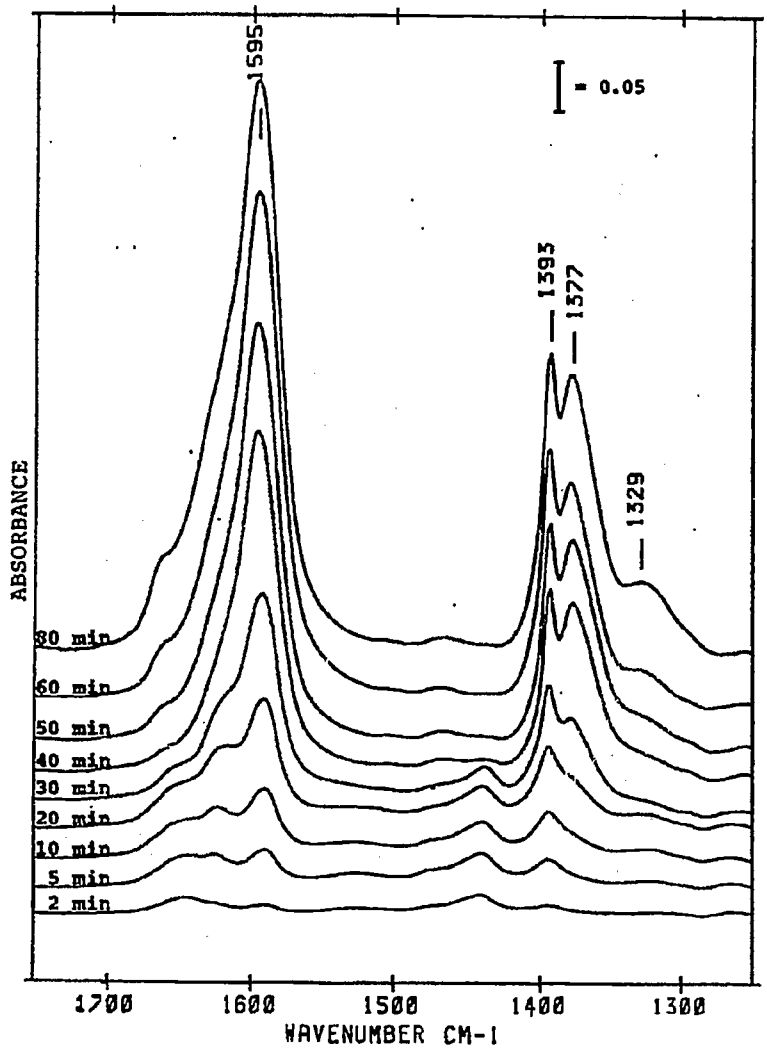

Fig. 5.2.8.3-3: **Infrared spectra of γ-Al_2O_3 (placed downstream of the sample cell) during CO hydrogenation.**

The times indicated represent those at which collection of interferograms was initiated.

CO hydrogenation conditions:
P_{Tot} = 6 bar, H_2/CO = 2, T = 473K

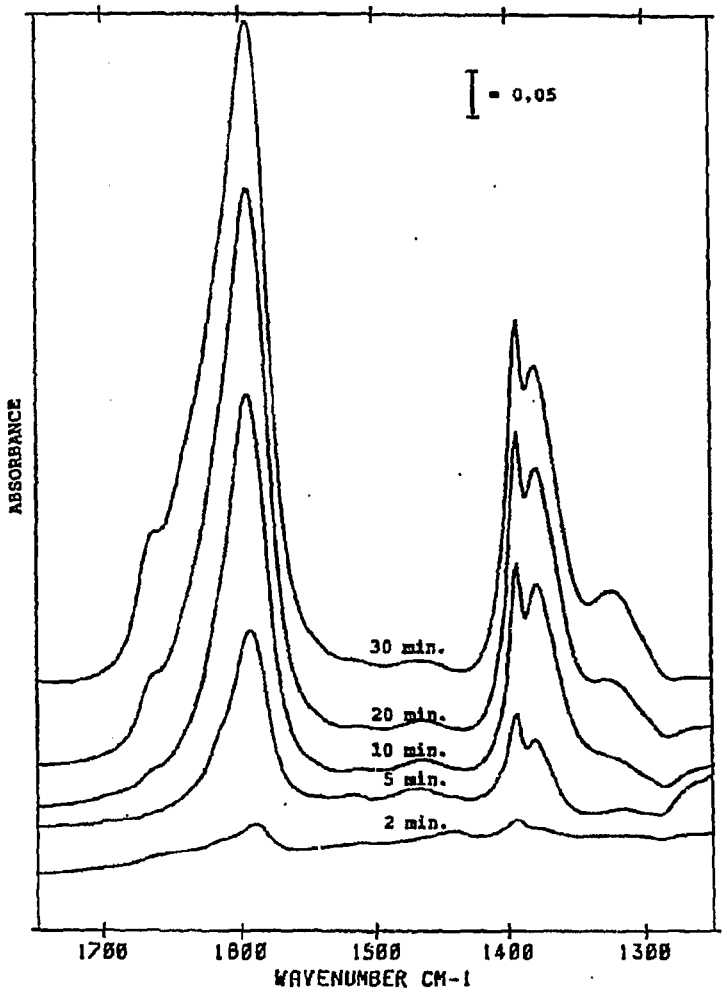

Fig. 5.2.8.3-4: **Infrared spectra of γ-Al_2O_3 in the region 1750-1250 cm^{-1} during CO hydrogenation.**

(The cell containing the alumina disk is placed downstream of the cell containing the alumina supported cobalt catalyst).

The times indicated represent those at which collection of interferograms was initiated.

CO hydrogenation conditions:
P_{Tot} = 6 bar, H_2/CO = 2, T = 523K

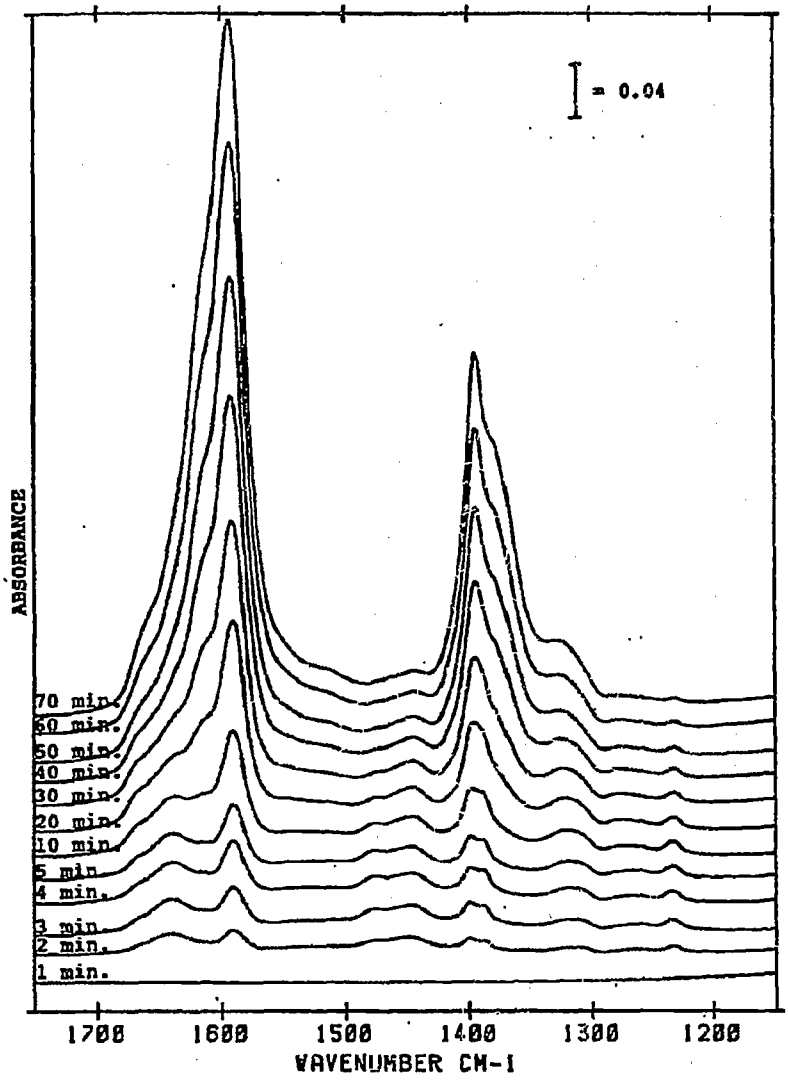

Fig. 5.2.8.3-5: **Infrared spectra of adsorbed species on γ-Al_2O_3 during CO hydrogenation.**

("single cell" experiment)

The times indicated represent those at which collection of interferograms was started.

CO hydrogenation conditions:
P_{Tot} = 6 bar, H_2/CO=2, T = 473K

a weakly resolved band is seen in this part of the spectrum, in contrast to the rather strong, distinct absorption band on 4.6% $Co/\gamma\text{-}Al_2O_3$.

4. A higher intensity of the bands at 1595, 1393 and 1377 cm^{-1} over $\gamma\text{-}Al_2O_3$ than over the alumina supported cobalt catalyst at 473 and 523K.
5. The location of a band near 1620 cm^{-1} on 4.6% $Co/\gamma\text{-}Al_2O_3$, exhibiting a considerably higher intensity than the 1665 cm^{-1} band on $\gamma\text{-}Al_2O_3$.

As can be seen, there exists a certain general similarity between the spectra in Fig. 5.2.8.3-1 to 5.2.8.3-4 and Fig. 5.2.8.3-5 concerning the position, intensity and behaviour of the observed infrared absorption bands.

It would seem though, as two shoulders develop on the high frequency side of the 1593 cm^{-1} band over the $\gamma\text{-}Al_2O_3$ blank (Fig. 5.2.8.3-5) during exposure to synthesis gas at 473K.

For a more exact and reliable determination of the frequencies of these shoulder peaks, deconvolution by fitting Gaussian and Lorentzian curves to the main absorption band in the 1700-1500 cm^{-1} region of Fig. 5.2.8.3-5 was carried out, resulting in the situation shown in Fig. 5.2.8.3-6 (basic curve fitting procedure input: 6-9 lines, 6000 iterations).

The principle peak can be regarded as being composed of at least six overlapping bands, the most interesting of these with frequencies at 1651, 1616 and 1591 cm^{-1}. Thus, the spectra of the pure $\gamma\text{-}Al_2O_3$ obtained above 1600 cm^{-1} during CO hydrogenation (Fig. 5.2.8.3-5) envelop both the bands, 1665 and 1620 cm^{-1}, found on 4.6% $Co/\gamma\text{-}Al_2O_3$ and $\gamma\text{-}Al_2O_3$, respectively, although the band intensities are different. In addition, a weak band is visible at 1231 cm^{-1}.

The stability of the infrared bands was investigated by replacing synthesis gas with He and then H_2 at reaction temperatures after 1-2 hours of exposure to H_2/CO. The typical behaviour of the adspecies giving rise to the bands is shown in Fig. 5.2.8.3-7 for 4.6% $Co/\gamma\text{-}Al_2O_3$ at 473K. All the bands except the one at 1622 cm^{-1} were rather unaffected by He and subsequent treatment with H_2. The intensity of the 1622 cm^{-1} band remained fairly constant in helium, while a minor decrease in the intensity of the band was observed in hydrogen, Fig. 5.2.8.3-7. Similar behaviour, that is, the negligible effect of He and H_2 upon the spectra of adsorbed species was also observed over $\gamma\text{-}Al_2O_3$ alone, either placed downstream of the alumina supported cobalt catalysts or investigated by a "single cell" experiment. Thus, the bands in this region appear to be strongly adsorbed due to their increase in intensity with temperature

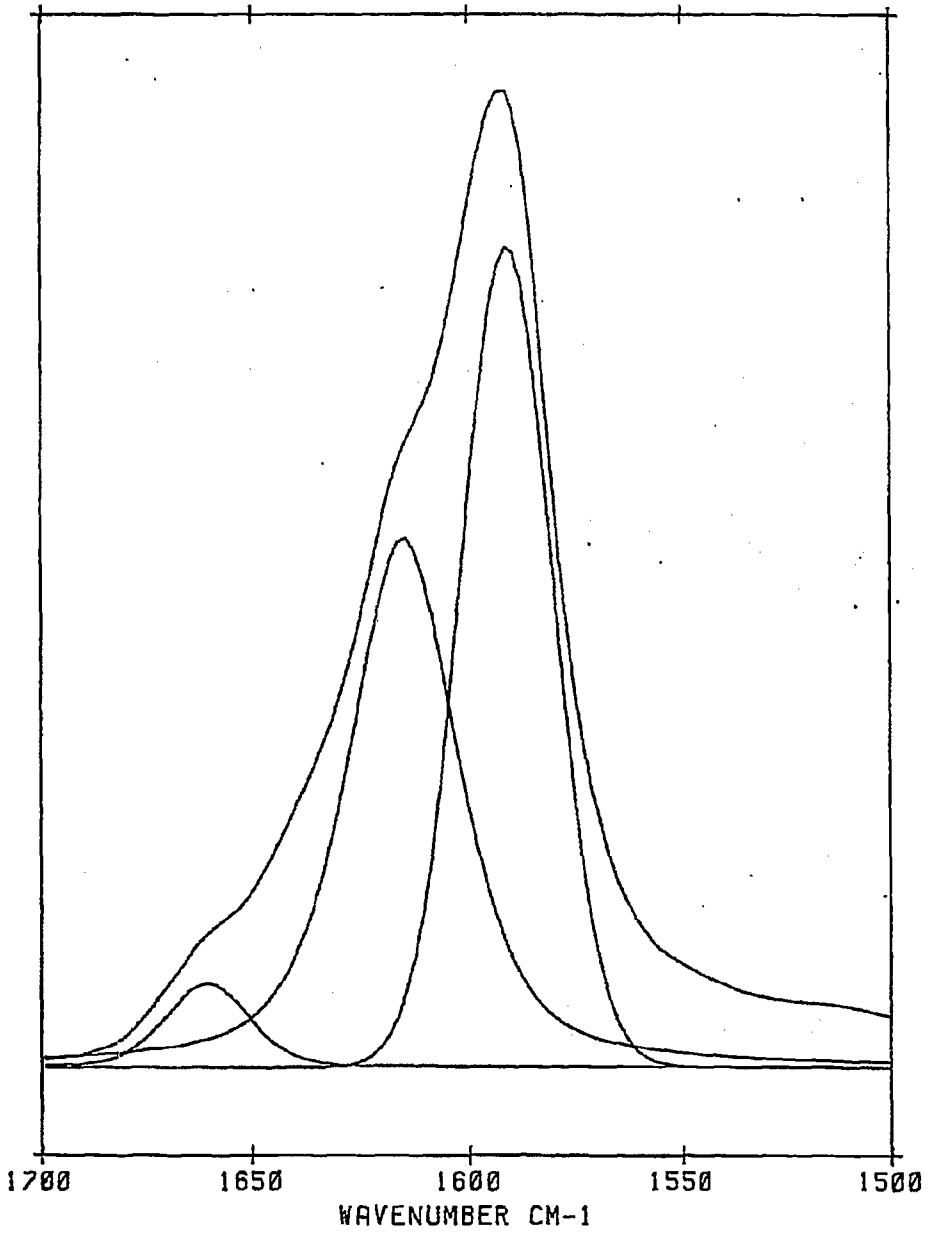

Fig. 5.2.8.3-6: **Deconvolution of the major peak appearing in the frequency region 1700-1500 cm^{-1} in Fig. 5.2.8.3-5.**

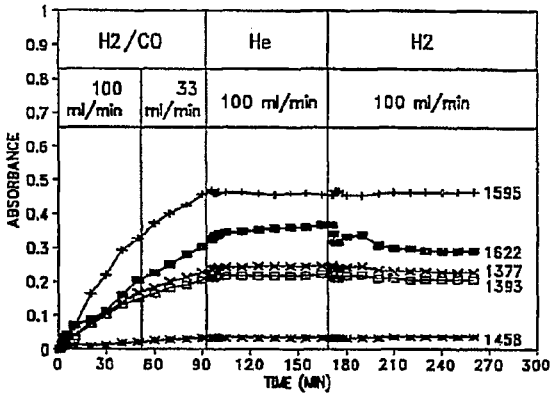

Fig. 5.2.8.3-7: Development of the intensities of selected bands in the 1700-1200 cm^{-1} range during CO hydrogenation, He-and H_2-treatment over 4.6% $Co/\gamma\text{-}Al_2O_3$.
CO hydrogenation conditions:
P_{Tot}=6 bar, H_2/CO=2, T=473K.

and their general lack of reactivity.

The identification of the bands, several of which were not observed with silica or the silica supported cobalt catalysts, is complicated by difficulties in comparing the surface species with the pure inorganic and organic compounds, for example cobalt carbonate complexes. A thorough review of the literature revealed that few investigations resembling the present work were available, although carbon monoxide containing species have been reported during catalytic oxidation of CO over cobalt oxide (Co_3O_4) /97/. A somewhat larger number of publications have appeared for Ru, and the assignment of the observed bands are thus aided and carried out in accordance with some of these reports /189,207/.

The most prominent features in the spectra of 4.6% $Co/\gamma\text{-}Al_2O_3$ and the $\gamma\text{-}Al_2O_3$ blank during CO hydrogenation are the bands at 1595, 1393 and 1377 cm^{-1}.

The 1393 and especially the 1377 cm^{-1} band showed relative variations in the peak intensity depending on the different reaction conditions, suggesting that different species contributes to the band observed at 1377 cm^{-1}.

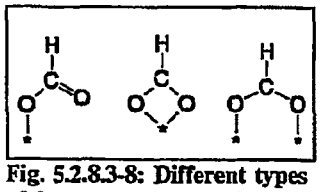

Fig. 5.2.8.3-8: Different types of formate structures /214/.

In agreement with previous studies /189,207/, it is believed that the bands at 1595 and 1377 cm^{-1} can be ascribed to the asymmetric and symmetric O-C-O stretching vibrations of adsorbed formate species. Possible structures are

depicted in Fig. 5.2.8.3-8, being of the type unidentate, bidentate or bridged formate. The C-H deformation mode of the surface formate species is suggested to be responsible for the 1393 cm^{-1} band. Support for these assignments is found upon the adsorption of formic acid on Ru/Al_2O_3 /189/, resulting in bands at 1585, 1392 and 1378 cm^{-1}. The appearance of these formate structures during a "single cell" experiment, in which H_2 and CO was reacted over γ-Al_2O_3 alone, indicate that cobalt metal does not have to be a necessary prerequisite for the formation of these adspecies. Furthermore, the intensity of these bands was higher over blank alumina than on 4.6% Co/γ-Al_2O_3, suggesting that cobalt may block adsorption sites required by the formate species. The positions of the bands are the same on both 4.6% Co/γ-Al_2O_3 and γ-Al_2O_3 alone, and due to the inertness of the bands when exposed to either helium and hydrogen, this may suggest that they are located on the support. Thus, it would seem that the formate bands are formed directly on the alumina support by interactions between H_2 and CO, or between carbon monoxide and surface hydroxyl groups of alumina.

Which type of formate compounds giving rise to the observed infrared bands can be determined using the frequency separation between the 1595 and 1377 cm^{-1} peaks. Differentiation between the different formate types is done by considering the separation in wavenumbers between the asymmetric and symmetric O-C-O stretching frequencies. In the case of bidentate, monodentate and the free formate ion, it has been suggested that the frequency separation between $\gamma\ (O\text{-}C\text{-}O)_{asy}$ and $\gamma\ (O\text{-}C\text{-}O)_{sy}$ should decrease in the order monodentate formate > free formate > bidentate formate /214/. Applying the empirical approach on the asymmetric and symmetric O-C-O frequencies at 1595 and 1377 cm^{-1} gives a separation of 218 cm^{-1}, suggesting a bidentate rather than a unidentate attachment to the surface.

The band located at 1458 cm^{-1} on 4.6% Co/γ-Al_2O_3 at 473K and 523K, but which is poorly resolved on blank γ-Al_2O_3, is in the position normally expected for unidentate carbonate complexes /210/. Thus, it may seem reasonable to assign the 1458 cm^{-1} band to the asymmetric $O_I\text{-}C\text{-}O_{II}$ stretching vibration of such a carbonate. The corresponding symmetric stretching frequency is expected around 1380-1350 cm^{-1}, and is probably hidden under the strong 1377 cm^{-1} formate band, or it may also contribute to the observed band. The decrease in intensity of the 1377 cm^{-1} peak observed on γ-Al_2O_3 alone can therefore be explained by the assignment of the bands (at 1458 and 1377 cm^{-1}) to the asymmetric and symmetric $O_I\text{-}C\text{-}$

O_n stretching vibrations of the unidentate complex, respectively. The 1458 cm^{-1} band on γ-Al_2O_3 is relatively weak, contrary to on 4.6% Co/γ-Al_2O_3, and consequently, the intensity of the 1377 cm^{-1} band is reduced relative to the 1393 cm^{-1} peak /207/.

In keeping with the preceding assignments of bands found in similar positions on 4.7% Co/SiO_2, one should also be aware of the possibility of CH deformation (in CH_2 and CH_3 groups) being the reason for or contributing to the 1458 cm^{-1} band.

The 1458 cm^{-1} band is also in such a position which, in principle, allows it to be attributed to at least two alternate (additional) adspecies, a simple carbonate ion, CO_3^{2-} or a carboxylate species.

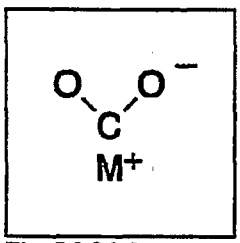

Fig. 5.2.8.3-9: Structure of carboxylate species /142/.

The carboxylate species can be envisioned as being formed on the surface by adsorption of carbon dioxide, possibly on a metal ion by the transfer of an electron from the adsorbent to the adsorbate /210/, see Fig. 5.2.8.3-9. The asymmetric and symmetric C-O stretching vibrations are typically located in the 1580-1560 cm^{-1} and 1400-1350 cm^{-1} range, while the (O-C-O) torsional vibration is usually observed at about 650 cm^{-1} /142,210/. The observed 1458 cm^{-1} band could therefore be proposed to arise from the symmetric C-O vibration, while the high frequency band (asymmetric C-O stretching vibration) could probably be included in or hidden by the strong, broad 1595 cm^{-1} formate band. Applying deconvolution procedures on the 1595 cm^{-1} peak resulted in an absorption band located near 1570 cm^{-1}.

An alternative assignment for the 1458 cm^{-1} band could be a simple carbonate ion, CO_3^{2-}, which has been reported to have infrared absorption bands in the spectral range 1450-1420 cm^{-1} /97,142/. Thus, the 1458 cm^{-1} band may also arise from this carbonate like structure, believed to be a result of matrix (MgO) stabilization of CO_2 /194/:

$$O^{2-} + CO_{2_{(g)}} \rightarrow CO_3^{2-} \qquad 5.14$$

Absorption bands in the region 1700-1600 cm^{-1} were observed at 1620 cm^{-1} (on 4.6% Co/γ-Al_2O_3) and 1665 cm^{-1} (on γ-Al_2O_3 alone). Also, the intensity of the 1665 cm^{-1} band was

noticeably lower than that of the 1620 cm^{-1} band. The presence of the 1665 cm^{-1} band was always accompanied by the appearance of the 1321 cm^{-1} band. Due to the parallel behaviour of the 1665 and 1321 cm^{-1} bands with time in synthesis gas, as illustrated in Fig. 5.2.8.3-3, it is suggested that they belong to the same adspecies, and that the 1620 cm^{-1} band can be associated with another species.

The band frequencies at 1665 and 1321 cm^{-1} could indicate the presence of a bidentate carbonate, even though the band position (for the low frequency band) lie slightly outside the range predicted for this kind of carbonate complexes /210/. Two possible types of the carbonate complex structures are shown in Fig. 5.2.8.3-10 /142/; bridged and bidentate.

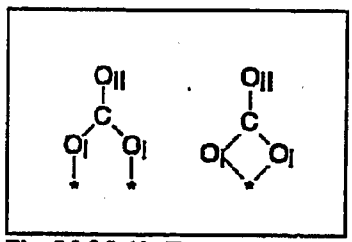

Fig. 5.2.8.3-10: Two types of bidentate carbonate structures /142/.

The separation of the features arising from the difference in the C-O_I and C-O_{II} stretching vibrations is used as a criterion to distinguish between these two modes of coordination and in addition, between the free carbonate ion (CO_3^{2-}) and unidentate carbonate. There would be no separation for a simple carbonate ion, *ca.* 100 cm^{-1} for the unidentate carbonate species and over 200-300 cm^{-1} for the bidentate structures and the bridged carbonate complex /210,215/. Based on the frequency separation, it seems reasonable to assign the 1665 cm^{-1} band to the C-O_{II} stretching and the 1321 cm^{-1} band to the asymmetric C-O_I stretching frequencies either in bidentate carbonate or bridged carbonate complexes. Since the two active centres is believed to induce a higher degree of frequency separation compared to a single point of attachment, the 1665 and 1321 cm^{-1} absorption bands are tentatively assigned to the bridged carbonate complex. The corresponding symmetric C-O_I stretching and out-of-plane bending of the bidentate carbonate is expected near 1040-1020 cm^{-1} and 840-820 cm^{-1}, respectively. The observation of both of these bands is unfortunately precluded by the progressive absorption of the alumina support in this region.

Another species which may require some consideration is that derived by comparison with the bicarbonate-ion, as shown in Fig. 5.2.8.3-11. Studies /216,217/ have on the basis of bands observed in the 1650-1630 cm^{-1} and 1390-1330 cm^{-1} region suggested this carbon monoxide containing complex. Compared to the frequencies observed in the present study, a structure

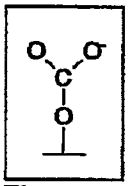

Fig. 5.2.8.3-11: Bicarbonate species /210/.

similar to that in Fig. 5.2.8.3-11 could suggestedly give rise to the 1665 cm^{-1} band (asymmetric O-C-O stretching vibration) and to one of the bands in the 1390-1330 cm^{-1} spectral range (symmetric O-C-O stretching vibration).

The 1620 cm^{-1} band could also be attributed to a bicarbonate species of the form $l\text{-}O\text{-}CO_2^-$. The corresponding low frequency band should be expected around 1390 cm^{-1}, and could possibly be included in the 1377/1395 cm^{-1} formate peak. Little et al. /217/ assigned these two bands to interaction of CO or CO_2 with surface hydroxyl groups resulting in a $H\text{-}O\text{-}CO_2^-$ structure.

A complexity of bands develop during CO hydrogenation in the range 3900-3400 cm^{-1}. Bands in this region are generally attributed to surface bound hydroxyl groups and chemisorbed water. The bending mode of adsorbed water is normally expected to be located in the region 1640-1600 cm^{-1}. Hence, the peak at 1620 cm^{-1} can possibly be due to the deformation mode of water. Such an assignment would be in agreement with previous studies, reporting the bending mode of adsorbed water at 1630 cm^{-1} /108/ and 1640 cm^{-1} /218/.

The 1620 cm^{-1} band is in an intermediate position between the frequencies given for bridged carbonate and bidentate carbonate /219/; 1620-1530 cm^{-1} (C=O), 1270-1250 cm^{-1} (O-C-O) and 1670-1620 cm^{-1} (C=O), 1270-1220 (O-C-O), respectively. The required low frequency band could not be observed in the spectra after prolonged exposure to synthesis gas, except in Fig. 5.2.8.3-5, where a weak band is visible at 1231 cm^{-1}. Thus, a definitive assignment for the 1620 cm^{-1} band can not be given.

In summary, the infrared spectra in Fig. 5.2.8.3-1 to 5.2.8.3-4 indicate the formation of monodentate carbonate species on 4.6% $Co/\gamma\text{-}Al_2O_3$, but not on $\gamma\text{-}Al_2O_3$ alone. On the other hand, bridged carbonate complexes are formed to a higher extent on the alumina support than on the alumina supported cobalt catalyst. King /207/, reporting a similar situation for alumina and alumina supported Ru, suggested that the bidentate carbonate could be converted to the monodentate form in the presence of water (from the Fischer-Tropsch reaction):

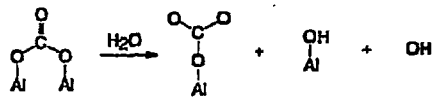

5.15

That there is a difference between the type of carbonate formed on γ-Al_2O_3 and 4.6% Co/γ-Al_2O_3 is contradicted by the spectra presented in Fig. 5.2.8.3-5 and 5.2.8.3-6, showing the presence of both the 1665 and 1620 cm^{-1} bands. The spectra in Fig. 5.2.8.3-5 does indicate, however, that the formate and carbonate compounds are adsorbed on the alumina support. Once formed, they appear to be quite stable and little influenced by treatment with He and hydrogen.

The formation of bidentate formate can be envisaged to occur according to equation 5.16:

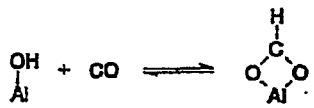

5.16

while interaction between CO_2 and the surface hydroxyl groups of alumina, or decomposition of formate, could result in carbonate formation.

An experiment was conducted, in which the reaction temperature was raised from 473K to 573K (2K/min) during CO hydrogenation (H_2/CO=2, P_{Tot}= 6 bar), followed by subsequent cooling (2K/min) to 473K in H_2/CO. The experimental procedure included a 30 min. dwell period at 473, 523 and 573K.

The effect of increasing temperature upon the bands in the 1750-1250 cm^{-1} region is illustrated in Fig. 5.2.8.3-12 to 5.2.8.3-14. By considering Fig. 5.2.8.3-12 and 5.2.8.3-14, a number of temperature dependent features can be observed.

The band intensities increase with time in synthesis gas at 473 and 523K, resembling the development shown in Fig. 5.2.8.3-1. An increase in the CO hydrogenation temperature resulted generally in increasing intensity of the absorption bands. Also, a distinct although weak absorption band at 1306 cm^{-1} develop with increasing reaction temperature (from 473 to 573K). The shoulder (at 1620 cm^{-1}) on the intense formate peak seems to get less resolved

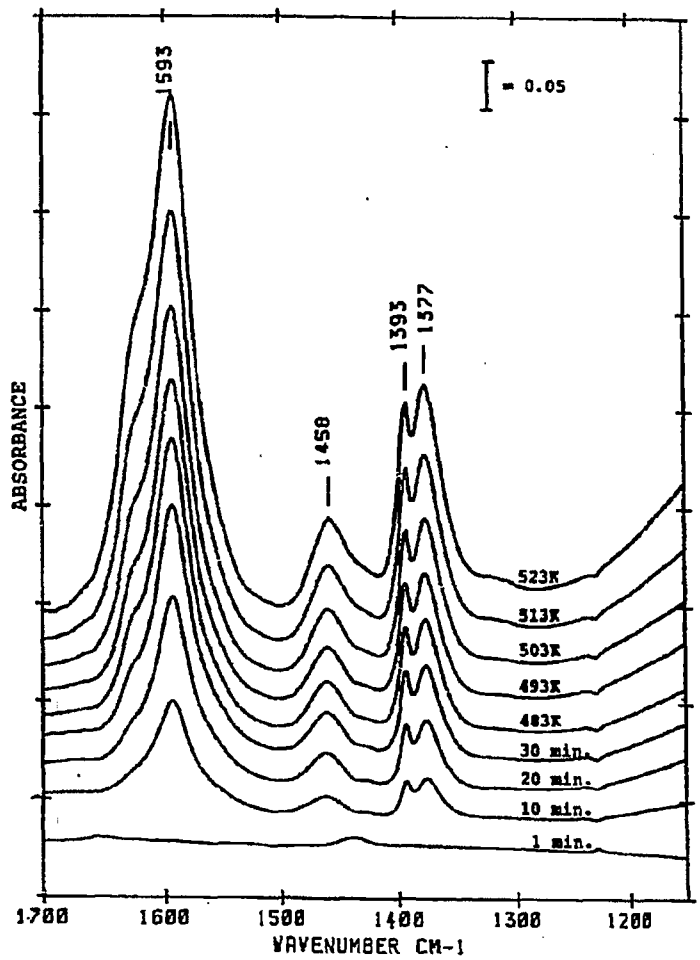

Fig. 5.2.8.3-12: **Infrared spectra of 4.6% Co/γ-Al_2O_3 at different times in synthesis gas at 473K and during heating to 523K (in H_2/CO).**

Heating rate: 2K/min.

The times and temperatures indicated represent those at which collection of interferograms was initiated.

CO hydrogenation conditions:
P_{Tot} = 6 bar, H_2/CO = 2, 100 Nml/min.

Fig. 5.2.8.3-13: Infrared spectra of 4.6% Co/γ-Al_2O_3 at various times in synthesis gas at 523K and during heating to 573K (in H_2/CO).

a: 1 min. (at 523K)
b: 10 min. (at 523K)
c: 20 min. (at 523K)
d: 30 min. (at 523K)
e: 533K
f: 543K
g: 553K
h: 563K
i: 573K

Heating rate: 2K/min.

CO hydrogenation conditions:
P_{Tot} = 6 bar, H_2/CO = 2, 100 Nml/min.

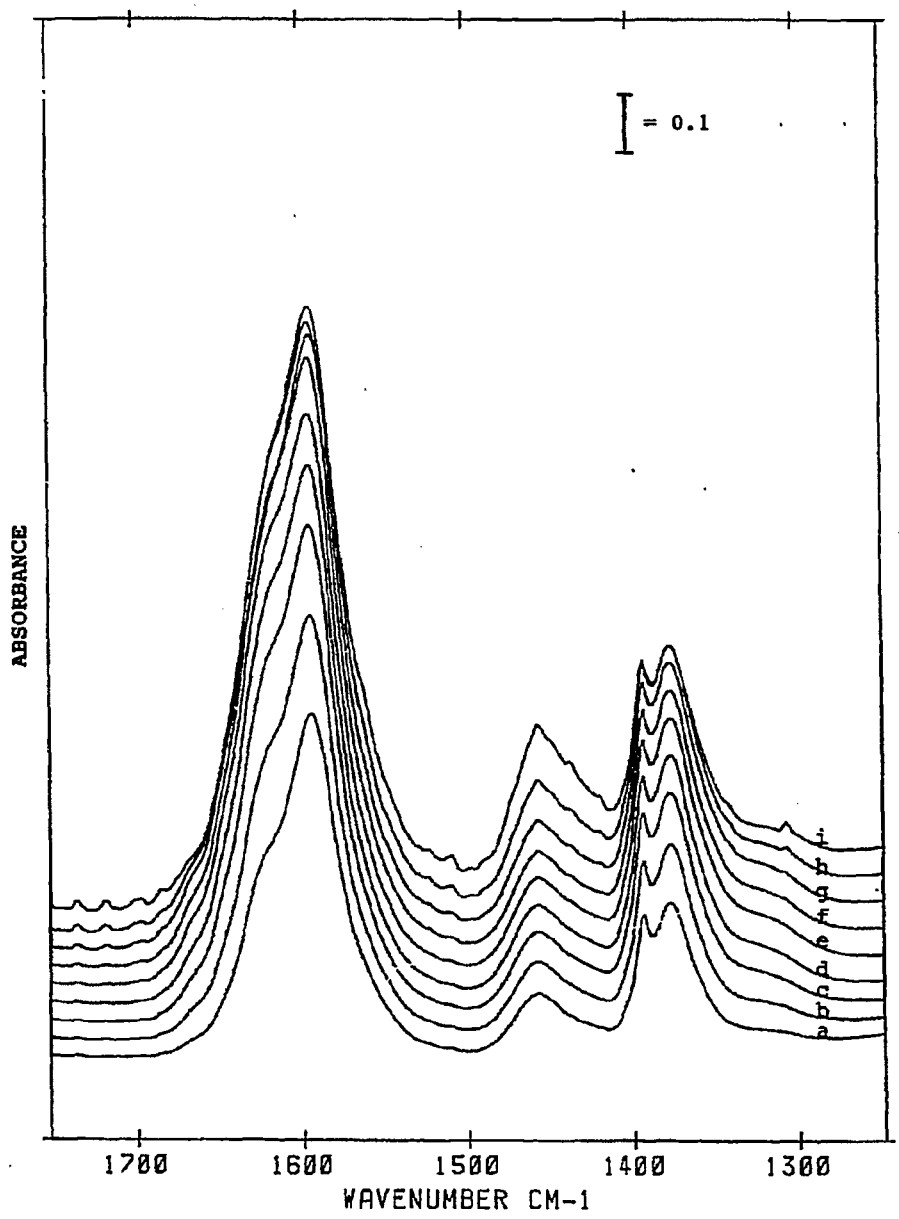
= 0.1
ABSORBANCE
1700
1600
1500
1400
1300
WAVENUMBER CM-1
i
h
g
f
e
d
c
b
a

Fig. 5.2.8.3-14: Spectra of 4.6% $Co/\gamma-Al_2O_3$ at various times in H_2/CO at 573K.

a: 1 min.
b: 10 min.
c: 16 min.
d: 24 min.
e: 30 min.

The times indicated represent those at which IR scanning was started.

CO hydrogenation conditions:
P_{Tot} = 6 bar, H_2/CO = 2, 100 Nml/min.

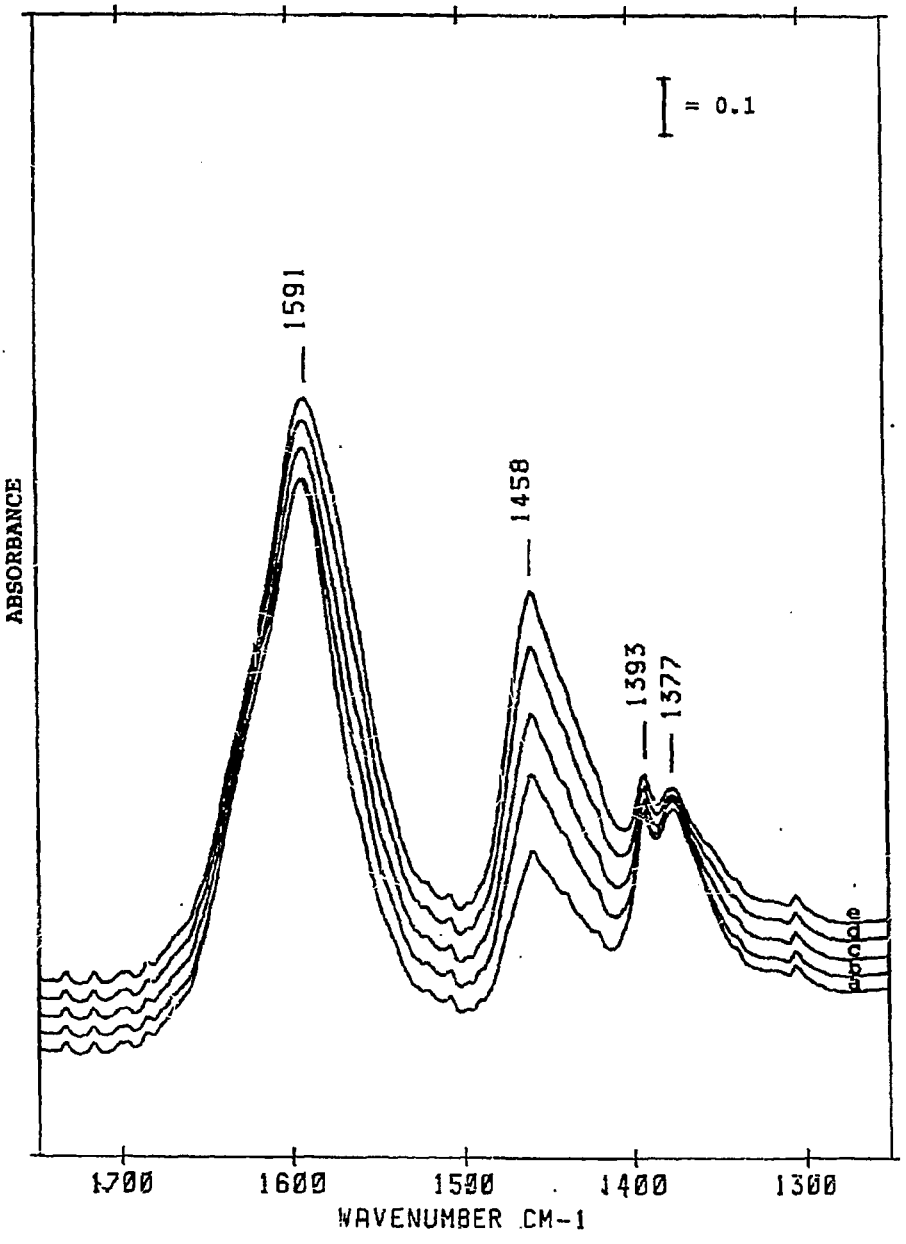
= 0.1
1591
1458
1393
1377
ABSORBANCE
1700
1600
1500
1400
1300
WAVENUMBER CM-1

as the reaction temperature is increased. Except for the 1306 cm^{-1} band, no new bands appear or none of the existing bands really disappear during the heating procedure.
The *major* increase in the intensity of the 1458 cm^{-1} band did not, however, occur during the temperature increase, but with time in H_2/CO at 573K, as shown by way of illustration in Fig. 5.2.8.3-14. At this temperature, the 1393 and 1377 cm^{-1} band intensities decrease. The intensity of the 1377 cm^{-1} band decrease at a faster rate compared to the band at 1393 cm^{-1}.

The 1595, 1393 and 1377 cm^{-1} peaks have previously been assigned to bidentate formate. If the decrease in the 1393 and 1377 cm^{-1} bands indicate decreasing amounts of the formate species, a similar behaviour would be expected for the high frequency band (at 1595 cm^{-1}). The intensity of this band remained relatively unaltered with time in synthesis gas at 573K. Thus, it does not seem likely that the decrease in the 1393 and 1377 cm^{-1} peaks reflects a decrease in the amount of bidentate formate at higher temperatures, due for example to decomposition or desorption.
Neither is it believed that the behaviour of these two bands represents formate interconversion, i.e. bidentate to monodentate formate. Since the frequency separation between the asymmetric O-C-O and symmetric O-C-O vibrations is more pronounced for the unidentate than bidentate type of formate, one would expect the appearance of bands in different positions corresponding to a larger frequency splitting. In this respect, it is difficult to reconcile a surface rearrangment from bidentate to monodentate formate as being responsible for the observed decrease in the intensities of the 1393 and 1377 cm^{-1} bands.

The band near 1620 cm^{-1} has previously been suggested to be caused by bicarbonate species. The corresponding O-C-O symmetric vibration would be expected near 1390 cm^{-1}. The decrease in the intensity of the 1393/1377 cm^{-1} band parallels the disappearance of the high frequency shoulder (at 1620 cm^{-1}) on the 1595 cm^{-1} formate peak. The simultaneous attenuation of these bands may point towards decomposition or desorption of the bicarbonate species due to the high temperature. Heating of the catalyst would cause a progressive elimination of the surface hydroxyl groups and adsorbed water. If the bicarbonate species can be said to have the structure $HO\text{-}CO_2^-$, as proposed by Little et al. /217/, increasing dehydroxylation of the 4.6% $Co/\gamma\text{-}Al_2O_3$ catalyst may possibly explain the behaviour of the 1620 and 1393/1377 cm^{-1} bands.

Unidentate carbonate has been suggested to be present on the surface of the 4.6% $Co/\gamma\text{-}Al_2O_3$ catalyst based on the 1458 cm^{-1} band and the decrease in the 1377 cm^{-1} peak intensity on alumina alone. An increase in the 1458 cm^{-1} band intensity would be expected to be accompanied by an increase in the 1377 cm^{-1} band, since the 1458 cm^{-1} band has been ascribed to the asymmetric C-O stretching vibration and a band, probably included in the 1377 cm^{-1}, to the symmetric vibration. This seems not to be the case, and it is therefore not likely that the changes in the 1458 cm^{-1} can be associated with the unidentate carbonate species.

One could speculate whether the high temperature induce surface rearrangements of existing carbonates. As previously discussed, there is an uncertainty in whether to assign the 1620 cm^{-1} band to bridged or bidentate carbonate, or to carbonate at all. A rearrangement of the type

5.17

could tentatively be proposed. An increasing fraction of bidentate carbonate would be expected to result in increasing absorption in the range 1620-1530 and 1270-1250 cm^{-1}. Even though very weak shoulders can be observed in the 1570-1500 cm^{-1} region (Fig. 5.2.8.3-13 and 5.2.8.3-14), such a surface rearrangement does not seem very likely in the present case. This is due to the fact that there appears no absorption bands in the range 1270-1250 cm^{-1}, and the lack of the low frequency band (belonging to bridged carbonate).

Since the 1377 cm^{-1} peak has been proposed to envelope the symmetric O-C-O stretching vibrations of bidentate formate and that of the unidentate complex, the increase in the 1458 cm^{-1} band intensity with time in synthesis gas would not be expected to be accompanied by a decrease in the 1377 cm^{-1} band. This raises the question whether the increased intensity of the 1458 cm^{-1} band can be related to the direct or indirect effect of deposition of carbon or carbonaceous materials. As shown in Chapter 5.2.5, bands near 1458 cm^{-1} have been assigned to the CH_3 deformation of adsorbed hydrocarbons. Thus, one could possibly attribute this peak

to a partially hydrogenated carbonaceous deposit. Anderson et al. /220/ reported a band in a similar position to C-H deformation in CH_2 or CH_3 groups, but their spectra indicate a considerable lower peak absorptivity than observed in Fig. 5.2.8.3-14. Deposition of carbon (by exposure to acetylene) on alumina at 525K was by Eischens /221/ found to result in absorption bands near 1580 and 1470 cm^{-1}. It was suggested that carbon in the deposit combined with oxygen from the alumina to form the carboxylate like species.

Previously in this section, the 1458 cm^{-1} band was assigned to carboxylate species or a simple carbonate ion, CO_3^{2-}. An increase in the band intensity may imply higher concentration of CO_2. Carbon dioxide can be formed from Boudouards reaction, by the water-gas shift reaction, by reaction of excess carbon monoxide with surface oxygen or by decomposition of the formate compounds. The CO_2 formed can either desorb, adsorb directly in the form of carboxylate species or it can be stabilized by reaction with the partly basic alumina support, resulting in a simple carbonate ion. The spectra indicate a higher intensity of the gas phase CO_2 (at 2369 and 2324 cm^{-1}) with increasing temperature. Whether this is due to enhanced CO disproportionation or contributions from the water-gas-shift reaction is not clear. The water-gas-shift reaction will probably not be in equilibrium with the applied reaction conditions and catalysts. The amount of CO_2 will depend on the partial pressure of water, which again will be related to the conversion of CO. Since the conversion is believed to be rather low due to the high space velocity [255320 Nml ($CO + H_2$)/g catalyst·h], it is doubtful whether the increased intensity of the 1458 cm^{-1} band can be ascribed to CO_2 formed in the water-gas-shift reaction.
Even though reasons for the increased intensity of the 1458 cm^{-1} band have been proposed and discussed, it is felt that a conclusive explanation for its behaviour has not been offered.

One final aspect of the observed behaviour of the bands in Fig. 5.2.8.3-12 to 5.2.8.3-14 deserves some attention. As previously mentioned, a band located at 1306 cm^{-1} appears at 543K. The intensity of this band increased with increasing temperature up to 573K, after which it remained relatively unaffected by prolonged exposure to syngas. This band also appears at the same temperature in the spectra recorded of alumina alone (placed downstream of the catalyst disk). It would be a minor problem to fit this band to the previous discussed formates/carbonates complexes, since its appearance and behaviour in a convenient way can

be related to those structures. However, the behaviour of the 1306 cm^{-1} band coincides with the band observed at 3017 cm^{-1}, earlier attributed to gas phase methane. Gaseous methane is expected to have Q branches at approximately 3017 and 1306 cm^{-1} accompanied by vibration-rotation P and R lines. Hence, it is felt that the new absorption band at 1306 cm^{-1} best can be explained by the vibrational-rotational structure of $CH_{4(g)}$.

The spectra obtained during heating of the alumina reference disk (placed downstream of the alumina supported catalyst disk) to 573K in synthesis gas is presented in Fig. 5.2.8.3-15. The intensity of the bands generally increased with increasing temperature, parallel to the situation in Fig. 5.2.8.3-12 to 5.2.8.3-14. Analogous to the separate experiments carried out at 473 and 523K discussed earlier in this section, the intensity of the 1595, 1393 and 1377 cm^{-1} was more intense over γ-Al_2O_3 compared to on 4.6% Co/γ-Al_2O_3 at all three temperatures.

Upon an increase in the reaction temperature from 473K to 523K, the intensity of the 1663 and 1323 cm^{-1} bands developed synchronously. This indicates that they belong to the same adspecies, thus confirming the earlier assignment of these bands to a bridged bidentate carbonate complex.

Also, the intensity of the 1458 cm^{-1} band on γ-Al_2O_3 lack the temperature and time dependent behaviour as was observed for the band over 4.6% Co/γ-Al_2O_3. The bands at 1458, 1393 and 1377 cm^{-1} were quite stable with time in synthesis gas at 573K, differing from the observed behaviour of these bands on 4.6% Co/γ-Al_2O_3.

Fig. 5.2.8.3-15: Infrared spectra of γ-Al_2O_3 (placed downstream of the sample cell) during heating to 573K.

A) Spectra recorded at various times in H_2/CO at 473K and while increasing the reaction temperature (2K/min.) to 523K.

B) γ-Al_2O_3 at various times in H_2/CO at 523K and during heating (2K/min.) to 573K.

C) Spctra recorded as a function of time in synthesis gas at 573K.

CO hydrogenation conditions:
P_{Tot} = 6 bar, H_2/CO = 2, 100 Nml/min.

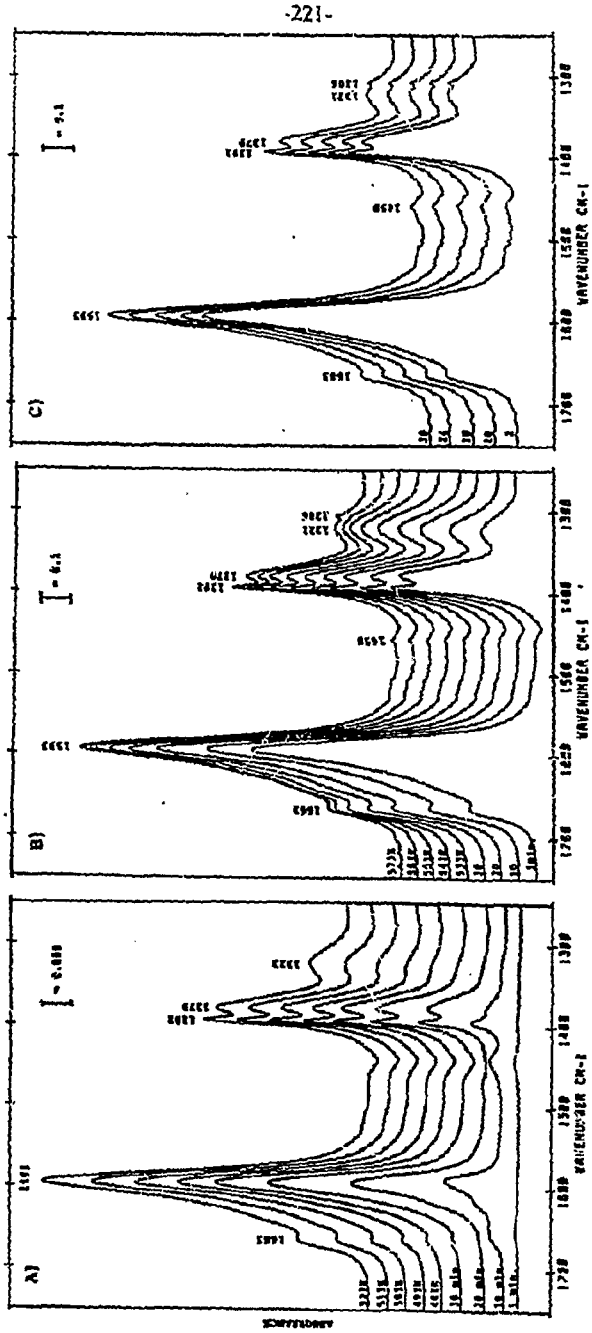
A)
B)
C)
WAVENUMBER CM-1

5.3. CATALYTIC ACTIVITY AND SELECTIVITY

5.3.1. Introduction

The determination of catalytic activity and selectivity was performed in both the combined microbalance/microreactor apparatus (described in Chapter 4.5) and in the microreactor apparatus described in Chapter 4.4.

The results reported below were obtained in the microreactor. The investigated catalysts were 1% and 4.6% Co/γ-Al_2O_3 and 4.7% Co/SiO_2. Data for the low metal loading silica supported catalyst, 0.82% Co/SiO_2, is not available. Since the dispersion is only known for the 4.6% Co/γ-Al_2O_3 catalyst, the activity is expressed as mole CO converted/g Co-s. Even though such a presentation provides little information about the active site itself, it does provide a common foundation for comparison of the activity of the different catalysts.

5.3.2. CO hydrogenation activity and selectivity of silica and alumina supported cobalt catalysts

Fig. 5.3.2-1 and 5.3.2-2 shows the activity of 4.7% Co/SiO_2 and 4.6% Co/γ-Al_2O_3, respectively, with time during CO hydrogenation at 523K. As can be seen from the figures, the activity of the investigated catalysts is of the same order of magnitude. However, there is a different time dependent behaviour for the silica and the alumina supported cobalt catalysts. At an early stage of reaction, the activity of the 4.7% Co/SiO_2 catalyst is higher than that of the alumina supported 4.6% Co-catalyst. With increasing time on stream, the silica supported catalyst experienced a continuing decrease in activity, while the opposite behaviour could be observed for 4.6% Co/γ-Al_2O_3.

In addition to 4.7% Co/SiO_2 and 4.6% Co/γ-Al_2O_3, the CO hydrogenation activity of the 1% Co/γ-Al_2O_3 catalyst was also investigated as a function of time. After prolonged exposure to synthesis gas at 523K, the activity of the 1% Co/γ-Al_2O_3 catalyst is lower than the CO hydrogenation activities reported in Fig. 5.3.2-1 and 5.3.2-2. The experiment with the 1% Co/γ-Al_2O_3 catalyst was conducted with a space velocity being one-third of that applied for 4.6% Co/γ-Al_2O_3 and 4.7% Co/SiO_2.

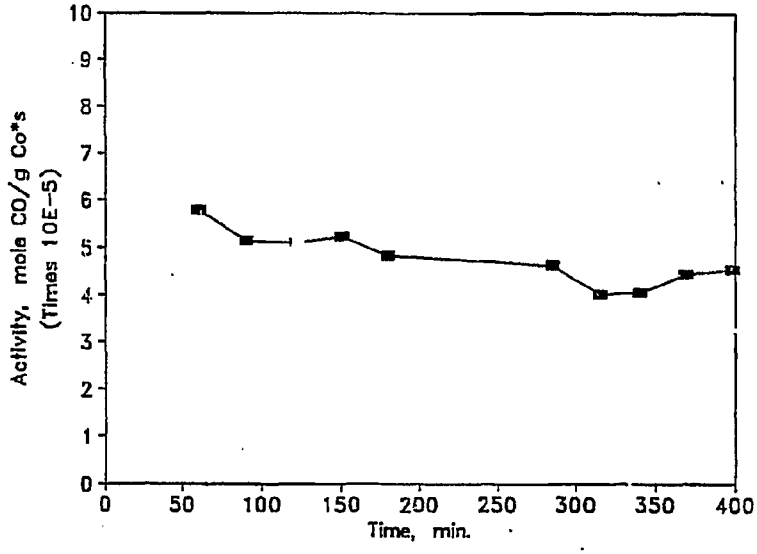

Fig. 5.3.2-1: Variation in CO hydrogenation activity with time for 4.7% Co/SiO_2. Reaction conditions: P_{Tot}= 6 bar, H_2/CO=2, T=523K.

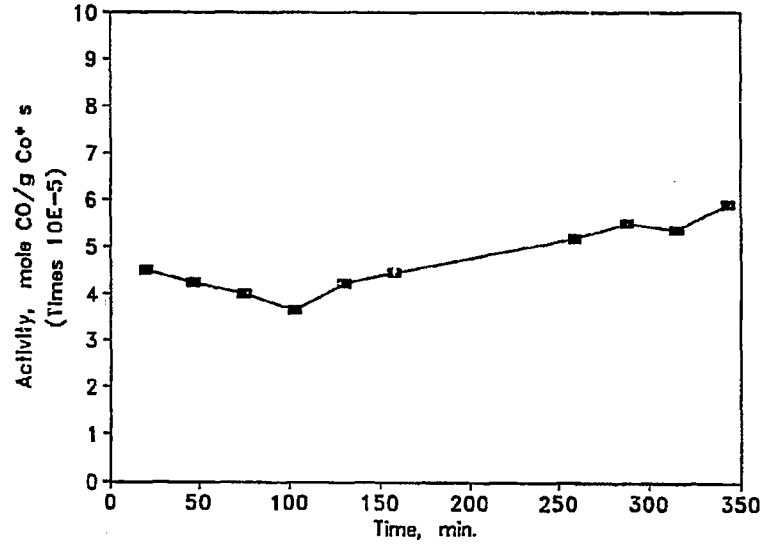

Fig. 5.3.2-2: Variation in CO hydrogenation activity with time for 4.6% Co/γ-Al_2O_3. Reaction conditions: P_{Tot} = 6 bar, H_2/CO=2, T=523K.

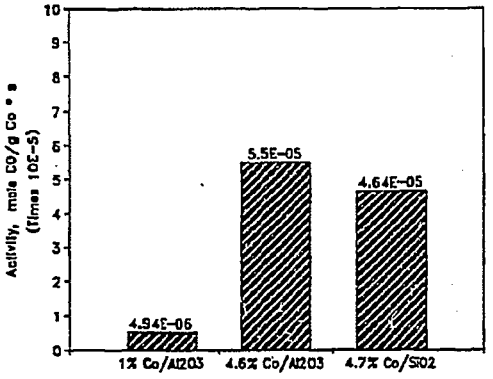

Fig. 5.3.2-3: Activity of the catalysts after 4.5 hours on stream.
Reaction conditions: 523K, 6 bar, $H_2/CO=2$

Fig. 5.3.2-3 shows the activity of the investigated catalysts after approximately 4.5 hours of reaction. The reaction rates of the high metal loading Co-catalysts, 4.6% Co/γ-Al_2O_3 and 4.7% Co/SiO_2 are compared at approximately the same conversion of CO (2%), while the CO conversion over the 1% Co/γ-Al_2O_3 catalyst at the given time of reaction was 0.17%. The activity of the low metal loading alumina supported catalyst is an order of magnitude lower compared to the other catalysts.

The activities of the supported Co catalysts are likely to be associated with the reduction peaks appearing in the TPR spectra previously shown and discussed in Chapter 5.1.

The low and almost negligible activity of 1% Co/γ-Al_2O_3 can be discussed in terms of the extent of metal-support interactions. From TPR analysis of the 1% and 4.6% Co/γ-Al_2O_3 catalysts, it was suggested that the absence of any resolved peak (on the 1% Co/γ-Al_2O_3 catalyst) due to the reduction of cobalt oxide could indicate complete diffusion of cobalt into the γ-Al_2O_3 lattice, or this peak could possibly be included in the nitrate decomposition peak. Also, the decrease in the extent of reduction with decreasing cobalt loading can be explained in light of the formation of stable surface cobalt aluminate species. UV-VIS spectra featured an absorption triplet ascribed to tetrahedrally coordinated Co^{2+} in cobalt aluminate. Of further note is that the infrared spectra of this catalyst showed the absence of absorption bands attributable to molecularly adsorbed CO during CO hydrogenation.

These observations supports the theory of inaccessible cobalt stabilized in the alumina lattice, which may explain why 1% Co/γ-Al_2O_3 is essentially inactive in the Fischer-Tropsch synthesis. When expressed in mole CO converted per gram catalyst and per second, the activity of the 1% Co/γ-Al_2O_3 catalyst is close to that obtained during CO hydrogenation over γ-Al_2O_3 alone /222/. Even though the low loading alumina supported catalyst can be

considered fairly inactive, trace amounts of methane, ethane, ethene and propane was still detected in the FID product analysis. Likewise, CH_4 was detected on the TCD during reaction, albeit in small amounts. This may be related to impurities, for example iron in the γ-Al_2O_3 or effects of the reactor wall.

As mentioned previously, the activity of the 4.6% Co/γ-Al_2O_3 increased with time during prolonged exposure to synthesis gas. The total extent of reduction of this catalyst was from the TPR measurements estimated to 42.1%. The continuing increase in activity during CO hydrogenation (Fig. 5.3.2-2) could, in principle, be explained by an increase in the number of adsorption sites due to additional reduction of cobalt species-probably by carbon monoxide- during the reaction. Kuznetsov et al. /86/ stated that there was a greater thermodynamic probability of reducing cobalt oxides in CO than in H_2. A similar conclusion was reached by Rosynek et al. /51/ to account for the observed increase in Co^0 after 4 hours exposure of an uncalcined, silica supported cobalt catalyst to H_2/CO at 523K.
A further reduction of cobalt species ought to result in an increase in the intensity of the principal CO band at 2050 cm^{-1}, ascribed to linearly adsorbed CO. Even though the quality of the infrared spectra after subtraction of the gas phase CO to some extent precluded an exact determination of the behaviour of the linear CO band, the intensity of the 2050 cm^{-1} band remains approximately unchanged during reaction. Thus, it is not possible, from the infrared data alone, to unambigously verify the assumption of increasing reducibility of cobalt species as an explanation of the increasing activity with time in H_2/CO.

A decrease in catalytic activity with time, as observed for the 4.7% Co/SiO_2 catalyst in Fig. 5.3.2-1, is generally associated with deactivation of the catalyst. In this context, two effects are frequently discussed, namely (pore) diffusion limitations and the formation of carbon or carbonaceous deposits.
By considering Fig. 5.3.2-1, one can assume that a reasonable explanation for the decrease in activity with time can be the formation of carbon, for instance during carbon monoxide disproportation or dissociative adsorption of carbon monoxide. Catalyst deactivation would result as a consequence of the formation of inactive carbon or for example metal carbides. The blockage of active sites by graphite and/or polymeric carbon was by Lee et al. /25/ found to result in a decrease in activity. Machocki /41/ stated that cobalt carbide was formed after

an induction period of about 20 hours, during which the formation of stable carbide nucleus was assumed. Niemantsverdriet et al. /223/ suggested that the time dependent behaviour of cobalt catalysts could be explained by considering the activation energies for diffusion of carbon into the metal and the CO hydrogenation reaction. The lower activation energy for the Fischer-Tropsch reaction (27±4.4 kcal/mole) compared to that of carbon diffusion (34.7 kcal/mole) could mean a higher Fischer-Tropsch reaction rate, resulting in a progressive loss of catalytically active sites with time in synthesis gas.

The observed decline in the activity of 4.7% Co/SiO_2 during prolonged exposure to synthesis gas could be explained by the accumulation of liquid hydrocarbons in the catalyst pores. The liquid hydrocarbons may retard the rate of reaction by slowing down the mass transport of hydrogen and carbon monoxide within the pores. The accumulation of liquid hydrocarbons in a catalyst pore was treated mathematically by Huff et al. /224/. The effects of reaction variables such as temperature, pressure, chain growth probability, etc. were reported. Using these results and the estimated chain growth probability in the present study, typically of the order of 0.6-0.7, it can be shown that the predicted time to fill the first pore is considerably longer (> 25 h) than the duration of the experiment reported in Fig. 5.3.2-1. One may suggest that intraparticle pore-diffusion limitations due to accumulation of liquid products do not prevail at an early stage of reaction, but may become more significant in terms of retardation of the reaction rate with extended time on stream.

The effect of water should also be noted when reasons for decreasing acitvity with time is being discussed. One may envisage two effects of water:

Firstly, water vapour may influence the state of the metal during prolonged exposure to synthesis gas. Since the hydroxyl groups may act as oxidizing agents, water formed during the CO hydrogenation reaction could influence the cobalt species present on the surface, for example by partial re-oxidation of reduced cobalt, thus decreasing the Co^0/Co^{2+} ratio. Such an explanation was proposed by Rosynek et al. /51/ in order to explain differences in surface composition of the catalyst ($CoCl_2/SiO_2$) before and after exposure to synthesis gas at 523K.

Secondly, it is possible that sintering (crystalline growth) leading to a reduction of the metal surface area may occur in the presence of water. This could mean an increased ability of the metal atoms to participate in surface migration due to the presence of hydroxyl groups. Dry /26/ stated that water vapour enhanced the rate of sintering, causing loss of active surface area

and thus decreasing dispersion.
The extent of deactivation due to the effect of water will mainly depend on the ratio of P_{H_2}/P_{H_2O}. It seems reasonable to assume, in the present study, that the overall atmosphere is reducing, since a low CO conversion is obtained. This implies a partial pressure ratio >1, and it can thus be questioned whether the effect of product water will be of considerable influence in terms of induced sintering of the cobalt particles. If water vapour has any noticeable effect, its presence is rather believed to result in the formation of metal oxides /225/.

At elevated temperatures, coalescence of metal (or metal oxide) particles can occur. Since the reaction temperature (523K) was lower than the reduction temperature (673K), it is not believed that the decreasing activity with time can be related to temperature induced sintering of the metal particles.

It can be understood that several factors can influence the deactivation process resulting in decreasing activity with time during prolonged exposure to synthesis gas. The interplay of these factors and the major contributing factor can not be determined unambigously on the basis of the presently available data.

The distribution of the hydrocarbon product selectivities could reasonably well be described by polymerization kinetics predicted by the Anderson-Schulz-Flory-model. Selected examples of ASF plots of carbon number distributions are shown in Fig. 5.3.2-4 and 5.3.2-5. The reported selectivities are normalized within the hydrocarbon fraction. This can be done since the selectivity to CO_2 in all cases was low (<1%). Hence, trends in the development of CO_2 as a function of reaction time have not been considered.

The hydrocarbon product distributions in both figures are characterized by deviations from the Anderson-Schulz-Flory distribution at low and high carbon numbers, that is at carbon cut 1, 2 and greater than 9 for 4.6% Co/γ-Al_2O_3 and 4.7% Co/SiO_2. In addition, higher fractions of C_1-C_5 hydrocarbons are evident for the 4.7% Co/SiO_2 compared to the alumina supported catalyst, while the C_{6+} fraction is higher for 4.6% Co/γ-Al_2O_3, as seen more clearly in Fig. 5.3.2-6. The IR investigations showed stronger and more distinct absorption bands at for

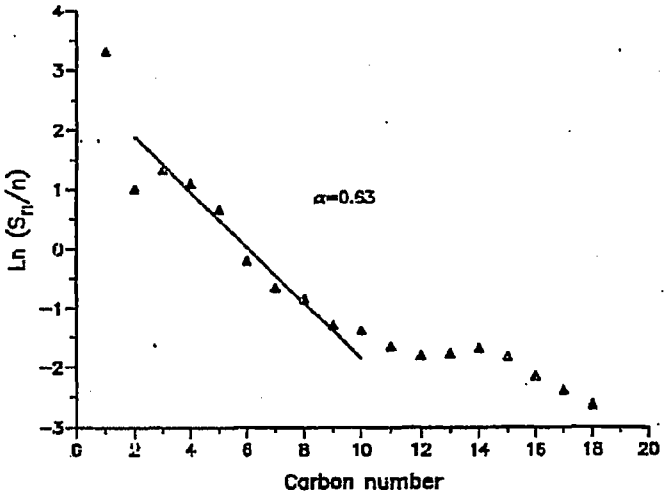

Fig. 5.3.2-4: Anderson-Schulz-Flory plot for 4.7% Co/SiO_2 at 523K, 6 bar after 435 min. of reaction.

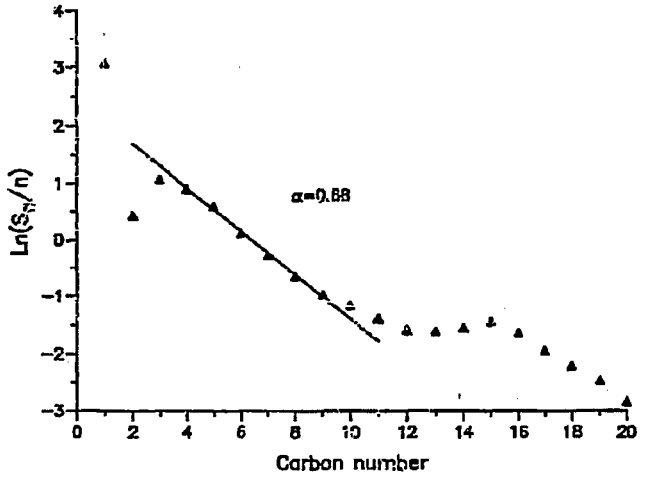

Fig. 5.3.2-5: Anderson-Schulz-Flory plot for 4.6% $Co/\gamma\text{-}Al_2O_3$ at 523K, 6 bar after 379 min. of reaction.

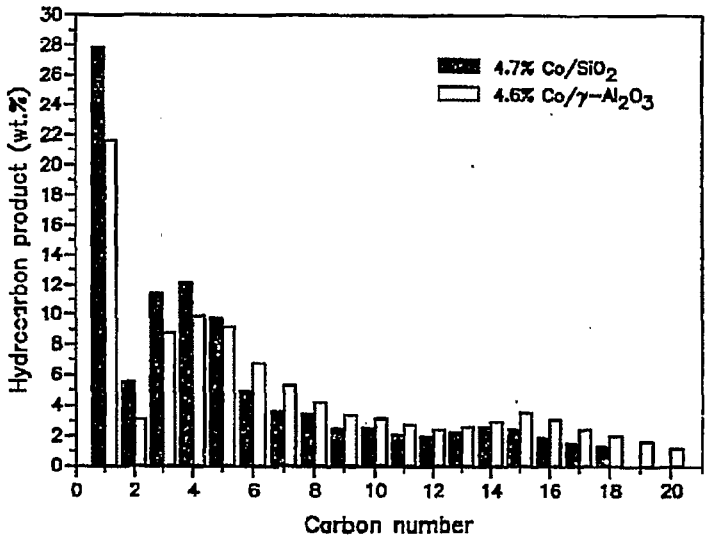

Fig. 5.3.2-6: Hydrocarbon product selectivity (wt.%) for 4.6% Co/γ-Al_2O_3 and 4.7% Co/SiO_2 at 523K, 6 bar after 379 and 435 min. of reaction.

example 3017 cm^{-1} (ascribed to methane) over the silica supported catalyst than on the alumina supported cobalt catalyst. On the other hand, Vannice /120/ stated that the higher production of methane over alumina supported Fe-catalysts compared to the silica supported was due to the less acidic character of silica.

As previously mentioned, the product distributions observed in this study are relatively consistent with ASF kinetics within a certain carbon number. It was found that the deviations for the C_{9+} carbon cuts could be explained by experimental artifacts. This could mean that condensation of higher boiling products occured in the heated lines or in the GC FID injector of the analysis system. Accordingly. the carbon balances were not very accurate.

Irrespective of the type of catalyst, a characteristic low C_2-selectivity can be observed, see Fig. 5.3.2-4 and 5.3.2-5. The C_2-value is typically lower than both the selectivity to CH_4 and

C_3. This apparent misfit in product distribution is commonly observed with Fischer-Tropsch catalysts, and several explanations have been proposed to account for it /26,121/:

* partial hydrogenolysis of C_2H_4 to CH_4
* more readily incorporation of ethylene in growing chains than the longer chained olefines
* higher probability of chain growth
* a higher oligomerization rate to higher hydrocarbons

Anderson et al. /226/ stated that C_2H_4 thermodynamically should have higher tendency to incorporate than higher carbon number olefines. Ready incorporation of C_2H_4 into Fischer-Tropsch products was indicated from the results of Smith et al. /227/, but also propene and butene was found to be incorporated in the products on a cobalt catalyst /228/.

The reason for the difference in the hydrocarbon product distribution of the two catalyst at higher carbon number ($> C_6$) is not known. The higher C_{6+} fraction of 4.6% Co/γ-Al_2O_3 may be a characteristic feature for a poorly reduced low dispersed catalyst. Bartholomew et al. /9/ correlated the hydrocarbon selectivity with the dispersion, stating that highly dispersed cobalt catalysts produced large amounts of lighter hydrocarbons. Whatever the reason for the difference in the carbon number distribution between the two catalysts, it can not be given within the confines of the limited available data.

5.4. GRAVIMETRIC INVESTIGATIONS OF 4.7% Co/SiO_2 AND 4.6% Co/γ-Al_2O_3 DURING CO HYDROGENATION

5.4.1. Introduction

The catalysts which were investigated in the combined microreactor and microbalance apparatus were 4.6% Co/γ-Al_2O_3 and 4.7% Co/SiO_2. The high pressure microbalance/micro-reactor allowed *in situ* detection of the weight changes of the catalyst sample during reaction conditions as well as the possibility of taking GC analysis of the reactor effluent. In this chapter, emphasis is put on the observed changes in the catalyst mass during CO hydrogenation over the silica and alumina supported catalysts. The intention behind the presentation of data related to catalyst activity and selectivity is merely to illustrate and substantiate trends in the experimental data and conclusions drawn from these.

As described earlier (Chapter 4.5.1), the catalyst was contained in a finely perforated stainless steel basket connected to one arm of the microbalance. In this context, several aspects are of interest. Bypass of the feed gas can not be avoided, since it is necessary with free space between the basket and the reactor wall. This is in order to achieve a freely suspended basket, avoiding contact between the reactor wall and the basket, which would result in erroneous measurements. To check and ensure that the basket was hanging freely without touching the reactor walls, two methods were applied. Firstly, by visual inspection of the quartz fiber to which the basket was connected (see Fig. 4.5.1-2 in microbalance experimental section). Secondly, when the reactor was assembled and pressure tested, tapping gently on the outside of the reactor wall while at the same time monitoring the development of the weight curve. No attempt was carried out in order to quantify the fraction of the reactant gas channelling the basket containing the catalyst.

The effect of buoyancy has to be considered, especially upon switching between different gases or during unsteady conditions (increase or decrease in the feed gas flowrate). The flow of the gas past the catalyst basket will exert a drag force, which may lead to changes in the weight curve upon changes in the reaction conditions, i.e. GHSV. Separate control experiments (blank runs) were conducted, in which the basket was filled with glass-spheres and subjected to identical experimental procedures as the catalyst samples themselves in order

to gain information about the effect of buoyancy on the weight curves upon introduction of the applied gases and weight changes which possibly can be associated with the basket itself. In the presented weight curves, small downwards "peaks" are observed at regular intervals regardless of the temperature and type of gas in the reactor. This is clearly seen in Fig. 5.4.2-1 for the experiment conducted at 723K. These "dips" in the weight curves are due to disturbances of the flow through the reactor induced by the sampling of the GC-analysis.

5.4.2. Gravimetric studies of 4.7% Co/SiO_2

Fig. 5.4.2-1 shows the effect of the reaction temperature on the weight curves obtained during CO hydrogenation over 4.7% Co/SiO_2.

At the lowest temperature investigated, 473K, a continuous weight increase with time in synthesis gas is observed. The weight curves obtained at 523 and 573K are qualitatively similar showing a relatively flat weight curve featuring negligible weight changes during the course of the run. Fig. 5.4.2-1 indicates a slightly higher amount of deposited material at 523K compared to 573K. Also, at 523K, increasing the flow of synthesis gas to 200 Nml/min. results in an weight decrease of approximately 22 mg/g Co, see Fig. 5.4.2-1.

CO hydrogenation carried out at 723K, the temperature at which the literature often report the formation of inactive carbon (graphitic carbon) shows a different progress with time compared to the other temperatures investigated. After a period of about 100 minutes without extensive buildup of deposited material, the weight curve increases steadily with time in synthesis gas, reaching approximately 470 mg/g Co immediately before introduction of helium. Reproducing the experiment at 723K resulted in a similar experimental progress of the weight curve with time in synthesis gas. The estimated rates of weight increase at the reaction temperatures 473K and 723K are given in Table 5.4.2-1.

Following exposure to synthesis gas for various lengths of time, the catalysts were flushed with either helium and then hydrogen or directly by hydrogen, in order to study the stability and reactivity of the deposited species. The effect of helium and hydrogen flushing was most pronounced at 473K, while no significant weight changes were observed at the other temperatures in either helium and/or hydrogen.

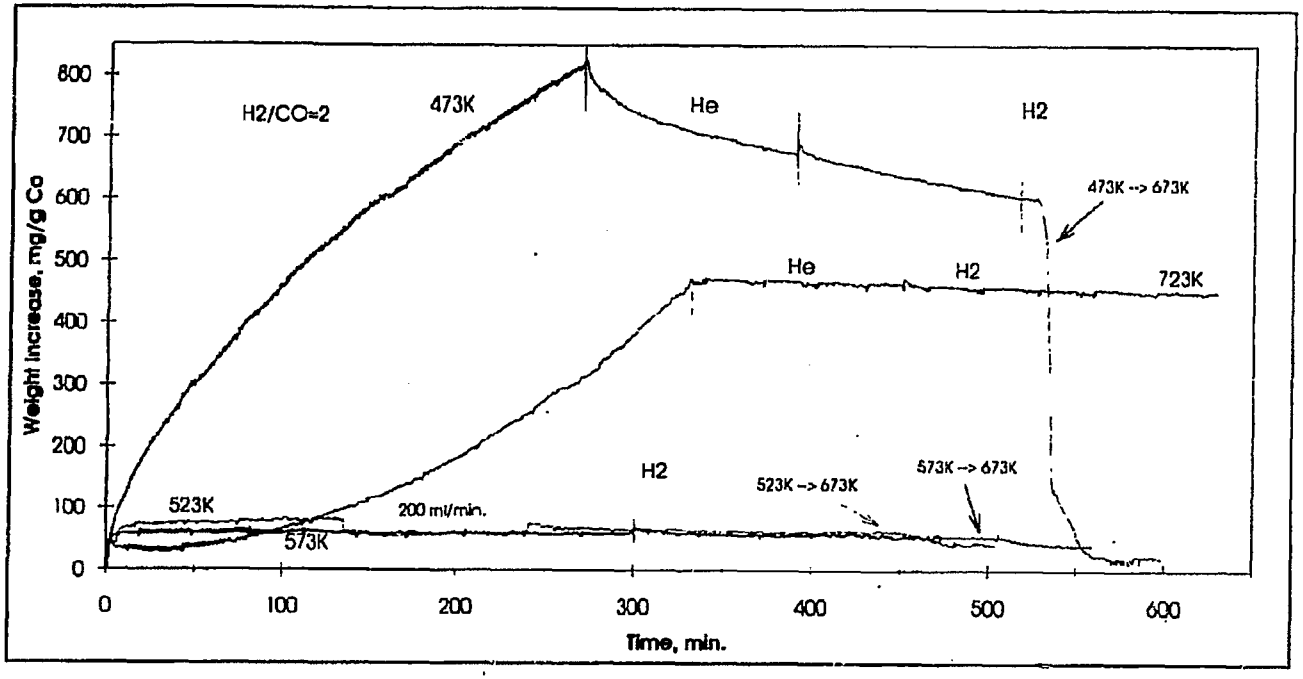

Fig. 5.4.2-1: Weight curves obtained during CO hydrogenation over 4.7% Co/SiO_2 followed by flushing with He and then hydrogen, or directly by hydrogen.

The investigated temperatures were: 473K, 523K, 573K and 723K.

CO hydrogenation conditions: P_{Tot} = 6 bar, H_2/CO = 2

Table 5.4.2-1: **Rates of weight increase for 4.7% Co/SiO_2 during CO hydrogenation.**
Reaction conditions : P_{Tot}=6 bar, H_2/CO=2.

TEMPERATURE (K) [1]	*RATE OF WEIGHT INCREASE (mg/g Co·min.)*
473	2.86 [2]
723	2.07 [3]

[1]: CO hydrogenation reaction temperature

[2]: TOS = 100 min.

[3]: TOS = 250 min.

When the reaction temperature was lower than 723K, the silica supported cobalt catalyst samples were heated to 673K (heating rate of 5K/min.) while still keeping a flow of hydrogen through the reactor. The experiments carried out at 723K were not subjected to this temperature treatment.

As can be seen from Fig. 5.4.2-1, the reaction temperature influenced the amount of the deposited material which could be removed by hydrogen treatment. Virtually all the deposited material at 473K was removed by increasing the temperature to 673K in hydrogen, while higher CO hydrogenation temperature resulted in decreasing amounts of removable species. Hydrogen treatment at 723K following CO hydrogenation at the same temperature showed no pronounced decrease in the weight curve, as was found to be the case at the lower reaction temperatures.

GC-analysis of the reactor effluent stream obtained at different temperatures during the heating process and while keeping the temperature at 673K for some time, showed mainly methane in addition to small amounts of higher hydrocarbons (C_{2+}). The fraction of higher hydrocarbons generally decreased with increasing CO hydrogenation and H_2 treatment temperature (during the linear temperature increase in hydrogen).

5.4.3. Gravimetric studies of 4.6% $Co/\gamma\text{-}Al_2O_3$

The increase in the catalyst sample mass of 4.6% $Co/\gamma\text{-}Al_2O_3$ during CO hydrogenation at 473, 523 and 573K is shown in Fig. 5.4.3-1.

Generally, increasing reaction temperature resulted in increasing amounts of deposited material, as indicated by the weight curves in Fig. 5.4.3-1. The weight curves obtained in synthesis gas can generally be divided into two regimes. A rapid weight increase occured during the first 15-20 minutes of reaction. Following this regime, a second slower regime in the deposition process took place with a different progress as a function of time.

At 473 and 523K, the weight of the catalyst sample increased steadily with time although at a lower rate and without showing any tendency of stabilization.

With a reaction temperature of 573K, however, the initial rapid weight increase is followed by a short period of time characterized by the absence of any weight increase, rather a temporary weight decrease can be observed. In the next stage, the catalyst shows an almost exponential weight increase before entering a regime similar to the second slower regime at 473 and 523K.

The applied reaction temperature influences the time location of the regimes. Increasing CO hydrogenation temperature results in a displacement of the first regime, appearing after shorter times of reaction with increasing temperature. The increasing temperature also makes the transition between the two regimes more pronounced.

Flushing with He followed by hydrogen or direct introduction of hydrogen following CO hydrogenation resulted in a weight decrease of the catalyst, with the highest weight loss occuring at the highest applied reaction temperature. Regardless of the deposition temperature, substantial parts of the adsorbed compounds could be removed by increasing the temperature to 673 or 723K (directly or stepwise) in flowing hydrogen. It is clear that increasing reaction temperature during CO hydrogenation resulted in the formation of deposits showing decreasing reactivity towards hydrogen.

Fig. 5.4.3-2 shows changes in the mass of a 4.6% $Co/\gamma\text{-}Al_2O_3$ catalyst (diluted with $\alpha\text{-}Al_2O_3$, weight dilution ratio 1:2) during CO hydrogenation at 723K. As can be seen, the weight curve lacks the two regimes appearing at the lower temperatures. Instead, an almost linear relationship between the weight increase and time of reaction is observed (after approximately 150 min. of reaction).

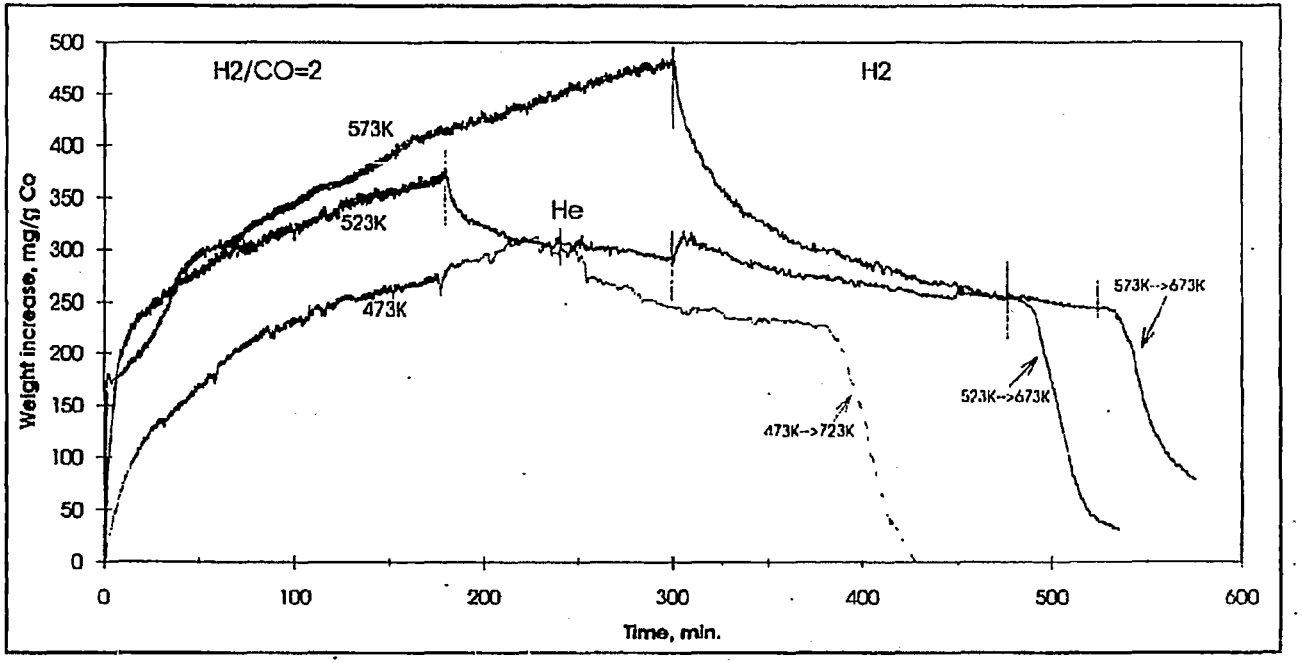

Fig. 5.4.3-1: **Weight changes observed during CO hydrogenation over 4.6% Co/γ-Al_2O_3 and subsequent flushing with He and then hydrogen, or directly by hydrogen.**

The temperatures investigated were: 473K, 523K and 573K.

CO hydrogenation conditions: P_{Tot} = 6 bar, H_2/CO = 2

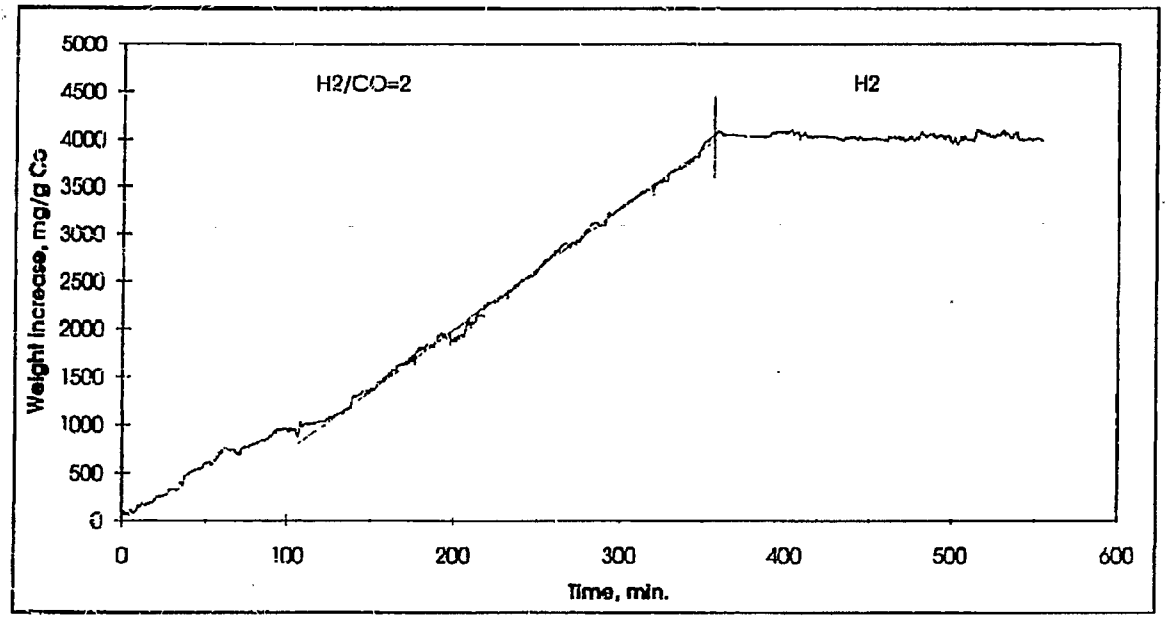

Fig. 5.4.3-2: Weight increase of 4.6% Co/γ-Al_2O_3 during CO hydrogenation and subsequent treatment with hydrogen at 723K.

CO hydrogenation conditions:
P_{Tot} = 6 bar, H_2/CO = 2

The catalyst was diluted with α-Al_2O_3 (weight ratio 1:2)

GHSV = 35003 Nml ($CO+H_2$)/g catalyst · h from 0-136 min.
GHSV = 46670 Nml ($CO+H_2$)/g catalyst · h from 136 min.

The rate of the weight increase in synthesis gas was calculated to 12.8 mg/g Co·min. The weight increase immediately before introduction of hydrogen is approximately an order of magnitude higher compared to the weight of the alumina supported catalysts in the temperature range 473-573K. Comparison with the weight curve for 4.7% Co/SiO_2 obtained at 723K (see Fig. 5.4.2-1 and Fig. 5.4.3-2) reveals at least two common features. During CO hydrogenation, the deposition process can in both cases be regarded as qualitatively similar, in the sense that the weight increase curve can be said to be of the linear form. Quantitatively, there is a pronounced difference, as deduced above. Furthermore, the reactivity of the accumulated species towards hydrogen is similar. No decrease in the catalyst masses is observed upon introduction of hydrogen and in flowing hydrogen, regardless of the time of exposure. This may imply that the materials deposited at the high temperature are "inactive" and resistant towards hydrogenation.

Fig. 5.4.3-3 shows the reaction rate (expressed as mole CO/g Co·s) at the different investigated CO hydrogenation temperatures for 4.6% $Co/\gamma\text{-}Al_2O_3$. The activity increases with increasing temperature, while it generally decreases as a function of time during the course of a run at a given reaction temperature.

A comparison of the reaction rate obtained in the microbalance at 523K to that presented in Chapter 5.3 indicates a lower activity when the experiment was conducted in the combined microbalance/microreactor mode. These discrepancies can be accounted for if the difference in the design of these two systems are taken into consideration. In the microbalance apparatus, bypass of the synthesis gas may explain the reduced conversion. In addition, a constant flow of He was maintained through the taring counter weight part of the microbalance, which also passed further down through the reactor. The amount of inert gas corresponded to 14.3 and 25% of the total feed gas, depending on the applied space velocity of the reactant flow. The flow of He will reduce the possibility of runaway upon introduction of H_2/CO and prevent condensation of reaction products, but it will also influence the partial pressures of carbon monoxide and hydrogen in the reactor. Both these aspects are expected to lead to a lower activity.

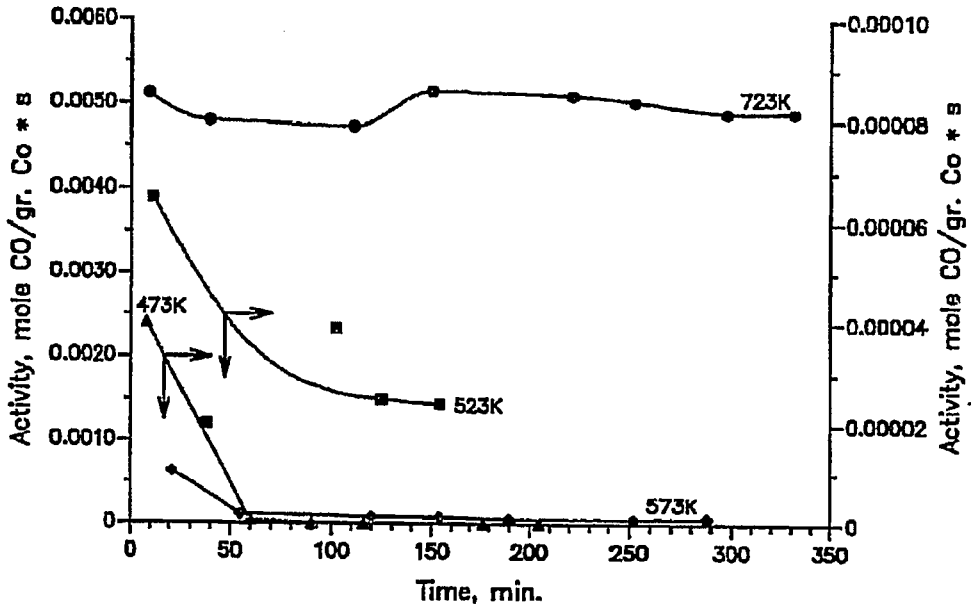

Fig. 5.4.3-3: CO hydrogenation activity for 4.6% Co/γ-Al_2O_3 at different temperatures at 6 bar, $H_2/CO=2$.

The following main conclusions can be drawn by comparison of the weight curves obtained during CO hydrogenation over the silica (Fig. 5.4.2-1) and alumina (Fig. 5.4.3-1 and 5.4.3-2) supported cobalt catalysts:

* The weight increase of the silica supported Co-catalyst progressively declined upon an increase in the reaction temperature from 473K to 573K, while the opposite behaviour was registered for the alumina supported catalyst.

* Increasing reaction temperature during the deposition process results in decreasing amounts of removable species by an increase in the temperature to 673/723K in hydrogen. With a CO hydrogenation temperature of 723K, virtually no changes in the weight curve are observed in hydrogen following exposure to synthesis gas.

* The deposition process for the alumina supported Co-catalysts can be divided into two regimes. A similar behaviour can not be associated with the silica supported high metal loading Co-catalysts.

In order to clarify whether the observed weight changes of the catalyst samples obtained during reaction conditions are due to for example reactions occuring on the support or to buoyancy effects, several experiments were conducted in which the pure supports (silica and alumina) as well as inert glass-spheres were investigated at different temperatures.
Fig. 5.4.3-4 summarizes the resulting weight changes of the different supports at the specified reaction conditions. It should be noted that these samples were subjected to the same pretreatment and reduction procedures as the supported cobalt catalysts.
A control experiment with inert glass-spheres at 523K resulted in negligble weight changes upon introduction of H_2/CO, while switching to hydrogen following exposure to synthesis gas resulted in a negligible weight increase. From this, it can be concluded that the increase in the sample weight of the supported cobalt catalysts occuring during the first minutes after onset of the reaction (introduction of H_2/CO) are not due to buoyancy effects.
The pure silica support was investigated at the temperatures 473 and 723K, which in the experiments with the silica supported Co-catalysts resulted in the most pronounced weight gains. No significant weight increase was observed for silica alone during CO hydrogenation at 473K, while at 723K, the weight of the catalyst continuously increased with time in synthesis gas. However, the weight curve lacks the initial time period without extensive build-up of large amounts of deposited species, as was observed for the silica supported Co-catalyst at the same temperature (723K). Of further notice is that a fraction of the deposited material could be removed by hydrogen, in contrast to the findings shown by way of illustration in Fig. 5.4.2-1.

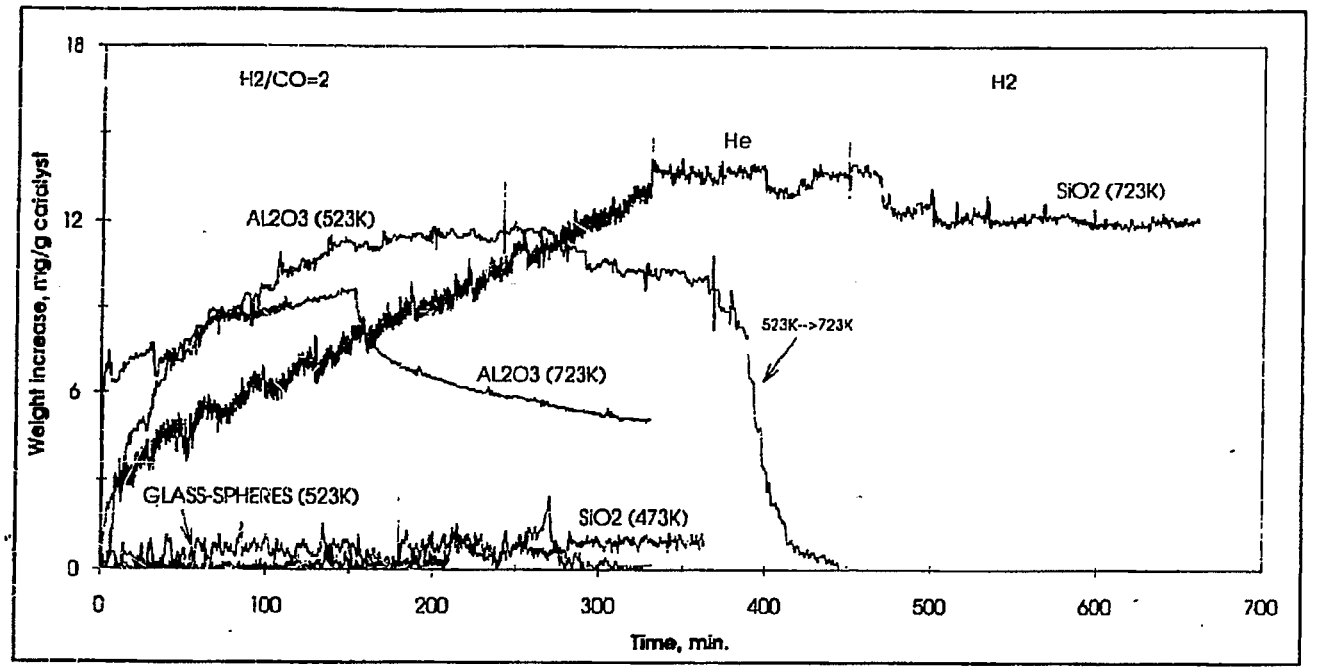

Fig. 5.4.3-4: Weight changes observed during CO hydrogenation followed by flushing with either He and then hydrogen, or directly by hydrogen.

The materials investigated were: SiO_2 (at 473 and 723K), γ-Al_2O_3 (at 523 and 723K) and glass-spheres (at 523K).
The supports and glass-spheres were subjected to the same pretreatment as the supported cobalt catalysts.

CO hydrogenation conditions:
P_{Tot} = 6 bar, H_2/CO = 2

Experiments were conducted in which pure alumina was employed as "catalyst". The temperatures investigated were 523 and 723K. As seen from Fig. 5.4.3-4, the weight curve of pure alumina obtained during CO hydrogenation at 523K is characterized by the absence of the first regime and the rate of the weight increase show signs of stabilization at a certain level, which could not be observed in the case of the alumina supported catalyst. The characteristic features are shown more clearly in Fig. 5.4.3-5. Similar to previous observations, most of the species accumulated during CO hydrogenation could be removed by heating to 673 or 723K in flowing hydrogen.

CO hydrogenation over pure alumina at the reaction temperature 723K resulted in a smaller amount of deposited material compared to at 523K. The deposited species showed a moderate reactivity towards treatment with hydrogen. Both the shape of the weight curve and the reactivity of the adsorbed species are in contrast to what was observed in the case of the alumina supported Co-catalysts at comparable temperature.

5.4.4. Discussion of the weight curves obtained during CO hydrogenation over silica, alumina, 4.6% Co/γ-Al_2O_3 and 4.7% Co/SiO_2

In the preceeding section, the observed weight changes of the different samples subjected to CO hydrogenation at different temperatures were described. The nature and origin of the species being responsible for the detected weight increases in H_2/CO are the topics of the following section.

The weight changes can possibly be explained by:

1. The formation of carbides and/or carbonaceous materials
2. Deposition of polymerization products on the catalyst surface
3. The presence of stable formate and/or carbonate compounds
4. Oxidation/reduction of the different Co-phases, especially related to the alumina supported cobalt catalysts
5. The adsorption/absorption of water from the Fischer-Tropsch reaction
6. Additional effects; contributions from the background, i.e. the basket and reactor walls

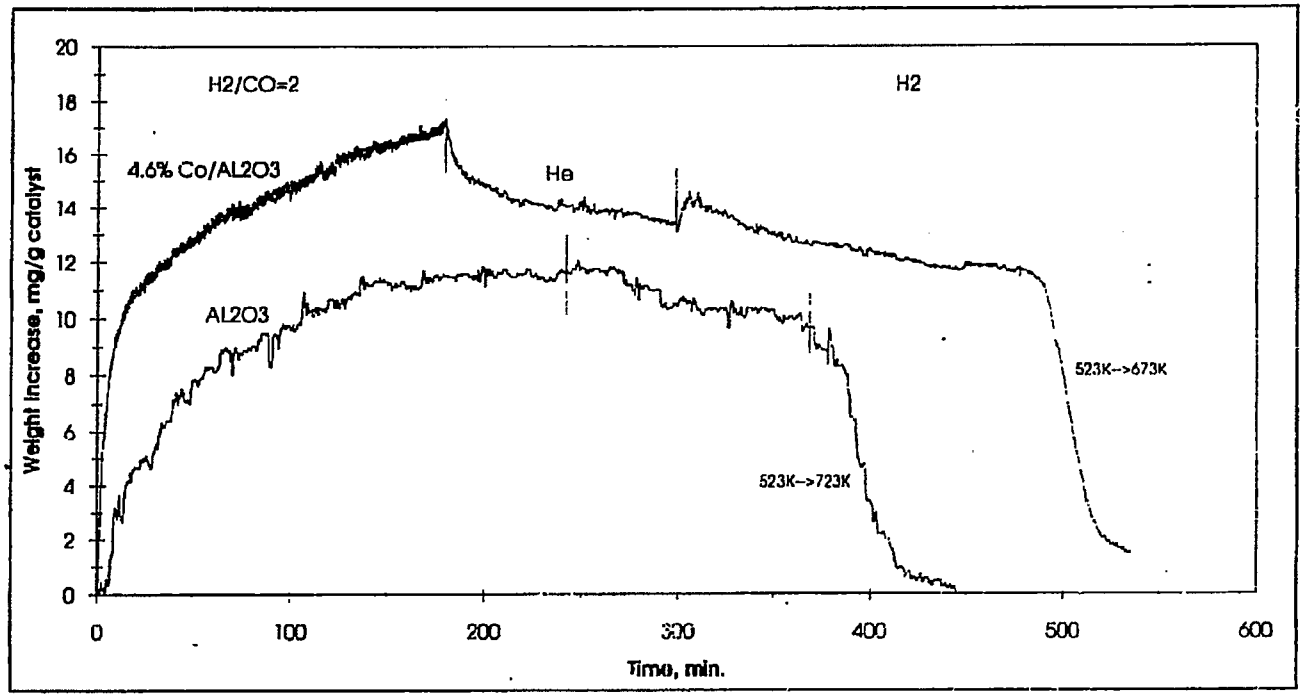

Fig. 5.4.3-5: Changes in sample mass of 4.6% Co/γ-Al_2O_3 and γ-Al_2O_3 during CO hydrogenation followed by treatment with He and then H_2 (4.6% Co/γ-Al_2O_3) or directly by hydrogen (γ-Al_2O_3).

CO hydrogenation conditions:
P_{Tot} = 6 bar, T = 523K, H_2/CO = 2

In principle, all of the above explanations may be regarded as more or less likely in an attempt to explain the observed weight curves. The problem related to the way the weight curves were obtained is that only the net weight change is recorded. This may imply that reactions associated with a weight decrease, for example reduction of the cobalt phase may be balanced and even exceeded by reactions associated with an increase in the mass of the catalyst sample, exemplified by deposition of carbon or carbonaceous materials and the accumulation of high-boiling hydrocarbon products. Thus, parallel reactions and/or complex combinations of point 1. to 6. introduce limitations in the interpretations of the weight curves and on the determination of the actual major effect causing the increase (or the absence) in the catalyst mass. Keeping this in mind, an attempt is nevertheless carried out in order to discuss the possible influence of the different aspects listed on page 242 in connection with the observed weight curves, presented in Fig. 5.4.2-1 to 5.4.3-5. The route chosen to approach the problem was to determine, on a theoretical basis, the maximum likely effect of the different possible reasons and consider these options in light of the observed weight changes at the different reaction conditions.

The observed weight increase in the catalyst sample mass can possibly be related to the formation of cobalt carbides and/or carbonaceous deposits. On a weight basis, the amount of carbon in cobalt carbides like Co_2C and Co_3C is 9.24% and 6.36%, respectively. The weight increase expected to be observed if all available cobalt metal participate in the formation of carbides can be estimated using the following stoichiometric equations:

$$2Co + 2CO \rightarrow Co_2C + CO_2 \qquad 5.18$$

$$3Co + 2CO \rightarrow Co_3C + CO_2 \qquad 5.19$$

The weight ratio between cobalt and carbon in the cobalt carbides Co_2C and Co_3C is 0.102 and 0.068, respectively. The theoretical weight change due to carbon associated with the metal carbide formation is given in Table 5.4.4-1. Examples of how to estimate the amount of cobalt carbide are shown in more detail in Appendix A9.

Table 5.4.4-1: Theoretical weight increase for 4.6% Co/γ-Al_2O_3 and 4.7% Co/SiO_2 provided formation of cobalt carbide.

Co_2C (mg/g Co)	*Co_3C (mg/g Co)*
−100	−68

Comparing the theoretical values with the observed weight changes in Fig. 5.4.2-1 to Fig. 5.4.3-2 indicates that the weight of the catalysts already after short times of reaction exceeds those predicted in Table 5.4.4-1. These values represent the extreme case, and it may well be that the formation of cobalt carbide proceed simultaneously with other reactions. The rate of metal carbide formation must be considered in view of the rate of hydrogenation of surface carbon formed by the dissociation of carbon monoxide. If the rate of the hydrogenation of surface carbon is higher than that of the cobalt carbide formation, a relatively slow migration of carbon into the cobalt lattice would be expected. The preferential route for surface carbon between the two competing reactions depends on the surface concentration of hydrogen and on the temperature of the reaction. Cobalt is known to exhibit a relatively high hydrogenation activity, thus providing decreasing amounts of carbon available for metal carbide formation. Thus, one should expect that if cobalt carbides actually are formed during CO hydrogenation, the reaction would probably proceed over a longer time scale than the one in the present experiments.

Machocki /41/ stated that bulk cobalt carbide (Co_2C) was formed after an induction period of 20 hours. Niemansverdriet et al. /223/ compared the activation energies for the Fischer-Tropsch reaction and carbon diffusion, and concluded that for cobalt, the Fischer-Tropsch

reaction rate would be higher than the carbidation rate. Whether cobalt carbides are formed or not during CO hydrogenation is an intriguing question. Weller et al. /229/ stated that Co_2C was not formed in any appreciable amounts during steady-state Fischer-Tropsch synthesis at 498K over a cobalt:thoria:kieselguhr (100:18:100) catalyst. However, exposure of a cobalt:thoria:magnesia:kieselguhr (100:6:12:200) catalyst to CO for 20 hours resulted in an conversion of 70% of available cobalt to cobalt carbide, Co_2C. Dry /26/ was of the opinion that stable carbides were produced upon exposure of cobalt to CO alone at normal Fischer-Tropsch temperatures, but that this phase was not present when used F-T catalysts were examined. In view of the above argumentation and the present data, it seems unlikely that the increase in the mass of the catalysts solely can be explained by bulk carbide formation.
Also, the effect of a possible deposition of carbidic and/or graphitic carbon species should be taken into consideration. Differentiation between the two species is commonly achieved by considering the deposition temperature. Generally, in the literature, it is believed that carbon deposited below 500-510K results in carbidic carbon, while above this temperature, the formation of graphitic carbon normally tends to occur. Deposition by Boudouard's reaction below 500-510K followed by heating to 703K was usually found to result in a conversion of the carbidic carbon to graphitic carbon /42/. Employing these arguments on the weight curves presented in Fig. 5.4.2-1 and 5.4.3-2 makes it reasonable to suggest that a major part of the weight increase observed over the 4.6% Co/γ-Al_2O_3 and 4.7% Co/SiO_2 catalysts during CO hydrogenation at 723K can be ascribed to the formation of inactive (graphitic) carbon.
A strong confirmation of this is found in the almost negligble reactivity of the deposited species towards hydrogen, which by several authors has been mentioned as the most characteristic feature of this type of deposited carbon species. Also, the course of the deposition process is relatively similar for the two catalysts at 723K and then again quite different compared to that occuring at lower temperatures for each of the alumina and silica supported cobalt catalysts. Furthermore, when the reactor was disassembled and the basket containing the catalyst was checked, a black deposit was observed on the catalyst particles and the basket itself which not was observed when CO hydrogenation was carried out in the temperature interval 473-573K.

One can also possibly anticipate that the background effects constitute a certain contribution to the observed weight curves, both at lower temperatures as well as at 723K. In this context,

contributions from the alumina support itself and possibly also from the stainless steel basket may be of importance. Considering the latter option first, iron in the stainless steel basket can be regarded as a possible source for carbide formation. However, blank runs with glass spheres in the basket showed negligble weight changes, indicating that contributions from the basket itself is of little or no importance, see Fig. 5.4.3-4. This assumption is believed to be valid for all of the experiments regardless of the catalyst or applied reaction conditions. Another iron containing compound is the alumina support. Iron impurities in the alumina may be envisioned to serve as a "reactant" for the formation of iron carbides such as Fe_2C, Fe_5C_2 and Fe_7C_3. The iron content in the applied γ-Al_2O_3 was 0.02 wt-%, according to the specifications given by the supplier (Akzo). Assuming the content of iron in the diluent α-Al_2O_3 to be of the same magnitude as in γ-Al_2O_3, the total amount of iron in the sample used in the CO hydrogenation experiment at 723K (see Fig. 5.4.3-2) is 0.15 mg. This would be expected to result in a small, and totally ignorable weight increase of 0.332 mg, assuming complete conversion of the present iron into Fe_2C, the most carbon rich iron carbide. The effect of such a background contribution will to a certain extent be of even less importance, since the majority of the experiments were carried out without dilution of the supported cobalt catalysts with α-Al_2O_3. Nevertheless, it is believed that contributions from the alumina support itself still contribute to the observed weight changes, as will be discussed in connection with the weight gains and losses over γ-Al_2O_3 alone and the alumina supported Co catalyst.

The magnitude of the weight increase indicates that the catalysts may retain other species deposited on the sample surface. As previously suggested, possible species may include carbon monoxide, water and hydrocarbons.

The *in situ* infrared measurements during CO hydrogenation at reaction conditions over silica and alumina supported cobalt catalysts showed distinct absorption bands for linearly adsorbed CO and bands tentatively ascribed to bridgebonded CO. It is not likely that the associative adsorption of carbon monoxide can explain the observed weight increase, since the weight of adsorbed CO molecules probably is too small for this to be the case. This is supported by a simple calculation based on the dispersion and the amount of available cobalt metal. Using the 4.6% Co/γ-Al_2O_3 as an example, Table 5.4.4-2 shows the expected weight increase of this catalyst at different temperatures if molecularly adsorbed CO is retained by metallic cobalt in a monolayer coverage. The infrared investigations revealed no indications of adsorbed CO

in the linear or bridgebonded mode on either of the pure supports, silica or alumina. Details of the calculations leading to the values reported in Table 5.4.4-2 are given in Appendix A10.

Table 5.4.4-2: **Weight increase associated with a monolayer coverage of CO on 4.6% Co/γ-Al_2O_3. Dispersion 1%. Adsorption stoichiometry: linear form (Co:CO)1:1, bridgebonded form 1:2.**

Temperature (K) [1]	*Catalyst mass (g)*	*Stoichiometric ratio 1:1 (mg)*	*Stoichiometric ratio 1:2 (mg)*
473	0.7064	0.1540	0.0772
523	0.7215	0.1578	0.0789
573	0.7229	0.1580	0.0790
723	0.2506	0.0550	0.0274

[1]:Temperature at which CO hydrogenation was carried out

The numbers in Table 5.4.4-2 actually represent the extreme case since factors like for example the temperature dependence of the equilibrium constant and the extent of reduction are not considered in this context. The expected loss of a quantitative amount of cobalt strongly associated with the γ-Al_2O_3 lattice is not included in the calculations. If the above aspects were taken into consideration, the expected weight increase would then be even less than the predicted values in Table 5.4.4-2.

Applying the previously assumed dispersion of 7% for 4.7% Co/SiO_2, calculations similar to those above can be carried out for this catalyst. The obtained values are shown in Table 5.4.4-3. The calculations show that the weight of molecularly adsorbed carbon monoxide on the silica and alumina supported cobalt catalysts is too small to explain the observed weight increase.

Table 5.4.4-3: **Theoretical estimate of the weight of adsorbed CO on 4.7% Co/SiO_2 based on an assumed dispersion of 7.0 % for 4.7% Co/SiO_2. Adsorption stoichiometry; 1:1.**

Temperature (K) [1]	*Mass of catalyst (g)*	*Weight of CO (mg)*
473	0.7092	1.1090
523	0.7140	1.1165
573	0.7209	1.1273
723	0.7215	1.1283

[1]:Temperatures at which the CO hydrogenation reaction was performed

To elucidate the significance of polymerized species being a possible reason for the weight increase, a simple approach to the problem is achieved by considering the pore volume of the catalyst. The cumulative pore volume was found to be 2.19 cm^3/g for 4.7% Co/SiO_2 7230/. This means that the total volume which can be filled with liquid hydrocarbons is known, since the catalyst sample mass is known. GC analysis showed that C_8 was the highest hydrocarbon detected. Thus, octane is used as a representative of the hydrocarbons present on the surface. The density of octane is 0.698 g/cm^3, and the weight increase associated with a complete filling of the catalyst pores with this hydrocarbon can then be estimated. The results are presented in Table 5.4.4-4.

Such an approach is believed to be valid at least for the reactions taking place at lower temperatures, since the infrared spectra in the C-H stretching region revealed dominating absorption bands ascribed to asymmetric and symmetric C-H stretching in CH_2 groups. Also, the estimated average chain length at these temperatures was found to be higher than unity, indicating longer chained hydrocarbons present during reaction conditions.

It is of interest to compare the values calculated by the pore volume approach to those estimated from the IR-measurements. As shown in Chapter 5.2.5, the estimated volume of adsorbed CH_2 and CH_3 species was found to be 0.00109 and 0.00014 cm^3, respectively, during CO hydrogenation at 473K.

Table 5.4.4-4: **Theoretical estimates of the weight increase associated with filling of the catalyst pores of 4.7% Co/SiO_2 with hydrocarbones.**

Temperature (K) [1]	*Mass of catalyst (g)*	*Weight of hydrocarbon (mg)*
473	0.7092	1084
523	0.7140	1091
573	0.7209	1102

[1]: Temperature at which CO hydrogenation was carried out

The weight of the accumulated hydrocarbons can be estimated according to the equation:

$$n_{CH_x} = \frac{S_{CH_x} \cdot A_C}{B_{CH_x} \cdot m_{cat}} \cdot 10^{-3} \qquad 5.20$$

where S_{CHx} = integrated area under the absorption band (cm^{-1})

A_C = cross-sectional area of the catalyst wafer (cm^2)

B_{CHx} = integrated infrared intensity (cm/mol)

m_{cat} = weight of the pressed catalyst disk (g)

The equation indicates the amount of adsorbed CH_2 and CH_3 species in mol/g catalyst. By the use of equation 5.20, the weight of long chained hydrocarbons on 4.7% Co/SiO_2 at 473K is estimated to 0.161 mg/g catalyst assuming the dominant surface species to be $>CH_2$. In comparison, the weight gains observed in the microbalance was 35-40 mg/g catalyst. Thus, the amount of accumulated hydrocarbons as indicated by infrared spectroscopy is approximately one and a half order of magnitude lower than the observed weight increase when the comparison is made at similar reaction conditions (H_2/CO=2, P_{Tot}= 6 bar, 100 Nml/min., ~2 hours of reaction). The development with time of the infrared bands attributable to hydrocarbon species is in fair agreement with the changes in the catalyst sample weight with reaction time. The intensity (measured as peak heights) of the absorption bands increased

steadily with time in synthesis gas, comparable with the observed continuous increase in the catalyst sample weight. Of further interest is it to note that the development of the infrared band intensities upon introduction of He and hydrogen showed the same trend as registered for the weight curves under similar reaction conditions. Furthermore, the chain length was estimated to approximately 8 at 473K from the IR measurements. Also, it is generally known that the chain growth probability decreases with increasing temperature. For these reasons, it is believed that the formation and presence of higher hydrocarbons can account for a significant part of the weight increase during CO hydrogenation at 473K over 4.7% Co/SiO_2.

Regarding the weight curves obtained for 4.6% $Co/\gamma\text{-}Al_2O_3$, it would be tempting to draw the conclusion that accumulated hydrocarbons is responsible for the increase in catalyst weight with increasing temperature. However, the experimental results indicate that this can not be the only explanation for the increase in catalyst mass. Firstly, the probability of chain growth is expected to decrease with increasing temperature, which would result in the formation of lighter hydrocarbon products. The hydrocarbon product distribution for 4.6% $Co/\gamma\text{-}Al_2O_3$ is shown in Table 5.4.4-5.

Table 5.4.4-5: **Hydrocarbon product distribution for 4.6% $Co/\gamma\text{-}Al_2O_3$ during CO hydrogenation.**
Reaction conditions: P_{Tot}=6 bar, H_2/CO=2.

Temperature (K)	*Weight percentage hydrocarbon selectivities*				
	CH_4	C_2	C_3	C_4	C_{5+}
473	74.52	0	25.48	0	0
523	73.66	0	26.34	0	0
573	46.93	10.26	14.65	14.985	13.2
723	99.23	0.276	0.499	0	0

If deposition of hydrocarbons was the sole reason for the observed weight increase, one would probably not expect the catalyst to gain weight with increasing temperature. The infrared results indicate a decrease in the total amount of $>CH_2$ and $-CH_3$ with increasing temperature. Secondly, the intensity and position of the C-H stretching bands on 4.6% $Co/\gamma\text{-}Al_2O_3$ differed significantly compared to those on 4.7% Co/SiO_2. Typically, they were displaced to lower frequencies (2916/2907 cm^{-1}) and of lower intensity. Also, the bands remained relatively stable when flushing with He or during hydrogen treatment. Hence, it was suggested that the presence of formate/carbonate species was the most likely explanation of the observed behaviour. The development of the intensity of the formate/carbonate bands with time in synthesis gas resembled the progress of the weight deposition process. By comparison of Fig. 5.4.3-1, Fig. 5.4.4-1 and Fig. 5.4.4-2, the presence of the two regimes is evident. Likewise is the shift in the time location of the first regime with increasing temperature easily recognized. Moreover, the intensity of the formate/carbonate bands increased with increasing temperature. Consequently, it is believed that the observed weight increase over 4.6% $Co/\gamma\text{-}Al_2O_3$ during CO hydrogenation predominantly is due to the presence of formate/carbonate species and hydrocarbon structures.

It is evident that the formate/carbonate IR band intensities are rather stable in He, while increasing temperature results in a small, gradual decline in the band intensity during exposure to hydrogen, as seen in Fig. 5.4.4-1 and Fig. 5.4.4-2. Fig. 5.4.3-1 indicates a decline in the catalyst sample mass of the 4.6% $Co/\gamma\text{-}Al_2O_3$ catalyst upon introduction of He and H_2, while the weight changes observed for pure alumina (Fig. 5.4.3-5) are rather small in comparison during hydrogen treatment. This is in accordance with the infrared results obtained when $\gamma\text{-}Al_2O_3$ alone was exposed to He and then hydrogen following CO hydrogenation at 473K, as illustrated in Fig. 5.4.4-3. The difference in the observed behaviour can possibly be related to the presence of formate/carbonate and hydrocarbon species. While the former is stable and rather unaffected by flushing with He and H_2, hydrocarbon end products or biproducts are easier to remove, and are most probably the reason for the observed weight losses upon introduction of helium, as discussed further in the next paragraph.

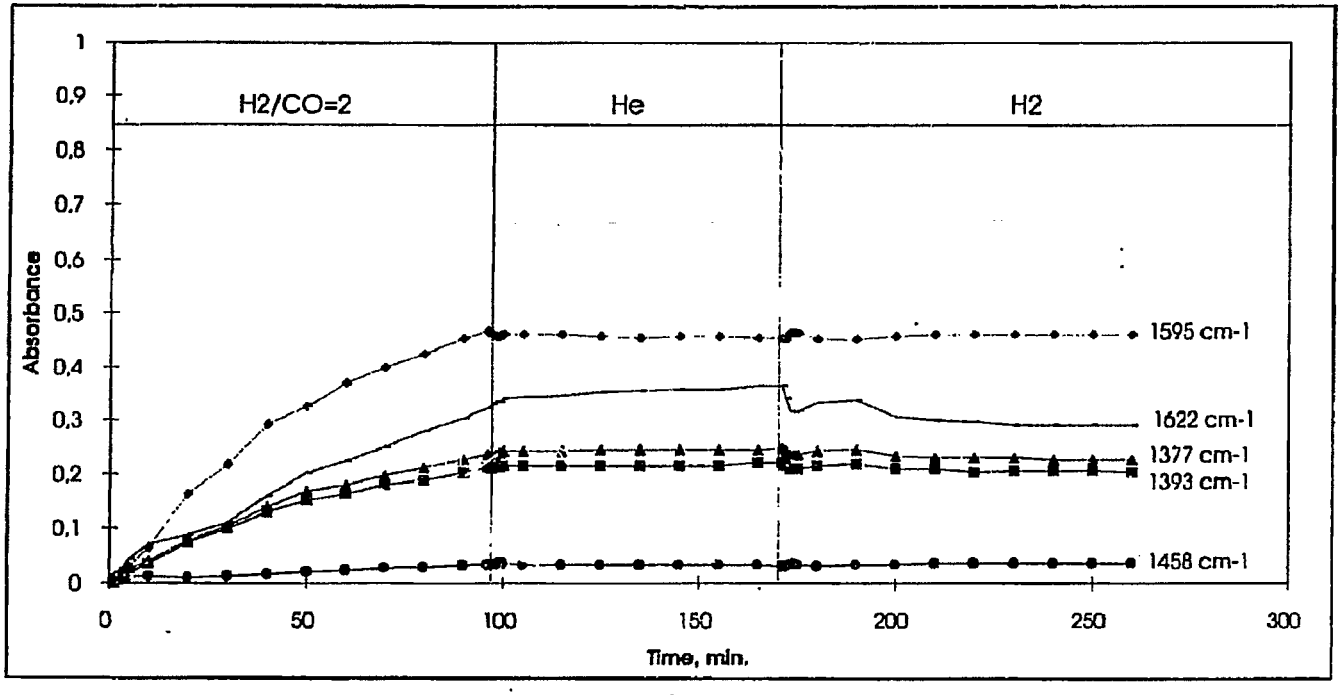

Fig. 5.4.4-1: Development of the intensity of infrared bands assigned to formate/carbonate species during CO hydrogenation, He-purging and H_2-treatment on 4.6% Co/γ-Al_2O_3.

CO hydrogenation conditions:
P_{Tot} = 6 bar, T = 473K, H_2/CO = 2

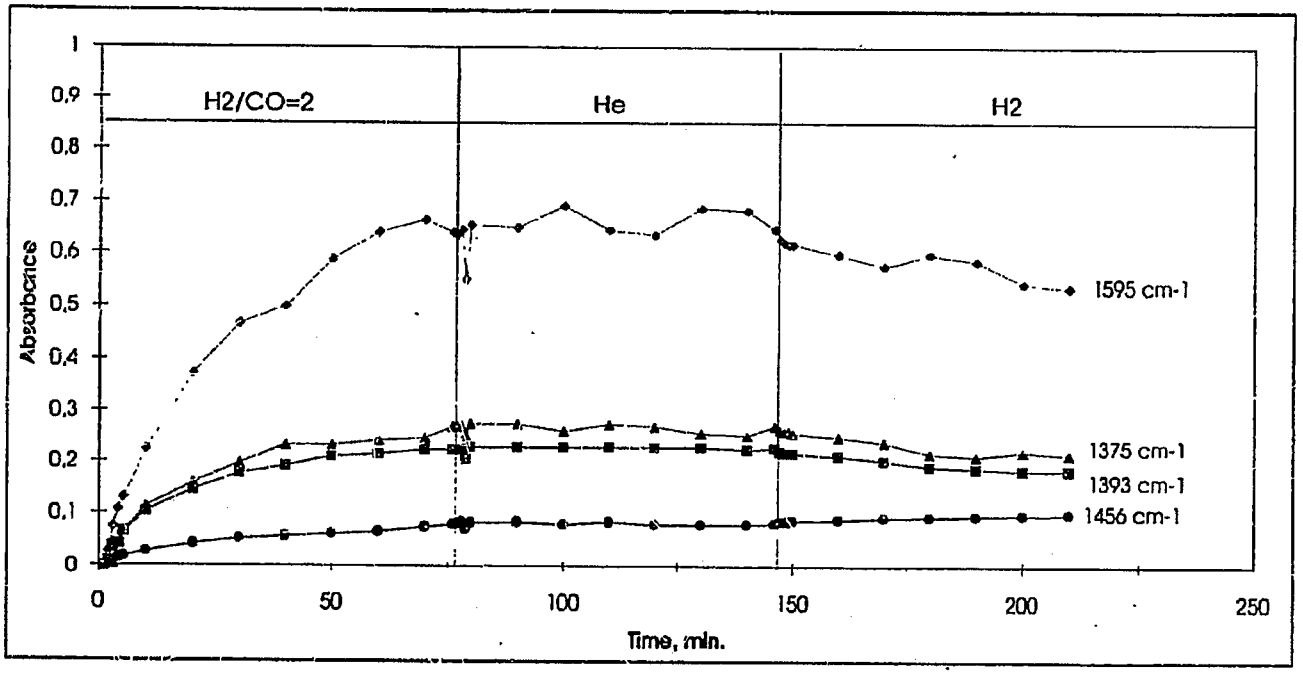

Fig. 5.4.4-2: **Development of the intensity of infrared bands assigned to formate/carbonate species during CO hydrogenation, He-purging and H_2-treatment on 4.6% Co/γ-Al_2O_3.**

CO hydrogenation conditions:
P_{Tot} = 6 bar, T = 523K, H_2/CO = 2

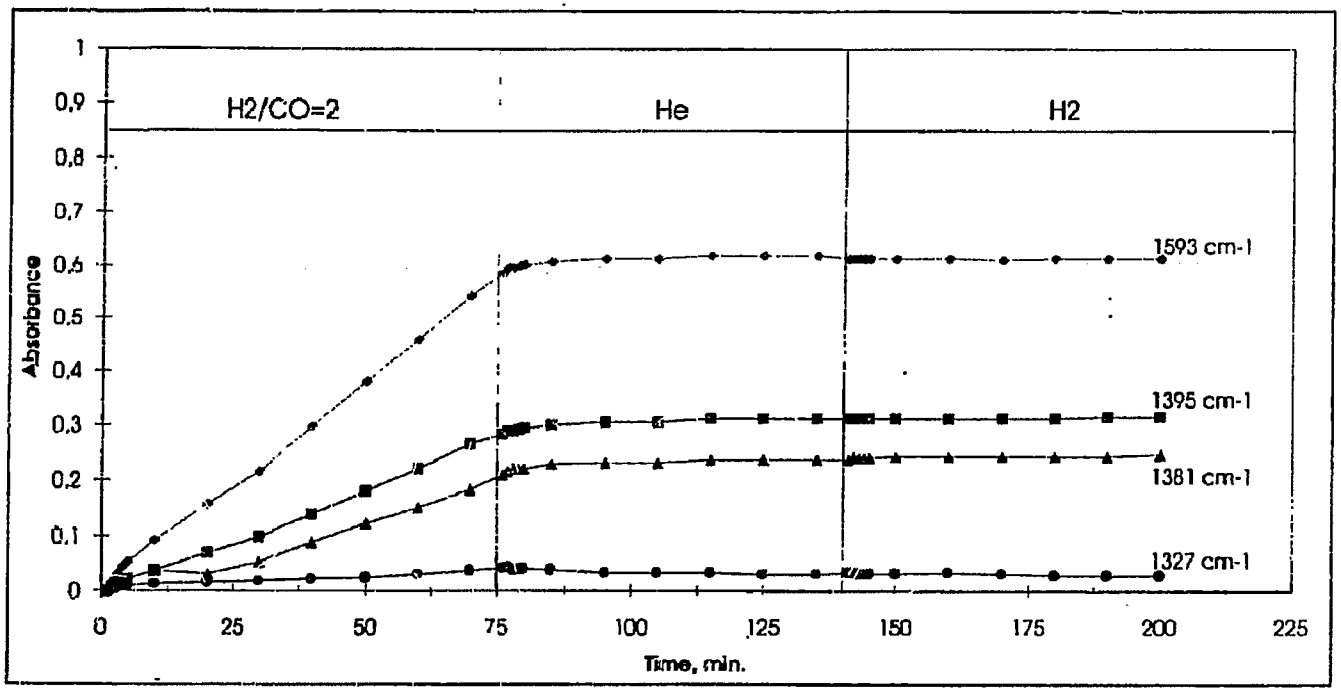

Fig. 5.4.4-3: Development of the intensity of infrared bands in the 1800-1200 cm^{-1} during CO hydrogenation, He-purging and H_2-treatment of blank γ-Al_2O_3.

CO hydrogenation conditions:
P_{Tot} = 6 bar, T = 473K, H_2/CO = 2

A common feature observed for both of the catalysts was a characteristic weight loss upon introduction of either He and then hydrogen, or directly by hydrogen. For the silica supported catalysts, a similar variation in the intensity of the C-H stretching bands could be observed at 473K when exposed to He followed by hydrogen. Table 5.4.4-6 and 5.4.4-7 shows the composition of the effluent stream during He and hydrogen treatment after exposure of the 4.7% Co/SiO_2 catalyst to synthesis gas ($H_2/CO=2$) at 473K.

Table 5.4.4-6: **Composition of the effluent gas during He treatment as determined from GC-analysis.**
Reaction conditions : P_{Tot}=6 bar, T=473K.

Time in He (min.)	*Effluent gas composition (wt.%)*				
	CH_4	C_2	C_3	C_4	C_{5+}
11	7.03	0	2.80	21.24	62.59
43	2.67	0	0	39.97	57.36
74	3.78	0	0	46.80	49.42
103	1.12	0	0	18.12	79.39

Table 5.4.4-7: **Composition of the effluent gas in H_2 as determined by GC analysis.**
Reaction conditions : P_{Tot}=6 bar, T=473K.

Time in H_2 (min.)	*Effluent gas composition (wt.%)*				
	CH_4	C_2	C_3	C_4	C_{5+}
12	70.39	1.01	0	10.81	17.79
49	54.20	0	0	0	45.79
80	54.86	0	0	13.12	32.02
113	63.05	0	0	13.58	20.68

At higher reaction temperatures, hydrogen treatment of the catalyst after exposure to synthesis gas resulted in increasing amounts of methane and less amounts of C_2-C_{5+}. The possibility exists, that the observed weight changes upon switching from synthesis gas to He and then hydrogen or directly to hydrogen may be caused by buoyancy effects induced by changes in the density of the gas phase. Using the same approach as outlined in Appendix A11, the influence of the gas phase density upon the the weight changes can be estimated. The calculations showed that the weight changes associated with changes in the gas phase density in all cases are too small to alone explain the weight decrease observed upon introduction of the different gases, He and H_2. Rather, based on the calculations of the gas phase density, a weight increase and not decline should be expected, since switching to He and/or hydrogen generally resulted in a lower gas phase density compared to H_2/CO. Thus, based on the above argumentation and the data in Table 5.4.4-6 and 5.4.4-7, it seems reasonable to assume that the weight decrease observed for 4.7% Co/SiO_2 during flushing with He at reaction temperature (473K) most likely are due to desorption of accumulated hydrocarbons. The lack of any significant weight changes for this catalyst at 523 and 573K are presumably due to the low formation of long chained hydrocarbon structures, as indicated in Table 5.4.4-8.

The weight curves obtained during CO hydrogenation over 4.7% Co/SiO_2 at 523 and 573K deserves a further discussion. As seen from Fig. 5.4.2-1, the weight increase observed at these temperatures is rather small compared to that observed at 473K. There also seems to be small differences in the weight gains between 523 and 573K. Another reason which may explain the negligble weight changes at these temperatures is the possibility of the basket being in contact with or touching the reactor wall. However, this is not believed to be the case for the following reasons:

1. Before starting an experiment, two things were done in order to ensure a freely suspended basket.

    a) When the basket containing the fresh catalyst was hooked onto the quartz fiber, the position of the quartz fiber and the basket was checked. The quartz fiber should be located in the center of the tube (see Fig. 4.5.1-2) and the basket should hang in the plumb line.

b) By gently touching the basket/quartz fiber while monitoring the deflections of the balance. A freely hanging basket was achieved when the deflection of the balance returned to its starting point.

2. The experiments were reproduced resulting in similar results as those presented in Fig. 5.4.2-1.

Thus, it is not believed that the basket is in contact with the reactor walls during the experiments at 523 and 573 over 4.7% Co/SiO_2, and that this may explain the stable weight curve obtained at these temperatures.

Doubling of the flowrate of the reactant gases resulted in a weight decrease, as seen in Fig. 5.4.2-1. This could possibly be explained by a chemical and/or a fluiddynamic effect. Considering the last option first, the changes in the flowrate lead to a change in the gas phase density, with the possibility of a buoyancy effect. If such an effect were present, a decrease in the the weight curve would be expected to be observed. Estimation of the density of the gas phase before and after the increase in flowrate yields 1.243 and 1.342 kg/m^3, respectively. The mass of the gas displaced by the basket due to the differences in the gas phase density is 0.155 mg., as the calculations in Appendix A11 show. The observed weight decrease was approximately 1.1 mg/g catalyst, which indicates that the buoyancy effects associated with changes in the gas phase density is of minor importance and not the main reason for the decrease of the weight curve.

Counteracting the buoyancy effects is the drag forces, which would be expected to be higher due to the increased flowrate, and result in a deflection in the opposite direction of that observed. The microbalance would record the resultant (net) effect of these two opposing forces. This indicates that chemical in addition to the above mentioned effects must be considered when trying to elucidate the observed weight decrease.

Increasing the flowrate will generally result in decreasing conversion of CO, while the activity should remain constant, assuming differential reactor conditions. The reaction rates at the different CO hydrogenation temperatures are shown in Fig. 5.4.4-4. By an increase in the flowrate of the reactants, the activity increases and then declines. This could possibly be explained by concentration gradients in the catalyst bed due to non-differential conditions.

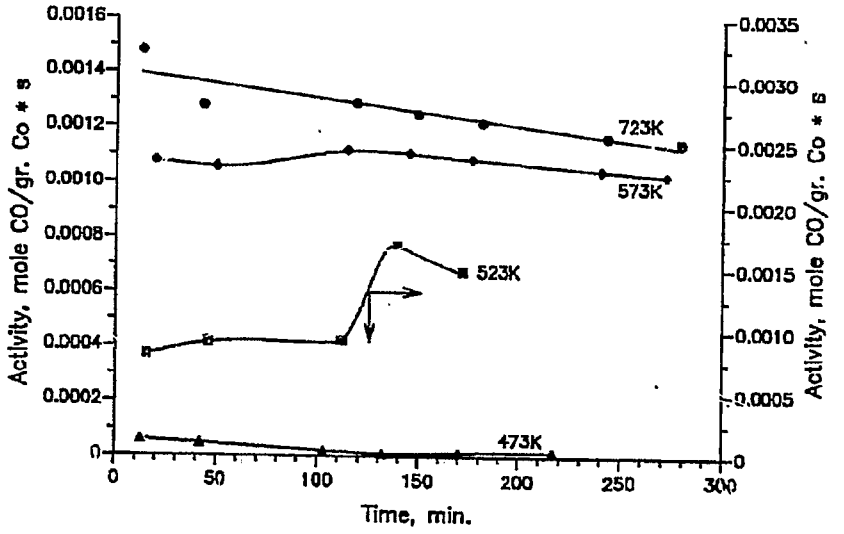

Fig. 5.4.4-4: CO hydrogenation activity of 4.7% Co/SiO_2 at different temperatures. Reaction conditions: P_{Tot}=6 bar, H_2/CO=2.

Higher flowrate could mean higher concentrations of CO and H_2 in the catalyst bed, thereby increasing the activity. Higher flowrate could also mean a higher probability of desorption of adsorbed species, for example hydrocarbons, resulting in a weight decrease. As can be seen from Fig. 5.4.4-4, the reaction rates at the higher temperatures (523, 573 and 723K) are approximately an order of magnitude higher compared to that at 473K, and the weight curves at these temperatures is characterized by lower amounts of deposited species. At this point, it may be appropriate to consider the results from the GC-FID analysis. Table 5.4.4-8 lists the hydrocarbon group selectivities (in weight-%) based on the total hydrocarbon products. As can be seen there is a significant difference in the hydrocarbon product distribution between 473K and the higher temperatures. At temperatures ≥ 523K, methane is the abundant hydrocarbon detected, with neglectable amounts of C_{2+}. At 473K, the C_{2+} consitutes the dominant hydrocarbon fraction, 61.5% of the hydrocarbons are in the C_{2+} fraction. Thus, CO at 473K is converted to a range of hydrocarbons, but mainly to methane at 523, 573 and

723K. The development of the weight curves of 4.7% Co/SiO_2 as a function of increasing reaction temperature can reasonably well be explained in view of the results above. That is, high conversions and high selectivity for methane formation are observed at higher temperatures. This can possibly be interpreted in terms of CO adsorption followed by dissociation and removal of oxygen as CO_2 or H_2O. Hydrogenation of surface carbon (carbidic carbon) results mainly in CH_4 formation, but deposition of carbon may also occur.

Table 5.4.4-8: **Hydrocarbon product distributions for 4.7% Co/SiO_2 during CO hydrogenation.**
Reaction conditions: P_{Tot}= 6 bar, H_2/CO=2.

Temperature (K)	*Weight percentage hydrocarbon selectivities*				
	CH_4	C_2	C_3	C_4	C_{5+}
473	38.42	7.3	10.6	17.4	26.2
523	98.2	1.4	0.17	0.19	0.053
573	99.5	0.29	0.062	0.075	0.059
723	98.24	0.94	0.58	0.147	0.088

Based on the decreased intensity and the concurrent downscale shift in the frequency of the linear CO band, it has earlier been suggested that this behaviour could possibly be explained by the deposition of carbon or carbonaceous deposits. Such a conclusion is not necessarily in contrast to the results presented in Fig. 5.4.2-1. Table 5.2.3.6-1 on page 134 gives an estimate of the amount of adsorbed CO on 4.7% Co/SiO_2 at selected reaction conditions. Using these values as starting points, it can be calculated that if all available cobalt metal is covered by carbon, this would correspond to a weight increase of 0.76, 0.52 and 0.36 mg/g at 473, 523, and 573K, respectively. The weight increase associated with such a reaction could then not be resolved under the present circumstances.

Oxidation and reduction of the cobalt phase are reactions expected to be associated with weight gains and losses. The presence of water formed during the Fischer-Tropsch reaction and/or surface hydroxyl groups may act as potential oxidants. While it is difficult to predict the surface oxidation of metal crystallites, thermodynamic calculations can be used to evaluate the possibility of bulk oxidation of cobalt in the presence of water /200/. The standard Gibbs free energy of formation for bulk cobalt oxide (CoO) from Co and water vapour, according to the reaction

$$Co + H_2O \rightarrow CoO + H_2 \qquad \Delta G_f = +8\,kJ/mole \qquad 5.21$$

indicate that cobalt does not exhibit any tendency toward bulk oxidation at reaction conditions. The formation of cobalt oxide will to a certain extent depend on the conversion of carbon monoxide. At high conversions the atmosphere will be oxidizing, while reducing at low conversions. GC-analysis taken during CO hydrogenation at 523 and 573K indicate a CO conversion of about 30-40%, implying a relatively high production of water and hence higher probability of oxidation of the cobalt metal. Therefore, one should expect that oxidation would give rise to a weight increase of greater magnitude than the experiments indicate. One can argue that a possible oxidation effect would be included in the significant weight increase observed at 473K in synthesis gas, but since the rate of oxidation would be favoured by increasing temperature, this would be expected to lead to a more pronounced weight increase at 523 and 573K than the ones observed. Thus, it can be concluded that oxidation of cobalt metal is probably not a likely reason explaining the obtained weight changes. In accordance with this, Dry et al. /26/ stated that Co was not oxidized under normal Fischer-Tropsch conditions.

As can be seen from Fig. 5.4.3-1, increasing reaction temperature resulted in increasing amounts of deposited materials. Also, when blank alumina was exposed to synthesis gas at 523K and 723K, a significant weight increase could be observed, although CO conversion was negligible (less than 0.5% at 523K). Fig. 5.4.3-5 compares the weight curves of 4.6% Co/γ-Al_2O_3 and γ-Al_2O_3 alone during CO hydrogenation at 523K. The noticeable weight increase obtained over pure alumina may be correlated with the observations from the IR measurements in the 1800-1200 cm^{-1} range. In section 5.2.8.3, strong infrared bands suggested

to be due to surface formate/carbonate species were observed. The intensity of these bands increased with time during the course of a run. The formate and carbonate bands were found to be present both on the support alone and on the alumina supported Co catalyst. It is of interest to relate the presence of these bands to the weight gains previously shown in Fig. 5.4.3-5. The area which a formate/carbonate molecule would be expected to occupy is roughly estimated to 20 $Å^2$. The weight of a formate and carbonate ion can be calculated to $7.48 \cdot 10^{-26}$ and $9.97 \cdot 10^{-26}$ kg, respectively. With a surface area of alumina of 186 m^2/g, the weight of formate molecules in a monolayer coverage can be estimated to 47.98 mg. Likewise, assuming that the complete surface is covered with carbonate species will result in a weight increase of 63.96 mg. It must be emphazied that these calculations do not include possible events like decomposition or interconversion as a result of specific reaction conditions. The calculations do however indicate that the weight of formate or carbonate species is of such a magnitude that it may explain the observed weight gains.

A striking similarity also exists between the development of the band intensities of the formate/carbonate bands and the weight curves. From Fig. 5.2.8.3-2 and 5.2.8.3-5, a continuous increase in the intensity of the bands can be observed, resembling the development in Fig. 5.4.3-5 Furthermore, introduction of He and/or hydrogen at reaction temperatures does not seem to invoke significant changes in the band intensity or in the catalyst sample mass. Thus, it can be inferred that the presence of surface formate/carbonate species - as also observed by FTIR spectroscopy - may explain the observed weight increase over alumina alone and partly that of the alumina supported Co-catalysts. The lower amount of adsorbed formate/carbonate species at the reaction temperature 723K compared to at 523K can possibly be related to a lower stability of the adsorbed species. Decomposition to carbonate species or CH_4, or thermal desorption are reactions that may occur due to the relatively high temperature.

The observed weight increase with increasing temperature over alumina alone can therefore most probably be explained by increased amounts of deposited formate/carbonate species. Such a suggestion is in accordance with the findings from the infrared investigation.

By comparison of Fig. 5.4.2-1 and Fig. 5.4.3-1, it can be seen that increasing reaction temperature results in decreasing amounts of deposited species for the 4.6% Co/SiO_2, while the opposite trend was observed for the alumina supported catalyst. Several explanations have

been put forward to account for this observation. It is difficult to pinpoint a single cause, but it is believed that the difference in the observed weight curves can be explained by the formation of hydrocarbons in the case of 4.7% Co/SiO_2 and in addition, the formation of formate/carbonate species on 4.6% $Co/\gamma\text{-}Al_2O_3$.

A common feature was observed for all the catalysts at reaction temperatures in the interval 473-573K upon an increase in the temperature to either 673K or 723K in flowing hydrogen, as seen in Fig. 5.4.2-1 to 5.4.3-5. The amount of species which could be removed by this temperature treatment decreased with increasing reaction temperature for both the silica and alumina supported catalysts. Various possible explanations can be offered to explain the observed decrease in the catalyst sample mass:

* Removal of water and/or surface hydroxyl groups
* Decomposition/interconversion of formate/carbonate species
* Further reduction of the catalyst
* Hydrogenolysis of hydrocarbons

The removal of hydroxyl groups may possibly occur by desorption or hydrocondensation in the form of water. An impression of the weight changes associated with such a reaction pathway can be achieved by considering the weight changes observed during the pretreatment procedure of the catalysts. As earlier described in section 4.5.2, the catalysts were dried overnight at 673K in He until a non-fluctuating weight curve was achieved. A subsequent increase in the temperature to 723K resulted in a small decrease in the sample weight. At these conditions, the major feature of the weight decrease must be due to dehydroxylation of the catalyst surface. Table 5.4.4-9 and 5.4.4-10 summarizes the observed weight decrease obtained by applying the above mentioned procedure.

It must be empasized that this way of evaluating the influence of hydroxyl groups and/or water on the weight curves does not consider the situation occuring between the reaction temperature and 673/723K. One must believe, however, that the removal of either hydroxyl groups or hydrogen bonded water also is facilitated in this temperature range. Thus, the tables 5.4.4-9 and 5.4.4-10 represent a simplified approach to the problem, but the values nevertheless express certain trends which relate to the problem. No attempt has been carried

Table 5.4.4-9: **Weight loss of 4.7% Co/SiO_2 observed during overnight drying in He at 673K followed by drying at 723K for different periods of time.**
Reaction conditions: P_{Tot}=6 bar, 300 Nml He/min.

Sample weight (mg)	*Sample weight at 673K (mg)* [1]	*Sample weight at 723K (mg)* [2]	*Δm (mg/g catalyst)*	*Drying time at 723K (h)*	*Reaction temperature (K)* [1]
709.2	586.08	585.05	1.45	5	473
714.0	586.00	584.60	1.96	4	523
720.9	584.39	583.17	1.69	4.5	573

[1]: Temperature at which the CO hydrogenation experiments were carried out

Table 5.4.4-10: **Weight loss of 4.6% Co/γ-Al_2O_3 observed during overnight drying in He at 673K followed by drying at 723K for different periods of time.**
Reaction conditions: P_{Tot}=6 bar, 300 Nml He/min.

Sample weight (mg)	*Sample weight at 673K (mg)* [1]	*Sample weight at 723K (mg)* [2]	*Δm (mg/g catalyst)*	*Drying time at 723K (h)*	*Reaction temperature (K)* [4]
706.4	566.46	565.09	1.94	5	473
721.5	580.62	-------[3]	----[3]	-[3]	523
722.9	563.90	562.90	1.40	4	573

[1]: The weight of the catalyst sample after overnight drying in He
[2]: The weight of the catalyst sample after drying at 723K for the specified time in He
[3]: Drying at 723K was not carried out
[4]: Temperature at which the CO hydrogenation was performed

out to quantify the amount of water and/or OH-groups which is removed by the increase in the temperature between the reaction temperature and 673/723K. The numbers in Table 5.4.4-9 and 5.4.4-10 indicate that drying at 723K following overnight drying at 673K results in a small weight decrease in the catalyst sample mass. The continuing loss of water or hydroxyl

groups with increasing temperature is in accordance with reports in the literature, indicating decreasing surface concentration of hydroxyl groups on silica and alumina with increasing temperature. This is shown by way of illustration in Fig. 5.4.4-5.

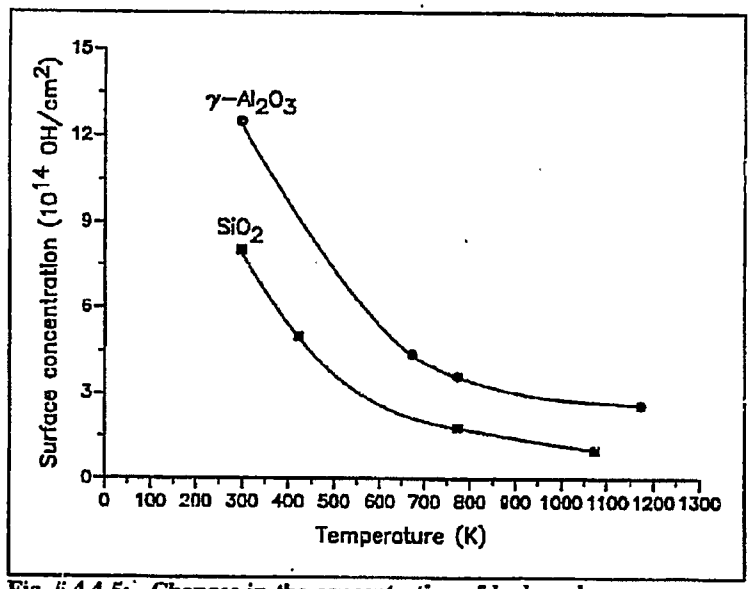

Fig. 5.4.4-5: Changes in the concentration of hydroxyl groups on SiO_2 and γ-Al_2O_3 with temperature /88,142/.

The values in Table 5.4.4-9 and 5.4.4-10 must be expected to represent a underestimate of the expected weight loss, since the water produced by the Fischer-Tropsch reaction is not included. This is corrected for by a simple calculation based on the conversion of CO at each temperatures, and selected results for the silica supported cobalt catalyst are summarized in Table 5.4.4-11. Thus, the values in Table 5.4.4-11 represent the weight loss associated with the removal of surface hydroxyl groups and water formed in the Fischer-Tropsch reaction.

Table 5.4.4-11: **Approximate estimates for the weight loss caused by temperature induced removal of hydroxyl groups and water from 4.7% Co/SiO_2 at reaction conditions (P_{Tot} = 6 bar, 200 Nml H_2/min.)**

Catalyst	*Temperature (K)* [1]	*Theoretical weight loss (mg)*
4.7% Co/SiO_2	473	24.9
	573	60.7

[1]: Temperature at which CO hydrogenation was performed

The underlying assumption which has to be considered is that the above approach assumes complete reconstitution of the hydroxyl groups on the dehydroxylated surface upon exposure to water. It is believed that neither the pretreatment temperature nor the reaction temperature used in this study is of such a magnitude that it is of significant influence to the above stated problem. Data in the literature confirm this view, reporting a complete reversible dehydration of silica up to about 673K /142/. Also, in cases where reconstitution of some, but not all of the surface hydroxyl groups occured upon readsorption of water, the temperature at which the γ-Al_2O_3 had been dehydrated was between 1073 and 1273K, significantly higher than those in the present study. Thus, the values in Table 5.4.4-11 can be regarded as the theoretical amounts of water/hydroxyl groups susceptible to removal by the performed temperature treatment. The calculations further indicated that the contribution from the OH groups is of minor importance compared to the amount of water which may condensate or desorb during the temperature treatment in hydrogen at higher reaction temperatures..

An increase in the temperature during treatment of the catalyst with hydrogen may facilitate a further reduction of the supported catalysts. In this respect, 4.6% Co/γ-Al_2O_3 has the lowest total degree of reduction as estimated from the TPR measurements and should in principle be most influenced assuming the above effect to be of importance. It can be questioned if the total degree of reduction (from the TPR-measurements) really is a valid measure of the actual extent of reduction obtained by the isothermal procedure generally applied throughout this study. The degree of reduction achieved by isothermal reduction at 673K will probably be lower than that from the TPR measurements, since the latter includes reduction of cobalt

species which is reduced at temperatures higher than 673K, for example cobalt aluminate. Since weight changes in the catalyst sample mass were recorded during the reduction procedure, there exists a possible mean of determining the extent of reduction of the catalysts applied in the microbalance experiments. The purpose of these calculations is to get a confirmation of the previous hypothesis and, if possible, to determine the associated weight changes. The results are summarized in Table 5.4.4-12, assumptions and calculations are shown in further detail in Appendix A12.

As anticipated, the degree of reduction of the alumina and silica supported cobalt catalysts are lower than those calculated from the TPR measurements. Furthermore, the extent of reduction of the 4.6% $Co/\gamma\text{-}Al_2O_3$ catalyst is lower than for the 4.7% Co/SiO_2 catalyst, confirming one of the main conclusions from TPR, namely that cobalt supported on silica is reduced to a higher extent than alumina supported cobalt. The values in Table 5.4.4-12 indicate that it is possible for cobalt to undergo further reduction upon the controlled temperature increase in hydrogen. It is difficult to achieve a good estimate for the expected decrease in the sample mass of the catalysts, since the historical effects complicates the picture rather seriously. Thus, one may only conclude that the observed weight decrease observed upon an increase in the temperature to 673/723K in hydrogen may be related to a further reduction of the catalyst.

The deposition of carbon or carbonaceous species has from the IR measurements been suggested as a possible reason for the decreased intensity and downscale shift in frequency of the linear CO band with increasing temperature. One could possible expect that the carbon containing materials would be hydrogenated to for example methane or other light gases upon introduction of hydrogen and the subsequent temperature increase. However, the common feature of the GC samples obtained during hydrogen treatment was a continuous decrease in the CH_4 concentration, suggesting that the hydrogenation of surface carbon is a slow process at the reaction conditions employed.

In the presence of hydrogen, hydrogenolysis of the adsorbed hydrocarbons to fragments with shorter chain length followed by desorption may be a reason for the observed weight decrease. Hydrogenolysis of alkanes, i.e. ethane, is generally believed to result in the formation of adsorbed C_1 fragments (CH or CH_2), which can be further hydrogenated to methane /231/.

Table 5.4.4-12: **Estimated degree of reduction for 4.6% Co/γ-Al_2O_3 and 4.7% Co/SiO_2 based on the observed weight changes during isothermal reduction.**
Reduction conditions: P_{Tot}=6 bar, 100 Nml H_2/min., T_{red} = 673K.

Catalyst	*Temperature (K)* [1]	*Theoretical weight loss (mg)*	*Observed weight loss (mg)*	*Extent of reduction (%)*
4.7% Co/SiO_2	473	12.07	5.97	49.47
	523	12.15	5.65	46.51
	573	12.27	5.23	42.64
	723	12.28	5.00	40.73
4.6% Co/γ-Al_2O_3	473	11.76	2.11	17.94
	523	12.02	3.10	25.80
	573	12.04	2.93	24.34
	723	4.173	1.23	29.47

[1]: Temperature at which CO hydrogenation was carried out.

The existence of formate and/or carbonate species on the catalyst during CO hydrogenation has been established from the IR-measurements. Their stability, evident from the infrared investigations, is in accordance with findings in the literature /232/, where it was reported that formate species did not react with surface hydrogen at temperatures less than 573K. Two principal decomposition pathways may be envisioned for the formate species, namely dehydration and dehydrogenation. Dehydration is catalysed by acidic oxides such as Al_2O_3, giving CO and water. The dehydrogenation reaction is more readily catalysed by metals and basic metal oxides /200/, resulting in the formation of CO_2 and hydrogen. Amenomiya /233,234/ stated that the formate ion was an intermediate in the water-gas-shift (WGS) reaction. The reactants as well as the products of the WGS reaction is involved in both of the possible decomposition pathways. From the IR investigations, the alumina support was regarded as the most likely adsorption sites for the formate structures. Since the inertness of the formate/carbonate bands argue against a surface metal association, a possible decomposition of the formate species may take place via dehydration to carbon monoxide and water.

6. SUMMARY AND CONCLUSIONS

6.1. TEMPERATURE PROGRAMMED REDUCTION

TPR-profiles of the silica supported cobalt catalysts, 0.82% Co/SiO_2 and 4.7% Co/SiO_2, showed that reductive decomposition of the metal precursor (cobalt nitrate) took place at 510 and 517K, respectively. The reduction of the cobalt oxide thus formed, Co_3O_4, is represented by peaks appearing at 535K (0.82% Co/SiO_2) and 564K (4.7% Co/SiO_2). The occurence of reduction peaks at higher temperatures has been ascribed to reduction of Co^{3+}/Co^{2+} interacting with the silica, forming mixed oxides (Co-Si-O) or cobalt silicates.

The TPR-spectrum of 4.6% $Co/\gamma\text{-}Al_2O_3$ showed peaks associated with reduction of Co_3O_4 (571K) and metal-support interactions (673-723, 984 and 1173K). The absence of any reduction peak for cobalt oxide in the spectrum of 1% $Co/\gamma\text{-}Al_2O_3$ indicate a strong coordination of cobalt with the alumina matrix, probably in the form of a cobalt aluminate spinel structure.

The total extent of reduction increased with increasing cobalt loading, irrespective of the applied support. The silica supported cobalt catalysts were reduced to a higher extent than their alumina supported counterparts.

6.2. INFRARED SPECTROSCOPY

In-situ infrared investigations of silica supported cobalt catalysts during CO hydrogenation showed the presence of linearly adsorbed carbon monoxide. The frequency of this band was constant, 2068 ± 4 cm^{-1} regardless of the H_2/CO ratio (2 or 3) or total pressure (2.5, 6 or 11 bar). This has been interpreted in terms of high local coverage of CO, akin to CO island formation.

With increasing CO hydrogenation temperature, deposition of carbon or carbonaceous materials caused a decreased band intensity and a concurrent shift in band frequency towards lower wavenumbers.

Flushing with inert gas (He) following CO hydrogenation resulted in a decrease in the linear CO band intensity accompanied by a downscale shift in frequency. Such behaviour was

related to reductions in the dipole-dipole interactions as a consequence of decreasing coverage of CO.

Absorption bands appearing in the frequency range 2000-1800 cm^{-1} during CO hydrogenation are not to be associated with brigdebonded CO, but due to lattice vibrations of the silica support.

The heat of adsorption of CO on 4.7% Co/SiO_2 was estimated to 40 ± 30 kJ/mole ($H_2/CO=2$, 2.5-11 bar, 473-573K).

Infrared absorption bands observed in the spectral region 3050-2700 cm^{-1} have been attributed to C-H stretching vibrations of adsorbed CH_2 and CH_3-groups. With increasing reaction temperature increasing fractions of CH_3-species was observed, while increasing pressure (at 473K) resulted in an increased intensity of the CH_2 absorption bands.

The absence of any effect of these structures on linearly adsorbed CO and the lack of any reasonable reaction capacity with H_2 indicate adsorption of the hydrocarbon species on the support. The variation in intensity with time during CO hydrogenation followed by treatment with He and/or H_2, suggest that the observed hydrocarbon structures do not represent reaction intermediates, rather spectator species of less significance with respect to the Fischer-Tropsch reaction mechanism.

The ratio of the CH_2 band intensities to the CH_3 band intensities (an expression of the hydrocarbon chain length) decreased with increasing CO hydrogenation temperature.

In the frequency range 1700-1300 cm^{-1}, two bands were observed on 4.7% Co/SiO_2 near 1560/1580 and 1450-1460 cm^{-1}. Various assignments have been proposed to account for these bands, such as asymmetric deformation of CH_3 groups, surface formate, carboxylate species in addition to carbonates. Based on the experimental data, no conclusive explanation can be given for the two bands appearing in the spectra below 1800 cm^{-1} during CO hydrogenation.

No absorption bands due to molecularly adsorbed CO was observed over 1% $Co/\gamma\text{-}Al_2O_3$. This is believed to be a result of cobalt located in tetrahedric interstices of the alumina lattice,

as indicated by the TPR and UV-VIS diffuse reflectance measurements. Calcination is not a necessary prerequisite for the formation of the cobalt aluminate phase.
The appearance of a pair of bands at 1996 and 1952 cm^{-1} during CO hydrogenation (473K, $H_2/CO=2$, 6 bar) over 4.6% $Co/\gamma\text{-}Al_2O_3$ have tentatively been assigned to bridgebonded CO, which possibly can be associated with the oxidic cobalt phase. The intensities of the two bands decreased with time during CO hydrogenation and upon an increase in the reaction temperature.

The frequency region 3050-2700 cm^{-1} of 4.6% $Co/\gamma\text{-}Al_2O_3$ during CO hydrogenation was dominated by absorption bands attributed to C-H stretching in adsorbed formate and hydrocarbon structures. The C-H stretching bands are believed to represent reaction products or by-products adsorbed on the alumina support.

Infrared bands below 1800 cm^{-1} in the spectra of $\gamma\text{-}Al_2O_3$ and 4.6% $Co/\gamma\text{-}Al_2O_3$ have been attributed to bidentate formate (1595, 1393 and 1377 cm^{-1}), unidentate carbonate (1458, 1377 cm^{-1}) and possibly bridged carbonate (bidentate, 1665 and 1321 cm^{-1}). The presence of these bands on blank $\gamma\text{-}Al_2O_3$ (at a higher intensity than on 4.6% $Co/\gamma\text{-}Al_2O_3$) and their behaviour as a function of the reaction temperature, indicate that these species are strongly adsorbed on alumina. Neither the band intensities nor frequencies were significantly influenced by treatment with He and hydrogen. Increasing CO hydrogenation temperature resulted generally in increasing band intensities, while the 1458, 1393 and 1377 cm^{-1} bands showed pronounced intensity variations with time at 573K.

6.3. CO HYDROGENATION ACTIVITY AND SELECTIVITY

The CO hydrogenation activity of 1% $Co/\gamma\text{-}Al_2O_3$, 4.6% $Co/\gamma\text{-}Al_2O_3$ and 4.7% Co/SiO_2 was studied in a microreactor at 523K, $H_2/CO=2$ and 6 bar total pressure.
At these conditions, 1% $Co/\gamma\text{-}Al_2O_3$ was nearly inactive in the Fischer-Tropsch synthesis, having an activity (expressed as mole CO converted/g Co·s) which was an order of magnitude lower than those of 4.6% $Co/\gamma\text{-}Al_2O_3$ and 4.7% Co/SiO_2.
The activity of 4.7% Co/SiO_2 was found to decrease with time of reaction, while the opposite behaviour was registered for 4.6% $Co/\gamma\text{-}Al_2O_3$. The increase in activity for the alumina

supported Co catalyst was suggested to be due to additional reduction of the catalyst. Various reasons for the decline in activity of 4.7% Co/SiO_2 were discussed, such as carbon deposition/carbide formation or reoxidation of cobalt due to the presence of water.
The hydrocarbon distribution could reasonably well be described by Anderson-Schulz-Flory polymerization kinetics, with deviations at carbon number 1 (positive) and 2 (negative).
The observed difference in the C_1-C_5 and C_{6+} hydrocarbon fractions between 4.7% Co/SiO_2 and 4.6% Co/γ-Al_2O_3 could not be explained and further experiments are required before a conclusive explanation can be offered.

6.4. GRAVIMETRY

Weight curves obtained during CO hydrogenation ($H_2/CO=2$, 6 bar) over 4.7% Co/SiO_2 at 473, 523 and 573K showed decreasing amounts of deposited materials with increasing reaction temperature. This has been interpreted as a result of accumulation of hydrocarbon products on the catalyst.
The preferred explanation of the observed weight increase during CO hydrogenation at 723K was the formation of inactive carbon, probably graphite.

In contrast, an increase in the amount of deposited material was observed with increasing CO hydrogenation temperature over 4.6% Co/γ-Al_2O_3. In addition, the support (γ-Al_2O_3) displayed a significant weight increase. A control experiment with glass-spheres resulted in negligible weight changes. Most of the weight increase observed over alumina alone and the alumina supported Co catalyst is believed to arise from the formation of formate and carbonate structures in addition to hydrocarbons, as indicated by the infrared results.

The weight changes observed as a consequence of increasing the reaction temperature in flowing hydrogen following CO hydrogenation can in principle be attributed to dehydroxylation of the catalysts, further reduction, decomposition of adsorbed formate and/or carbonate species or to hydrogenolysis of hydrocarbons.

7. REFERENCES

/1/ Sabatier, P., Senderens, J.B. : C. R. Acad. Sci., Paris, **134**. 514 (1902)

/2/ BASF : German Pat. 293, 787 (1913)

/3/ Fischer, F., Tropsch, H. : Brennst.-Chem. 4, 276 (1923)

/4/ Pichler, H. : Adv. Catal. (Frankenburg, Komarewsky and Rideal, Eds.), Academic Press Inc., New York, 4, 1952

/5/ Schanke, D. : Proceedings, European Applied Research Conference on Natural Gas, (EUROGAS), A105 (1992)

/6/ Bartholomew, C.H. : Stud. Surf. Sci. Catal. **64**, 158 (1991)

/7/ Ball, J. : Gas Matters, April 27, 1 (1989)

/8/ Haggin, J. : C&EN, April 29, 1991

/9/ Bartholomew, C.H., Reuel, R.C. : Ind. Eng. Chem. Prod. Res. Dev. **24(1)**, 56 (1985)

/10/ Hoff, A., Blekkan, E.A., Holmen, A., Schanke, D. : Proc. 10th Int. Congr. Catal. 1992

/11/ Sheppard, N., Nguyen, T.T. : *"Advances in Infrared and Raman Spectroscopy"* (Clarke and Hester, Eds.), New York, 5, 67, 1978

/12/ Masters, C. : *"Homogeneous Transition-metal Catalysis-a gentle art"*, Chapman & Hall Ltd., London, 1981

/13/ Massoth, F.E. : *"Advances in Catalysis"*, Academic Press, New York, 27, 265, 1978

/14/ Arnoldy, P., Franken, M.C., Scheffer, N., Moulijn, J.A. : J. Catal. **96**, 381 (1985)

/15/ Castner, D.G., Watson, P.R., Chan, I.Y. : J. Phys. Chem. **93**, 3188 (1989)

/16/ Augustine, R.L. : Catal. Rev. **13**, 285 (1976)

/17/ Winterbottom, K.M. : *"Catalysis and Chemical Processes"* (Pearce and Patterson, Eds.), Wiley, New York, 304, 1981

/18/ Rylander, P.N. : *"Catalysis:Science and Technology"* (Anderson and Boudart, Eds.), Springer-Verlag, New York, 4, 1, 1984

/19/ de Beer, V.H.J., van Sint Fiet, T.H.M., van der Steen, G.H.A.M., Zwaga, A.C., Schuit, G.C.A. . J. Catal. **35**, 297 (1974)

/20/ Wivel, C., Candia, R., Clausen, B.S., Mørup, S., Topsøe, H. : J. Catal. **68**, 453 (1981)

/21/ Prasad, R., Kennedy, L.A., Ruckenstein, E. : Combust. Sci. Technol. **22**, 271 (1980)

/22/ Garbowski, E., Guenin, M., Marion, M., Primet, M. : Appl. Catal. **64**, 209 (1990)

/23/ Sarup, B., Wojciechowski, B.W. : Can. J. Chem. Eng. **67**, 62 (1989)

/24/ Adesina, A.A., Hudgins, R.R., Silvestone, P.L. : Can. J. Chem. Eng. **64**, 447 (1986)

/25/ Lee, D.K., Lee, J.H., Ihm, S.K. : Appl. Catal. **36**, 199 (1988)

/26/ Dry, M.E. : *"Catalysis:Science and Tecnology"* (Anderson and Boudart, Eds.), Springer-Verlag, New York, **1**, 1981

/27/ Vannice, M.A. : J. Catal. **37**, 449 (1975)

/28/ Anderson, R.B. : The Fischer-Tropsch Synthesis, Academic Press, New York, 123, 1984

/29/ Delmon, B. : *"Proceedings, 3rd International Conference on the Chemistry and Uses of Molybdenum"* (Barry and Mitchell, Eds.), Climax Molybdenum Co., Ann Arbor, Michigan, 73, 1979

/30/ Farragher, A.L., Cossee, P. : Proc. 5th Int. Congr. Catal. 1972

/31/ de Beer, V.H.J., Schuit, G.C.A. : *"Preparation of Catalysts"* (Delmon, Jacobs and Poncelet, Eds.), Elsevier, Amsterdam, 343, 1976

/32/ Lo Jacono, M., Cimino, A., Schuit, G.C.A. : Gazz. Chim. Ital. **103**, 1281 (1973)

/33/ Biloen, P., Helle, J.N., Sachtler, W.M.H. : J. Catal. **58**, 95 (1979)

/34/ Araki, M., Ponec, V. : J. Catal. **44**, 439 (1976)

/35/ Goodman, D.W. : J. Vacuum Sci. Technol. **20**, 522 (1982)

/36/ Brady III, R.C., Pettit, R. : J. Am. Chem. Soc. **102**, 6181 (1980)

/37/ Joyner, R.W., Darling, G.R., Pendry, J.B. : Surf. Sci. **205**, 513 (1988)

/38/ Bell, A.T. : *"Structure and Reactivity of Surfaces"* (Morterra, Zecchina and Costa, Eds.), Elsevier Science Publishers BV, Amsterdam, **91**, 1989

/39/ Prior, K.A., Schwaha, K., Lambert, R.M. : Surf. Sci. **77**, 193 (1978)

/40/ Hofer, L.J.E., Peebles, W.C. : J. Am. Chem. Soc. **69**, 893 (1947)

/41/ Machocki, A. : Appl. Catal. **70**, 237 (1991)

/42/ Nakamura, J., Tanaka, K., Toyoshima, I. : J. Catal. **108**, 55 (1987)

/43/ Ihm, S.K., Lee, D.K. : *"Catalyst Deactivation"* (Bartholomew and Butt, Eds.), Elsevier Science Publishers VB, Amsterdam, 219, 1991

/44/ Nakamura, J., Toyoshima, I., Tanaka, K. : Surf. Sci. **201**, 185 (1988)

/45/ Papp, H. : Surf. Sci. **149**, 460 (1985)

/46/ Papp, H. : Ber. Bunsenges. Phys. Chem. **86**, 555 (1982)

/47/ Bridge, M.E., Comrie, C.M., Lambert, R.M. : Surf. Sci. **67**, 393 (1977)

/48/ Barcicki, J., Denis, A., Borowiecki, T., Grzegorczyk, W. : Chem. Stosow. **31(4)**, 497 (1987)

/49/ Choi, J-G., Rhee, H-K., Moon, S.H. : Appl. Catal. **13**, 269 (1985)

/50/ Lapidus, A., Krylova, A., Kazanskii,V., Borovkov, V., Zaitsev,A., Rathousky, J. Zukal, A., Jancalkova, M. : Appl. Catal. **73**, 65 (1991)

/51/ Rosynek, M.P., Polansky, C.A. : Appl. Catal. **73**, 97 (1991)

/52/ Arnoldy, P., Moulijn, J.A. : J. Catal. **93**, 38 (1985)

/53/ Chin, R.L., Hercules, D.H. : J. Phys. Chem. **86**, 360 (1982)

/54/ Chung, K.S., Massoth, F.E. : J. Catal. **64**, 320 (1980)

/55/ Choi, J.G., Rhee, H.K., Moon, S.H. : Korean J. of Chem. Eng. **1(2)**, 159 (1984)

/56/ Wang, W.J., Chen, Y.W. : Appl. Catal. **77**, 223 (1991)

/57/ Tung, H.C., Yeh, C.T., Hong, C.T. : J. Catal. **122**, 211 (1990)

/58/ Castner, D.G., Santilli, D.S. : ACS Symp. Ser. **248**, 39 (1984)

/59/ Okamoto, Y., Adachi, T., Nagata, K., Odawara, M., Imanaka, T. : Appl. Catal. **73**, 249 (1991)

/60/ Okamoto, Y., Nagata, K., Adachi, T., Imanaka, T., Inamura, K., Takyu, T. : J. Phys. Chem. **95**, 310 (1991)

/61/ Viswanathan, B., Gopalakrishnan, R. : J. Catal. **99**, 342 (1986)

/62/ Brown, R., Cooper, M.E., Whan, D.A. : Appl. Catal. **3**, 177 (1982)

/63/ Sexton, B.A., Hughes, A.E., Turney, T.W. : J. Catal. **97**, 390 (1986)

/64/ Paryjczak, T., Rynkowski, J., Karski, S. : J. Chromatogr. **188**, 254 (1980)

/65/ Van't Blik, H.F.J., Prins, R. : J. Catal. **97**, 188 (1986)

/66/ Blyholder, G. : J. Phys. Chem. **68**, 2772 (1964)

/67/ Blyholder, G., Allen, M.C. : J. Amer. Chem. Soc. **91**, 3158 (1969)

/68/ Ford, R.R. : Adv. Catal. **21**, 51 (1970)

/69/ Heal, M.J., Leisegang, E.C., Torrington, R.G. : J. Catal. **51**, 314 (1978)

/70/ Sato, K.S., Inoue, Y., Kojima, I., Miyazaki, E., Yasumori, I. : J. Chem. Soc., Faraday Trans. I **80**, 841 (1984)

/71/ Mostovaya, L.Ya., Petkevich, T.S., Kupcha, L.A. : Zh. Prikl. Spektrosk. **51(6)**, 968 (1989)

/72/ Rao, K.M., Spoto, G., Zecchina, A. : J. Catal. **113**, 466 (1988)

/73/ Zaitsev, A.V., Kozlova, G.V., Borovkov, V.Yu., Krylova, A.Yu., Lapidus, A.L., Kazanskii, V.B. : Iz. Akad. Nauk. SSSR, Ser. Khim. **11**, 2640 (1990)

/74/ Ferreira, L.C., Leisegang, E.C. : J. S. Afr. Chem. Inst. **23**, 136 (1970)

/75/ Ryberg, R. : Adv. Chem. Phys. **76**, 1 (1989)

/76/ Ponec, V. : Stud. Surf. Sci. Catal. **64**, 117 (1991)

/77/ Lee, W.H. : Ph.D Thesis, Brigham Young University, 1988

/78/ Arakawa, H., Takeuchi, K., Matsuzaki, T., Sugi, Y. : Sekiyu Gakkaishi **31(4)**, 335 (1988)

/79/ Gopalakrishnan, R., Viswanathan, B. : Chemical Age of India **37(6)**, 411 (1986)

/80/ Eischens, R.P., Pliskin, W.A. : Adv. Catal. **10**, 1 (1958)

/81/ Eischens, R.P., Pliskin, W.A., Francis, S.A. : J. Chem. Phys. **22**, 1786 (1954)

/82/ Eischens, R.P., Pliskin, W.A., Francis, S.A. : J. Phys. Chem. **60**, 194 (1956)

/83/ Blyholder, G. : Proc. 3rd. Int. Congr. Catal. 1964

/84/ Blyholder, G. : J. Phys. Chem. **79**, 756 (1975)

/85/ Zaitsev, A.V., Krasnova, L.L., Savel'ev, M.M., Borovkov, V.Yu., Lapidus, A.L., Kazanskii, V.B. : Kinet. Katal. **28**, 1194 (1987)

/86/ Kuznetsov, V.L., Aleksandrov, M.N., Bulgakova, L.N. : J. Mol. Catal. **55(1-3)**, 146 (1989)

/87/ Kavtaradze, N.N, Sokolova, N.P. : Russ. J. Chem. **38(4)**, 548 (1964)

/88/ Basila, M.R. : Appl. Spectr. Rev. **1(2)**, 289 (1968)

/89/ Park, R.L., Farnsworth, H.E. : J. Phys. Chem. **43**, 2351 (1965)

/90/ Park, R.L., Madden, H.L. : Surf. Sci. **11**, 180 (1968)

/91/ Little, L.H. : *"Infrared Spectra of Adsorbed Species"*, Academic Press, London, 1966

/92/ Little, L.H. : *"Chemisorption and Reactions on Evaporated Metallic Films"* (Anderson, Ed.), Academic Press, New York, 1970

/93/ Gardner, R.A., Petrucci,R.H. : J. Phys. Chem. **67**, 1376 (1963)

/94/ Voroshilov, T.G., Lunev, N.K., Roev, L.M., Rusov, M.T. : Dopov. Akad. Nauk. Ukr. RSR Ser B **4**, 319 (1975)

/95/ Busca, G., Lorenzelli, V., Escribano, V.S., Guidetti, R. : J. Catal. **131**, 167 (1991)

/96/ Yao, H.C., Shelef, M. : J. Phys. Chem. **78(24)**, 2490 (1974)

/97/ Hertl, W. : J. Catal. **31**, 231 (1973)

/98/ Busca, G., Guidetti, R., Lorenzelli, V. : J. Chem. Soc. Faraday Trans. **86(6)**, 989 (1990)

/99/ Queau, R., Poilblanc, R. : J. Catal. **27**, 200 (1972)

/100/ Baker, F.S., Bradshaw, A.M., Pritchard, J., Sykes, K.W. : Surf. Sci. **12**, 426 (1968)

/101/ Bradshaw, A.M., Pritchard, J. : Proc. Roy. Soc. Lond. **A316**, 169 (1970)

/102/ Hayward, D.O. : Paper presented at Gordon Conference on Catalysis, Colby College, New Hampshire, USA (1963)

/103/ Wojtczak, J., Queau, R., Poilblanc, R. : J. Catal. **37**, 391 (1975)

/104/ Harrod, J.F., Roberts, R.W., Rissmann, E.F. : J. Phys. Chem **71(2)**, 343 (1967)

/105/ Kuznetsov, V.L., Lisitsyn, A.S., Golovin, A.V., Aleksandrov, M.N., Yermakov, Yu.I. : Proceedings of the 5th international symposium on the relationship between Homogeneous and Heterogeneous Catalysis, VNU Science Press, Netherlands, 1065, 1986

/106/ Gupta, R.B., Viswanathan, B., Sastri, M.V.C. : J. Catal. **26**, 212 (1972)

/107/ Sastri, M.V.C., Gupta, R.B., Viswanathan, B. : J. Catal. **32**, 325 (1974)

/108/ Ansorge, J., Förster, H. : React. Kinet. Catal. Lett. **10(1)**, 99 (1979)

/109/ Savel'eva, G.A., Sass, A.S., Vozdvizhenskii, V.F., Tungatarova, S.A., Popova, N.M. : Russ. J. Phys. Chem. **62(4)**, 511 (1988)

/110/ Onishi, T., Maruya, K., Demen, K., Abe, K., Kondo, J. : Proc. 9th Int. Congr. Catal. 1988

/111/ Li, G., Ridd, M.J., Larkins, F.P. : Aust. J. Chem. **44**, 623 (1991)

/112/ Gopalakrishnan, R., Viswanathan, B. : J. Coll. Interf. Sci. **102(2)**, 370 (1984)

/113/ Dorokhina, T.S., Zaitsev, A.V., Borovkov, V.Yu., Kazanskii, V.B. : Kinet. Katal. **32(6)**, 1499 (1991)

/114/ Gardner, R.A., Petrucci, R.H. : J. Am. Chem. Soc. **82**, 5051 (1960)

/115/ Iglesia, E., Soled, S.L., Fiato, R.A. : J. Catal. **137**, 212 (1992)

/116/ Che, M., Bennett, C.O. : Adv. Catal. **36**, 55 (1989)

/117/ Moon, S.H., Yoon, K.E. : Korean J. of Chem. Eng. **5(1)**, 47 (1988)

/118/ Johnson, B.G., Rameswaran, M., Patil, M.D., Muralidhar, G., Bartholomew, C.H. : Catal. Today **6**, 81 (1989)

/119/ Reuel, R.C., Bartholomew, C.H. : J. Catal. **85**, 78 (1984)

/120/ Vannice, M.A. : J. Catal. **50**, 228 (1977)

/121/ Fu, L., Bartholomew, C.H. : J. Catal. **92**, 376 (1985)

/122/ Rameswaran, M., Bartholomew, C.H. : J. Catal. **117**, 218 (1989)

/123/ Johnson, B.G., Bartholomew, C.H., Goodman, D.W. : J. Catal. **128**, 231 (1991)

/124/ Kelly, R.D., Goodman, D.W. : Surf. Sci. **123**, L743 (1982)

/125/ Kelly, R.D., Goodman, D.W. : Am. Chem. Soc. Div. Fuel Chem. Prepr. **25(2)**, 43 (1980)

/126/ Lee, W.H., Bartholomew, C.H. : J. Catal. **120**, 256 (1989)

/127/ Lee, J.H., Lee, D.H., Ihm, S.K. : J. Catal. **113**, 544 (1988)

/128/ Moon, S.H., Yoon, K.E. : Appl. Catal. **16**, 289 (1985)

/129/ Ponec, V. : Catal. Today. **12**, 227 (1992)

/130/ Biloen, P., Sachtler, W.M.H. : Adv. Catal. **30**, 165 (1981)

/131/ Dry, M.E. : Catal. Today **6(3)**, 183 (1990)

/132/ Fischer, F., Tropsch, H. : Brennst.-Chem. **7**, 97 (1926)

/133/ Fischer, F., Koch, H. : Brennst.-Chem. **13**, 428 (1932)

/134/ Pannel, R.B., Kibby, C.L., Kobylinski, T.P. : Stud. Surf. Sci. Catal. **7A**, 447 (19??)

/135/ Rautavouma, A.O.I., van der Baan, H.S. : Appl. Catal. **1**, 247 (1981)

/136/ Wang, W.J., Chen, Y.W. : Appl. Catal. **77**, 21 (1991)

/137/ Lee, D.K., Ihm., S.K. : Appl. Catal. **32**, 85 (1987)

/138/ Schanke, D. : Ph.D Thesis, University of Trondheim, 1986

/139/ Hurst, N.W., Gentry, S.J., Jones, A., McNicol, B.D. : Catal. Rev.-Sci. Eng. **24(2)**, 233 (1982)

/140/ Subramanian, S. : Platinum Metals Rev. **36(2)**, 98 (1992)

/141/ Fierro, J.L.G. : Stud. Surf. Sci. Catal. **57B**, B67 (1990)

/142/ Hair, M.L. : *"Infrared Spectroscopy in Surface Chemistry"*, Marcel Dekker, New York, 1967

/143/ Delgass, N., Haller, Kellerman, Lunsford, :*"Spectroscopy in Heterogeneous Catalysis"*, Academic Press, New York, 1979

/144/ Herzberg, G. : *"Infrared and Raman Spectra of Polyatomic Molecules"*, Van Nostrand, Princeton, N.J., 1945

/145/ Cross, P.C., van Vleck, J.H. : J. Chem. Phys. 1, 350 (1933)

/146/ Sant, R. : Ph.D Thesis, University of Notre Dame, 1988

/147/ Bell, R.J. : *"Introductory Fourier Transform Spectroscopy"*, Academic Press, New York, 1972

/148/ Bell, A.T. : ACS Symp. Ser. **137**, 13 (1980)

/149/ Griffiths, P.R., de Haseth, J.A. : *"Fourier Transform Infrared Spectroscopy"*, John Wiley, New York, **83**, 1986

/150/ Griffiths, P.R. : *"Chemical Infrared Fourier Transform Spectroscopy"*, John Wiley, New York, **43**, 1975

/151/ Michelson, A.A. : Phil. Mag. Ser. 5 **31**, 256 (1891)

/152/ Michelson, A.A. : Phil. Mag. Ser. 5 **34**, 280 (1892)

/153/ Paper by A. Christy, University of Bergen, Norway

/154/ Griffiths, P.R., Sloane, H.J., Hanna, R.W. : Appl. Spec. **31**, 485 (1977)

/155/ Blekkan, E.A., Holmen, A., Vada, S. : Acta Chemica Scandinavia **47**, 275 (1993)

/156/ Hicks, R.F., Kellner, C.S., Savatsky, B.J., Hecker, W.C., Bell, A.T. : J. Catal. **71**, 216 (1981)

/157/ Hoff, A. : Ph.D Thesis, University of Trondheim, 1993

/158/ Written by B. Førre, SINTEF, Applied Physics, Trondheim

/159/ Roe, G.M., Ridd, M.J., Cavell, K.J., Larkins, F.P. : Stud. Surf. Sci. Catal. **36**, 509 (1988)

/160/ Ruger, M. : Ker. Rund. **31**, 79, 87, 99, 110 (1923); Chem. Abstr. **18**, 156 (1924)

/161/ Puskas, I., Fleisch, T.H., Hall, J.B., Meyers, B.L., Roginski, R.T. : Proc. 10th Int. Congr. Catal. 1992

/162/ Lund, C.R.F., Dumesic, J.A. : J. Catal. **72**, 21 (1981)

/163/ Castner, D.G., Watson, P.R., Chan, I.Y. : J. Phys. Chem. **94**, 819 (1990)

/164/ Polansky, C.A. : Ph.D Thesis, Texas A&M University, 1988

/165/ Gates, B.C., Katzer, J.R., Schuit, G.C.A. : *"Chemistry of Catalytic Processes"* , McGraw-Hill, New York, 1979

/166/ McDonald, R.S. : J. Phys. Chem. **62**, 1168 (1958)

/167/ Shigeishi, R.A., King, D.A. : Surf. Sci. **58**, 379 (1976)

/168/ Crossley, A., King, D.A. : Surf. Sci. **68**, 528 (1977)

/169/ Browne, V.M., Fox, S.G., Hollins, P. : Catal. Today **9**, 1 (1991)

/170/ Boudart, M., Djega-Mariadassou, G. : *"Kinetics of Heterogeneous Catalytic Reactions"*, Princeton University Press/Princeton, N.J., 26 (1984)

/171/ Hollins, P., Pritchard, J. : *"Vibrational Spectroscopies for Adsorbed Species"* (Bell and Hair, Eds.), ACS Symp. Ser. **137**, 51 (1980)

/172/ Hollins, P., Priv. Comm.

/173/ Ortega, A., Hoffman, F.M., Bradshaw, A.M. : Surf. Sci. **119**, 79 (1982)

/174/ Hardeveld, R. van, Montfoort, A. van : Surf. Sci. **17**, 90 (1969)

/175/ Reoethlein, R.J. : J. Electrochem. Soc. **116**, 37 (1969)

/176/ Breitev, M.W. : Electrochim. Acta **29**, 711 (1984)

/177/ Huff, G.A., Kobylinski, T.P. : Symp. Methane Upgrading, Div. Pet. Chem., 175 (1979)

/178/ Kartaradage, N.N., Sokolova, N.P. : Dokl. Phys. Chem. **172**, 39 (1967)

/179/ Golodets, G.I., Pavlenko, N.V., Tripol'skii, A.I. : Kinet. Katal. **28(4)**, 883 (1987)

/180/ Somorjai, G.A. : Stud. Surf. Sci. Catal. **64**, 462 (1991)

/181/ Rasband, P.B., Hecker, W.C. : J. Catal. **139**, 551 (1993)

/182/ Duncan, T.M., Yates, J.T., Vaughan, R.W. : J. Chem. Phys. **73(2)**, 975 (1980)

/183/ Ratnasamy, P., Knözinger, H. : J. Catal. **54**, 155 (1978)

/184/ Sass, A.S., Shvets, V.A., Savel'eva, G.A., Kazanskii, V.B. : Kinet. Katal. **26(5)**, 1149 (1985)

/185/ Neubauer, L.R. : Ph.D Thesis, Brigham Young University, 1986

/186/ Li, G., Priv. Commun.

/187/ Van Every, K.W., Ph.D Thesis, University of California, 1987

/188/ Stoop, F., Toolenaar, F.J.C.M., Ponec, V. : J. Catal. **73**, 50 (1982)

/189/ Dalla Betta, R.A., Shelef, M. : J. Catal. **48**, 111 (1977)

/190/ King, D.L. : J. Catal. **61**, 77 (1980)

/191/ Heal, M.J., Leisegang, E.C., Torrington, R.G. : J. Catal. **42**, 10 (1976)

/192/ Ekerdt, J.G., Bell, A.T. : J. Catal. **58**, 170 (1979)

/193/ Reuel, R.C., Bartholomew, C.H. : J. Catal. **85**, 63 (1984)

/194/ Rao, K.M., Scarano, D., Spoto, G., Zecchina, A. : Surf. Sci. **204**, 319 (1988)

/195/ Kellner, C.S., Ph.D Thesis, University of California, 1981

/196/ Dalla Betta, R.A., Piken, A.G., Shelef, M. : J. Catal. **35**, 54 (1974)

/197/ Wexler, A.S. : Spectrochim. Acta **21**, 1725 (1965)

/198/ Tamaru, K., Onishi, T. : Appl. Spectrosc. Rev. **9(1)**, 133 (1975)

/199/ Kellner, C.S., Bell, A.T. : J. Catal. **71**, 296 (1981)

/200/ Grenoble, D.C., Estadt, M.M., Ollis, D.F. : J. Catal. **67**, 90 (1981)

/201/ Trillo, J.M., Munuera, G., Criado, J.M. : Catal. Rev. **7**, 51 (1972)

/202/ Spinner, E. : J. Chem. Soc. 1964, 4217

/203/ Blyholder, G., Shihabi, D., Wyatt, W.V., Bartlett, R. : J. Catal. **43**, 122 (1976)

/204/ Arakawa, H., Fukushima, T., Ichikawa, M., Takeuchi, K., Matsuzaki, T., Sugi, Y. : Chem. Lett., 23 (1981)

/205/ Yamasaki, H., Kobori, Y., Naito, S., Onishi, T., Tamaru, K. : J. Chem. Soc., Faraday Trans. 1 **77**, 2913 (1981)

/206/ Pien, S.H., Chuang, S.C. : J. Mol. Catal. **68**, 313 (1991)

/207/ King, D.L. : Prepr. Amer. Chem. Soc. Div. Petrol. Chem. **23(2)**, 482 (1977)

/208/ Duchinskii, Y.W., Kuzyakin, E.B., Pasalskii, B.K. : Ukr. Khim. Zh. **53(7)**, 697 (1987)

/209/ Fujita, J., Martell, A.E., Nakamoto, K. : J. Chem. Phys. **36(2)**, 339 (1962)

/210/ Goodsel, A.J. : J. Catal. **30**, 175 (1973)

/211/ Edwards, J.F., Schrader, G.L. : Appl. Spec. **35(6)**, 559 (1981)

/212/ Eischens, R.P., Pliskin, W.A. : Adv. Catal. **9**, 662 (1957)

/213/ Taylor, J.H., Amberg, C.H. : Canad. J. Chem. **39**, 535 (1961)

/214/ Li, C., Domen, K., Maruya, K., Onishi, T. : J. Catal. **125**, 445 (1990)

/215/ Wang, G.W., Hattori, H. : J. Chem. Soc., Faraday Trans. 1 **80**, 1039 (1984)

/216/ Amerikov, V.G., Kasatkina, L.A. : Kinet. Katal. **12**, 122 (1971)

/217/ Little, L.H., Amberg, C.H. : Canad. J. Chem. **40**, 1997 (1962)

/218/ Makarova, M.A., Paukshtis, E.A., Thomas, J.M., Williams, C., Zamaraev, K.I. : Catal. Today **9**, 61 (1991)

/219/ Davydov, A.A. : *"Infrared Spectroscopy of Adsorbed Species on the Surface of Transition Metal Oxides"* (Rochester, Ed.), John Wiley & Sons, Chichester, 39 (1990)

/220/ Anderson, K.G., Ekerdt, J.G. : J. Catal. **116**, 556 (1989)

/221/ Eischens, R.P. : Stud. Surf. Sci. Catal. **44**, 51 (1989)

/222/ Ådnanes, E. : M.Sc.Eng. Thesis, University of Trondheim, 1991

/223/ Niemansverdriet, J.W., van der Kraan, A.M. : J. Catal. **72**, 385 (1981)

/224/ Huff, G.A., Satterfield, C.N. : Ind. Eng. Chem. Process Des. Dev. **24(4)**, 986 (1985)

/225/ Ruckenstein, E., Hu, X.D. : J. Catal. **100**, 1 (1986)

/226/ Anderson, R.B. : Catalysis **10** (Emmet, Ed.), Reinhold, New York, 1958

/227/ Smith, D.F., Hawk, C.O., Golden, P.L. : J. Amer. Chem. Soc. **52**, 3221 (1930)

/228/ Kölbel, H., Ruschenburg, E. : Brennst.-Chem. **35**, 161 (1954)

/229/ Weller, S., Hofer, L.J.E., Anderson, R.B. : J. Amer. Chem. Soc. **70**, 799 (1948)

/230/ Tronstad, O., Carlsen G.F. : Department of Industrial Chemistry, NTH

/231/ Sinfelt, J.H. : Catal. Lett., 159 (1991)

/232/ Yilu, F., Kraus, L., Knozinger, H. : Chinese J. Chem. Phys. **2(2)**, 125 (1988)

/233/ Amenomiya, Y. : J. Catal. **55**, 205 (1978)

/234/ Amenomiya, Y. : J. Catal. **57**, 64 (1979)

/235/ Francis, S.A. : J. Chem. Phys. **18**, 861 (1950)

/236/ Johansen, T. : M.Sc. Eng. Thesis, University of Trondheim, 1992

/237/ Toyoshima, I., Somorjai, G.A. : Catal. Rev. Sci. Eng. **19**, 105 (1979)

APPENDICES

Appendix A1: Analysis of catalysts.

Sample A: Co/SiO_2 Sample B: $Co/\gamma\text{-}Al_2O_3$

Analyserapport

SINTEF Teknisk kjemi
Gruppe for sensor- og analyseteknikk

STIFTELSEN FOR INDUSTRIELL OG TEKNISK FORSKNING VED NORGES TEKNISKE HØGSKOLE

Adresse: 7034 TRONDHEIM
Telefon: +47-7-59 30 00
Telex: 55 620 sintf n
Telefax: +47-7-59 31 62

SINTEF
Teknisk kjemi
7034 TRONDHEIM
Attn: Geir R. Fredriksen

Trondheim, 1991-05-28

Prosjekt nr. Z16110.12 J.nr. 1418/91

Deres ref.: Vår ref.: EK/vck

Oppdrag: **Bestemmelse av Co og vann**

Prøvemateriale	Antall	Form	Prøver mottatt
Co-holdige prøver	2		uke 20

Prøver uttatt av oppdragsgiver Utført av E. Kleven

Analysemetoder Co er løst ut og bestemt vha AAS
Vann er bestemt ved 100°C som vekttap

Anmerkning

Resultat

Prøve merket	%				
	Co-innhold			Vann-innhold	
	Parallellres.		Gj.snitt	Parallellres.	Gj.snitt
A	4.80	4.60	4.70	1.85 1.95	1.90
B	4.72	4.44	4.60	2.93 2.97	2.95

Kalman Nagy
fagsjef

E. Kleven

Appendix A2: Methods applied in pressing disks of silica, alumina and silica and alumina supported cobalt catalysts.

A number of ways were tested in order to press disks of acceptable quality for use in the FTIR investigations. At least two criteria were to be fulfilled:

1. The weight of the catalyst/support disk was to be as low as practically possible (in order to achieve optimum throughput).
2. The disks should be of sufficient mechanical strength.

One may argue that these criteria mutually exclude each other. It was found, that by proper loading of the KBr die with the powdered catalysts or pure supports, disks with acceptable mechanical strength and transparency could be obtained. The method of loading the powder into the die depended on the type of support, that is, whether it was silica or alumina which was to be pressed.

The different methods of loading the powdered catalysts or supports in the KBr die were as follows:

A. The material was placed in the center of the optical pellet.
B. The material was randomly distributed over the complete optical pellet surface.
C. The material was placed near the die wall on the edge of the optical pellet.

For silica alone, option (method) A gave the best result in combination with knocking of the die against the table, short pressing times and low pressure.
The optimum result for the silica supported catalysts was achieved by using method B, followed by banging the die towards the table two or three times. Occasionally, the die plunger was used to smooth the powder over the optical pellet surface after the former treatment. The optimal amount of catalyst powder was 13-18 mg.

The procedure used in pressing disks of alumina alone and the alumina supported Co-catalysts was a modified version of method A. After the material had been transferred to the centre of

the optical pellet, the die plunger was carefully placed on top of the catalyst/support powder and rotated several times, distributing the material over the complete optical surface. If an incomplete distribution took place, the disk would disintegrate in the centre where most of the powder was located.

Method C was generally not used, since the catalyst disk tended to stick to the wall and thus cracked from the edges when removed from the die.

Several variations and combinations of the amount of powder, loading methods and distribution methods were tried, but the above procedures gave the best overall results.

Furthermore, it was experienced that cleaning of the surface of the optical pellets with acetone and cottonwool between each attempt when pressing disks of the silica supported Co-catalysts resulted in a higher rate of successfully pressed disks. For the alumina supported catalysts, cleaning of the pellets gave poor results, since the powder after pressing was "glued" to the pellet surface.

It would seem that the difference between method A and B is of little importance from a practical point of view. However, the apparently minor differences had major influence on the final result.

The chosen pressing times and applied pressure were also factors which to a certain extent affected the outcome of the pressing procedure. As was expected, there was a relationship between the amount of catalyst/support and the magnitude of the applied pressure. Generally, high amounts of the material required high pressure. That, however, often tended to result in cracked disks, especially if the powder was loaded into the KBr die according to method C. Low pressure was usually applied in cases where relatively low amounts of the support or the supported catalysts were used. Silica itself or the silica supported Co-catalysts were such a case. Due to the dust like character of these compounds, it was easy to distribute them over the optical surface of the pellet, and the pressure did not need to be very high. After a screening of suitable pressures, the best results were obtained by using the body weight of the operator. Since the match weight of the operator was around 80 kg, the optimum pressure for

silica and the silica supported catalysts were approximately 60 kg/cm^2, even though pressures up to 100 kg/cm^2 were used, depending on the amount of the catalyst. The die was kept under the above pressure for relatively short periods of time, approximately 10 sec. Applying higher pressure and longer pressing times resulted in cracked disks.

The picture was a little bit different for alumina alone and the alumina supported cobalt catalysts. Since a higher amount of catalyst generally was used, the pressure also needed to be considerably higher. 2000-3000 kg/cm^2 usually worked very well when the KBr die was loaded with 15-25 mg. catalyst. The pressing times necessary to achieve acceptable disk was long compared to that used when pressing the silica based catalysts, 5-12 min. It did seem that it was necessary for the alumina and the alumina supported catalysts to "settle down", which was found to require the above mentioned time. When lower pressure and shorter pressing times where applied, the wafers disintegrated and had to be discarded.

Appendix A3: Gases applied in the different experimental apparatus.

1.	TPR apparatus:	H_2 5.0 (99.999%)
		Ar 6.0 (99.999%)
		7% H_2 in Ar
2.	FTIR apparatus	H_2 2.7 (99.7%)
		He 6.0 (99.999%)
		H_2/CO=2:1, 3:1
		He/CO=9:1
3.	Microreactor apparatus	
	Gas Cromatograph	He S4.5 (99.995%)
		H_2 2.7 (99.7%)
		Air kl.2 pkt. A
		CO_2 D3.0
	CO hydrogenation	H_2 2.7 (99.7%)
		He 4.5 (99.995%)
		7.5% N_2 in CO
4.	Gravimetric apparatus	H_2 2.7 (99.7%)
		8% N_2 in CO
		He 4.5 (99.995%)

Appendix A5: **Examples of TC and FID chromatograms obtained in the microreactor experiments during CO hydrogenation.**

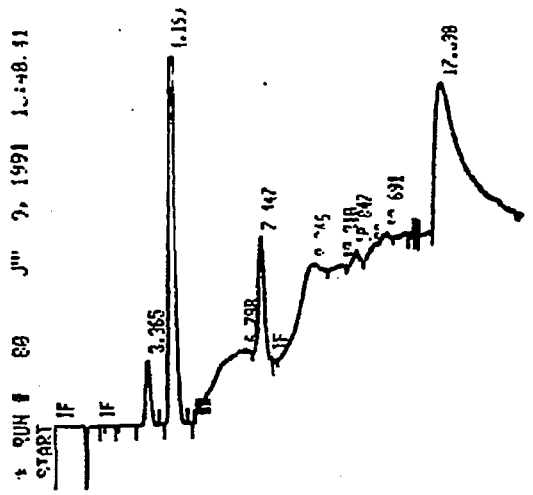

AREA%

RT	AREA	TYPE	WIDTH	AREA%
3.365	418297	PB	.172	6.8[illegible]50
4.199	4862621	PB	.225	[illegible]5.258
6.798	48787	PV	1.500	.79331
7.447	38856	VB	.258	.6.584
9.346	69802	PV	.915	1.14225
10.310	36957	VV	.742	.60477
10.847	26309	VV	.496	.43052
12.691	66632	VV	2.343	1.0838
17.590	542664	BB	3.185	8.83822

TOTAL AREA=6118925
MUL FACTOR=1.0000E+00

Fig. A5-1: **GC chromatogramme (TCD) obtained during CO hydrogenation over 4.7% Co/SiO_2.**

CO hydrogenation conditions:
P_{Tot}= 6 bar, H_2/CO=2, T=523K

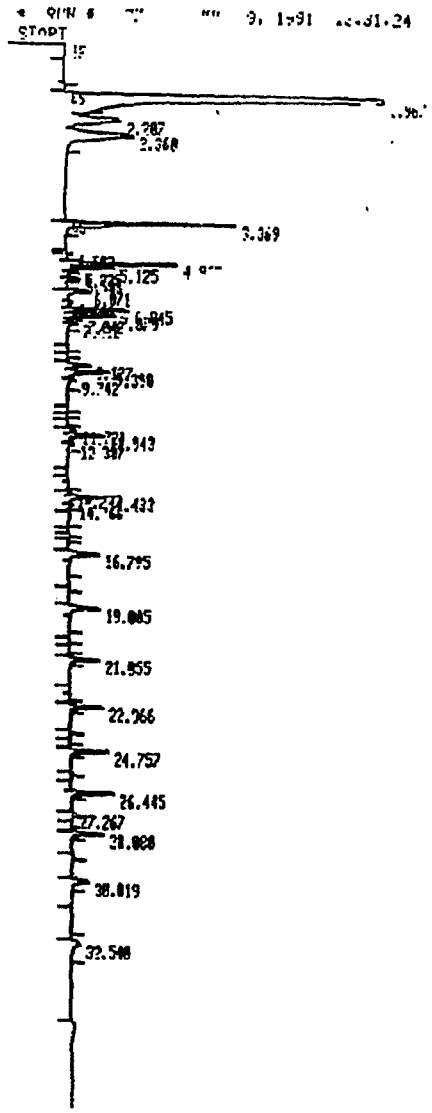

RT	AREA	TYPE	WIDTH	A.REA
1.967	1714958	PB	.062	2.3142
2.287	193827	PP	.056	0.2616
2.368	18249	PB	.066	0.0246
3.369	585521	PV	.069	0.7904
4.592	25197	BP	.103	0.0340
4.965	395385	PV	.082	0.5336
5.125	175580	VV	.083	0.2369
5.325	42699	VV	.048	0.0576
5.583	30554	VB	.071	0.0412
6.071	116231	BV	.125	0.1569
6.561	48283	VV	.174	0.0651
6.845	214914	VV	.081	0.2901
7.079	169284	VV	.082	0.2284
7.242	46277	VV	.079	0.0624
7.412	44192	VB	.102	0.0596
9.127	181583	BV	.185	0.2451
9.298	178173	VV	.096	0.2405
9.742	44216	VB	.120	0.0597
11.721	46681	BV	.120	0.0630
11.943	152239	VV	.096	0.2055
12.387	29751	VB	.106	0.0401
14.277	15896	BV	.100	0.0215
14.432	169826	VV	.112	0.2292
14.766	18208	VB	.105	0.0246
16.795	162432	BV	.128	0.2192
19.085	159258	BV	.119	0.2149
21.855	128488	BB	.079	0.1734
22.966	138835	BB	.092	0.1874
24.757	152338	BB	.093	0.2056
26.445	121511	BB	.093	0.1639
27.267	9325	PP	.098	0.1259
28.828	149561	PB	.107	0.2018
30.819	117139	BB	.157	0.2381
32.548	93463	BB	.255	0.2061

TOTAL AREA=5946243
AREA FACTOR=1.0000E+00

Fig. A5-2: GC chromatogramme (FID) obtained during CO hydrogenation over 4.7% Co/SiO_2.

CO hydrogenation conditions:
P_{Tot}= 6 bar, H_2/CO=2, T=523K

Appendix A6: Estimation of the heat of adsorption of CO on 4.7% Co/SiO_2 at reaction conditions.

By using the Langmuir-Hinschelwood expression relating the pressure of the gas to the volume adsorbed, it is possible to determine the equilibrium constant (K_{CO}) at different reaction conditions.

The starting point is the Langmuir-Hinschelwood equation:

$$\theta_{CO} = \frac{K_{CO} \cdot P_{CO}}{1 + K_{CO} \cdot P_{CO}} \qquad \text{A6.1}$$

where θ_{CO}= coverage of CO

K_{CO}= adsorption equilibrium constant

P_{CO}= partial pressure of CO

θ_{CO} can be expressed as A_a/A_∞, where A_a represents the actual absorbance at reaction conditions, and A_∞ the absorbance at infinite CO pressure corresponding to a complete coverage of carbon monoxide.

Substituting A_a/A_∞ for θ_{CO} in the above equation A6.1 and rearranging gives:

$$\theta_{CO} + \theta_{CO} \cdot K_{CO} \cdot P_{CO} = K_{CO} \cdot P_{CO} \qquad \text{A6.2}$$

$$\frac{A_a}{A_\infty} + \frac{A_a}{A_\infty} \cdot K_{CO} \cdot P_{CO} = K_{CO} \cdot P_{CO} \qquad \text{A6.3}$$

Multiplying both sides of equation A6.3 with $1/(A_a \cdot K_{CO})$ results in the relationship:

$$\frac{P_{CO}}{A_s} = \frac{P_{CO}}{A_\infty} + \frac{1}{K_{CO} \cdot A_\infty} \qquad \text{A6.4}$$

From the infrared investigations of 4.7% Co/SiO_2 during CO hydrogenation at different reaction conditions (P_{Tot}=2.5-11 bar, H_2/CO=2, T=473-573K), the following values were obtained, see Table A6-1.

Table A6-1: Experimental values of P_{CO}/A_s determined from the IR-measurements at the given reaction conditions (H_2/CO=2).

	P_{CO}/A_s[1] at different temperatures		
P_{CO} (bar)	473K	523K	573K
0.833	1.833	----	----
2.0	2.691	4.888	8.178
3.666	4.987	6.552	10.715

[1] : A_s is corrected for differences in the weight of the catalyst disks and the metal loading. A_s refers to the absorbance determined as peak height for the linear CO band (2068 ± 4 cm^{-1}).

When the P_{CO}/A_s values in Table A6-1 at each temperature is plotted versus the partial pressure of CO, the slope of the line will, according to equation A6.4, correspond to $1/A_\infty$, while the y-axis intercept represents $1/A_\infty \cdot K_{CO}$. Fig. 5.2.3.5-1 illustrates the result when the data are plotted in such a way. Linear regression was used to draw the lines and determine the values of $1/A_\infty$ at each of the selected reaction temperatures 473, 523 and 573K.

The values obtained from the statistical analysis were:

Temperature (K)	$1/A_\infty$	$1/(A_\infty \cdot K_{CO})$	K_{CO}
473	1.1313	0.7192	1.573
523	0.9983	2.8914	0.345
573	1.5192	5.1396	0.296

At each temperature, the value of A_∞ was determined. This value was then inserted into the expression $1/(A_\infty \cdot K_{CO})$. K_{CO} could then be calculated since the intercept between the line representing a given temperature and the y-axis was equal to $1/(A_\infty \cdot K_{CO})$.

Knowing the values of the equilibrium constant at each temperature, van't Hoffs equation A6.5 could be solved either graphically A6.6, or numerically A6.7:

$$\frac{d(\ln K)}{dT} = \frac{\Delta H}{R \cdot T^2} \qquad \text{A6.5}$$

$$\ln K_{CO} = -\frac{\Delta H}{R} \cdot \frac{1}{T} + \text{const.} \qquad \text{A6.6}$$

$$\ln \frac{K_{T_2}}{K_{T_1}} = \frac{-\Delta H}{R} \cdot \left(\frac{T_1 - T_2}{T_2 \cdot T_1}\right) \qquad \text{A6.7}$$

Plotting lnK versus $T^{-1} \cdot 1000$ resulted in a line with slope $-\Delta H/R = 4.6358$.
The heat of adsorption of CO was then calculated to 38.5 kJ/mole in the temperature range 473-573K.

Appendix A7: Estimation of the amount of adsorbed CO on the catalyst at reaction conditions.

The amount of adsorbed carbon monoxide on the silica and alumina supported Co-catalysts can be calculated using the integrated Beer-Lambert relation /181/:

$$S_{CO} = A_{CO} \cdot L \cdot C_{CO} \qquad \text{A7.1}$$

where S_{CO} = area under the IR CO absorbance peak (cm^{-1})
A_{CO} = the integrated absorption intensity (cm/mole)
L = sample thickness or path length (cm)
C_{CO} = concentration of CO ($mole/cm^3$)

Another way of expressing the Beer-Lambert equation in a more convenient form in view of solid samples in the pressed disk form, is achieved by replacing the term $L \cdot C_{CO}$ with:

$$L \cdot C_{CO} = m \cdot n_{CO} / A_C \qquad \text{A7.2}$$

and m = mass of the wafer (g)
n_{CO} = molar uptake of CO (mole/g)
A_C = cross sectional area of the wafer (cm^2)

Substituting the expression for $L \cdot C_{CO}$ in equation A7.2 in A7.1 and rearranging leads to:

$$n_{CO} = S_{CO} \cdot A_C / A_{CO} \cdot m \qquad \text{A7.3}$$

Equation A7.3 gives the amount of adsorbed CO in mole/g.

In order to evaluate the area under the linear CO absorption band, the method given by Rasband et al. /181/ was used to determine the upper and lower integration limits. The procedure was as follows :

1. The spectrum baseline was drawn beneath the individual peak(s) of interest.
2. A point was marked half way between the baseline and the local minimum or inflection point of the spectrum curve. The use of a local minimum or inflection point depended on the extent of overlap between adjacent peaks.
3. Through each midpoint(s) one line was drawn tangential to the right hand side of the peak of interest and one tangential to the left hand side of the adjacent peak.
4. The crossing points between the two tangent lines and the baseline determined the upper and lower integration limits.
5. The integrated band area was then computed based on the integration limits found by using the tangent method.

Fig. A7-1 illustrates the graphical approach applied in the determination of the integrated absorbance area.

The average value for the integrated absorption area under the 2072 cm^{-1} peak attributed to linearly adsorbed CO was (S_{CO}=) 18.075 cm^{-1} at the following reaction conditions:
4.7% Co/SiO_2, 473K, H_2/CO=2 and 6 bar.
The following values were obtained from measurements on the catalyst wafer used in the experiment at the reaction conditions specified above:

m = 0.0147 g $\qquad$ d_w = 1.3 cm (diameter of wafer)

The parameter A_{CO} was taken from data published by Duncan et al. /182/: $A_{CO} = 26 \cdot 10^6$ cm/mole.
The amount of adsorbed CO can then be calculated using equation A7.3:

$$n_{CO} = \frac{S_{CO} \cdot A_C}{m \cdot A_{CO}} = \frac{18.075 \cdot 1.33}{0.0147 \cdot 26 \cdot 10^6} = 6.3 \cdot 10^{-5} \text{ mole/g} = 63 \text{ µmole/g}$$

or, on a volume basis:

$$6.3 \cdot 10^{-5} \cdot 22414 \cdot \frac{473}{273} \cdot \frac{1}{6} = 0.41 \text{ cm}^3\text{/g}$$

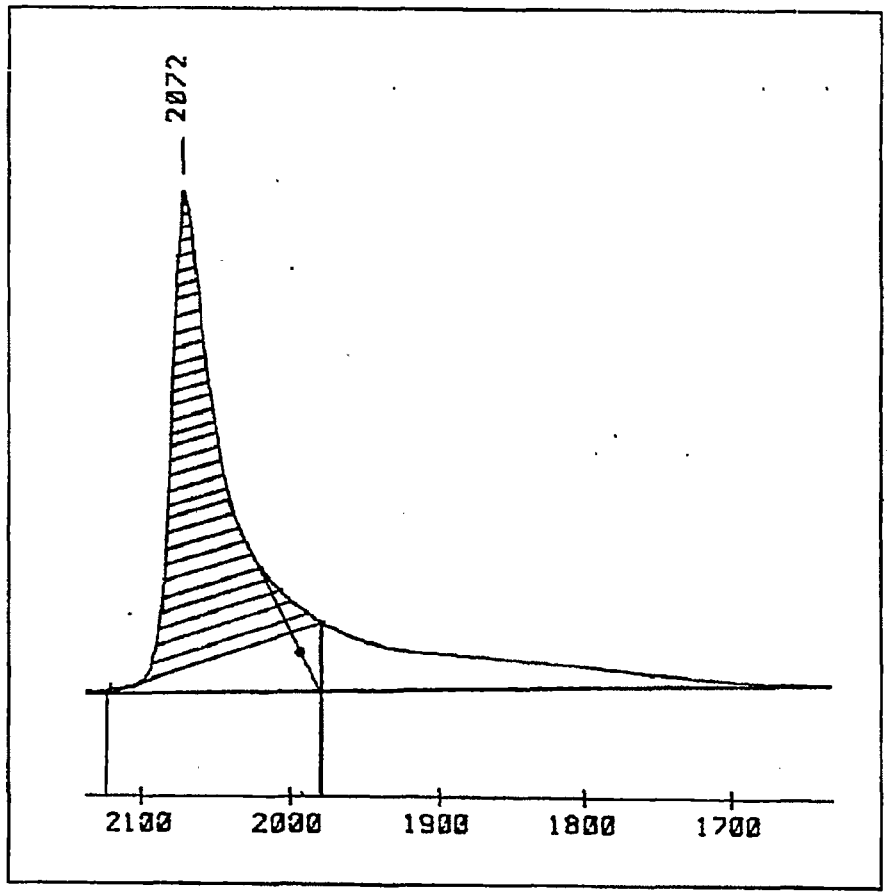

Fig. A7-1: Example on the use of the graphical method /181/ in determination of the upper and lower integration limits.
See text for further explanations.

Appendix A8: Estimation of the amount of adsorbed $>CH_2$ and $-CH_3$ species from the integrated intensities of the corresponding IR absorption bands.

The amounts of adsorbed $>CH_2$ and $-CH_3$ species accumulated on the surface during reaction can be calculated in a way similar to that shown in Appendix A7. The determination of the integrated absorbance area under the $>CH_2$ and $-CH_3$ bands were carried out using the graphical procedure given by Rasband et al. /181/.

The structural unit intensities, B_{CH_x}, for methyl and methylene stretching bands were reported to 4460 and 3740 $cm^{-2} \cdot dm^3 \cdot mole^{-1}$, respectively /197/. Francis /235/ reported intensity values of 3840 and 3320 $cm^{-2} \cdot dm^3 \cdot mole^{-1}$ for CH_3 and CH_2-groups, respectively, in liquid aliphatic hydrocarbons. Although there seems to be a slight discrepancy in the reported structural group intensities, the difference associated with the use of Wexlers in preferance to Francis' values is 12-16% lower values of v_{CHx} and m_{CHx}. The order of the "error" estimates is not of such a magnitude that it changes the conclusion drawn from these calculations. The values reported by Wexler /197/ are applied in the following calculations.

The amounts of $>CH_2$ and $-CH_3$ groups can be estimated according to the equation given by Yamasaki et al. /205/:

$$v_{CH_x} = \frac{S_{CH_x} \cdot A_C}{B_{CH_x} \cdot 10^3} \cdot \frac{T_m}{273} \cdot \frac{1}{P_m} \cdot 22414 \qquad (cm^3) \qquad \text{A8.1}$$

Considering the CO hydrogenation experiment performed at 473K and 6 bar over 4.7% Co/SiO_2, the amount of $>CH_2$ and $-CH_3$-groups on a volume basis is:

$$v_{CH_2} = \frac{0.475 \cdot 1.33}{3740 \cdot 10^3} \cdot \frac{473}{273} \cdot \frac{1}{6} \cdot 22414 = 0.00109 \ cm^3$$

$$v_{CH_4} = \frac{0.07229 \cdot 1.33}{4460 \cdot 10^3} \cdot \frac{473}{273} \cdot \frac{1}{6} \cdot 22414 = 0.00014 \text{ cm}^3$$

An expression for the chain length is obtained by dividing the amount of $>CH_2$ on $-CH_3$, thus giving the values reported in Table 5.2.5-2 on page 170.

In relation to the microbalance discussion, it is of interest to estimate the weight of adsorbed $>CH_2$ and $-CH_3$ present on the catalyst. This is done by using a similar expression as the one derived in Appendix A7, that is:

$$n_{CH_x} = \frac{S_{CH_x} \cdot A_C}{B_{CH_x} \cdot m_{cat}} \cdot 10^{-3} \qquad \text{(mole/g catalyst)} \qquad \text{A8.2}$$

$$m_{CH_x} = \frac{S_{CH_x} \cdot A_C}{B_{CH_x} \cdot m_{cat}} \cdot F_{CH_x} \qquad \text{(mg } CH_x\text{/g catalyst)} \qquad \text{A8.3}$$

The weight of accumulated $>CH_2$ and $-CH_3$ species during CO hydrogenation at 473K and 6 bar (H_2/CO=2) over 4.7% Co/SiO_2 was then found to be:

$$m_{CH_2} = \frac{0.475 \cdot 1.33}{3740 \cdot 0.0147} \cdot 14.01 = 0.161 \text{ mg} CH_2\text{/g catalyst}$$

$$m_{CH_3} = \frac{0.07229 \cdot 1.33}{4460 \cdot 0.0147} \cdot 15.01 = 0.022 \text{ mg} CH_3\text{/g catalyst}$$

Appendix A9: Theoretical estimates for the weight increase associated with cobalt carbide formation.

The weight change expected upon the possible formation of the cobalt carbides Co_2C and Co_3C can be calculated using the following expressions:

Co_2C : $$\frac{F_C \cdot m_{cat} \cdot wt\text{-}\%Co \cdot 1000}{F_{Co} \cdot 2} \qquad A9.1$$

Co_3C : $$\frac{F_C \cdot m_{cat} \cdot wt\text{-}\%Co \cdot 1000}{F_{Co} \cdot 3} \qquad A9.2$$

The above formula express the additional weight increase expected due to carbon atoms migrating into the cobalt lattice, forming interstitial carbides.

The weight of carbon participating in the carbide formation can be estimated for the experiment performed at the reaction conditions: 4.7% Co/SiO_2, 473K, H_2/CO=2 and 6 bar.

$F_C = 12.01$
$F_{Co} = 58.93$
$m_{cat} = 0.7092$ g
wt-% Co = 4.7

Co_2C : (12.01·0.047·0.7092·1000)/(58.93·2) = 3.400 mg.

Co_3C : (12.01·0.047·0.7092·1000)/(58.93·3) = 2.264 mg.

Appendix A10: Estimate of the weight of adsorbed carbon monoxide on 4.6% $Co/\gamma\text{-}Al_2O_3$.

The calculations are based on the dispersion of the catalyst, which was determined to 1% by volumetric chemisorption of hydrogen /236/.

The calculations are examplified by the CO hydrogenation experiment carried out at 473K, 6 bar and $H_2/CO=2$.

$F_{CO} = 28.01$
$F_{Co} = 58.93$
$m_{cat} = 0.7064$ g
wt-% Co = 4.6

number of moles of Co: $\frac{0.7064 \cdot 0.046}{58.93} = 5.514 \cdot 10^{-4}$

assuming an adsorption stoichiometry of 1:1 (linear form) results in:

the weight of adsorbed CO : $5.514 \cdot 10^{-4} \cdot 0.01 \cdot 28.01 = 0.154$ mg

or, assuming the bridgebonded form of adsorbed CO (adsorption stoichiometry of 1:2) gives:

the weight of adsorbed CO : $0.5 \cdot 5.514 \cdot 10^{-4} \cdot 0.01 \cdot 28.01 = 0.0772$ mg.

Appendix A11: Calculation of the density of the gas phase during CO hydrogenation over 4.7% Co/SiO_2 at GHSV=24538 and GHSV= 49706 Nml $(CO+H_2)$/g catalyst·h.

The gas phase density at GHSV=24538 and GHSV=49706 Nml $(CO+H_2)$/g catalyst·h was estimated in order to evaluate the possible effect of buoyancy as a cause for the observed weight decline upon changes in the flowrate.

The buoyancy effect due to changes in the gas phase density is represented by the following equation:

$$\Delta\rho_{gas} \cdot V_{basket} = \Delta m \qquad \text{A11.1}$$

where Δm = mass changes (g)

$\Delta\rho_{gas} = \rho_{GHSV=24538} - \rho_{GHSV=49706}$ (g/cm^3)

V_{basket} = volume of basket (cm^3)

The composition of the flow through the reactor at GHSV = 24538 and 49706 was:

GHSV = 24538	GHSV = 49706
92 Nml CO	184 Nml CO
8 Nml N_2	16 Nml N_2
200 Nml H_2	400 Nml H_2
100 Nml He	100 Nml He

$F_{CO} = 28.01$ $F_{N_2} = 28.02$ $F_{H_2} = 2.016$ $F_{He} = 4.003$

GHSV = 24538 Nml $(CO+H_2)$/g catalyst · h :

$$F_{gas} = 92/400 \cdot 28.01 + 8/400 \cdot 28.02 + 200/400 \cdot 2.016 + 100/400 \cdot 4.003 = 9.01145$$

$$\rho_{gas} = \frac{F_{gas} \cdot p}{R \cdot T} = \frac{9.01145 \cdot 0.6 \cdot 10^6}{8314 \cdot 523} = 1.243\,g/cm^3$$

GHSV = 49706 Nml ($CO+H_2$)/g catalyst · h :

F_{gas} = 9.7269

ρ_{gas} = 1.342 g/cm^3

$V_{basket} = \pi \cdot r^2 \cdot h = \pi \cdot (0.5)^2 \cdot 2 = 1.57$ cm^3

The difference in the gas phase density arises due to the flowrate of He, which was consta
(not doubled) when the flowrate of the reactant gases was increased twofold.

The buoyancy due to changes in the reactant flowrate is then:

$\Delta m = \Delta\rho_{gas} \cdot V_{basket} = (1.342-1.243) \cdot 1.57 = 0.155$ mg.

Appendix A12: Extent of reduction of 4.7% Co/SiO_2 and 4.6% $Co/\gamma\text{-}Al_2O_3$ estimated by the use of microbalance results.

The following assumptions were made in order to estimate the extent of reduction of the high loading silica and alumina Co-catalysts.

1. Cobalt is assumed to exist as Co_3O_4, and the reduction of this oxide is assumed to occur according to the stoichiometric reaction:

$$Co_3O_4 + 4H_2 \rightarrow 3Co + 4H_2O \qquad \text{A12.1}$$

2. The observed weight reduction is assumed to be due to loss of oxygen.

3. Adsorption of water on the catalyst is neglected.

With this in mind, the expression giving the degree of reduction of the catalyst is:

$$\frac{3/4 \cdot W_L \cdot F_{Co} \cdot 0.1}{F_O \cdot \%\text{-}Co \cdot m_{cat}} \qquad \text{A12.2}$$

where W_L = weight loss during reduction (mg)

m_{cat} = mass of catalyst (g)

F_{Co} = 58.93

F_O = 16

The degree of reduction of the 4.6% $Co/\gamma\text{-}Al_2O_3$ catalyst applied in the CO hydrogenation experiment at 573K and 6 bar (H_2/CO=2) is then:

$$\frac{3/4 \cdot 2.93 \cdot 58.93 \cdot 0.1}{16 \cdot 4.6 \cdot 0.7229} \cdot 100\% = 24.34\%$$

The theoretical weight loss during reduction can be estimated from:

$$\frac{\%Co \cdot 0.01 \cdot m_{cat}}{F_{Co}} \cdot F_O \cdot 4/3 \cdot 1000 \qquad \text{A12.3}$$

Using the experiment above as an example, the theoretical weight loss is calculated to:

$$(4.6 \cdot 10^{-2} \cdot 0.7229)/58.93 \cdot 16 \cdot 4/3 \cdot 1000 = 12.04 \text{ mg}$$

U.S. DEPARTMENT OF COMMERCE
Technology Administration
National Technical Information Service
Springfield, VA 22161 (703) 605-6000